DIRECT MEASUREMENT OF LAMINAR SKIN FRICTION AT HYPERSONIC SPEEDS

Thesis by

Manfred Eimer

In Partial Fulfillment of the Requirements

For the Degree of

Doctor of Philosophy

California Institute of Technology

Pasadena, California

1953

ACKNOWLEDGMENTS

While it is difficult to acknowledge individually all those who assisted in this investigation, mention must be made of those without whose continued help this project would not have been possible.

The author is deeply indebted to Dr. Henry T. Nagamatsu for his continued guidance and encouragement.

The author wishes to express his sincere appreciation to Professors H. W. Liepmann and L. Lees and Dr. T. Y. Li for many stimulating discussions.

Many of the members of the staff of the Hypersonic Research Group at GALCIT gave generously of their time, far more than their employment required. These include Mr. P. Baloga, whose skill and ingenuity contributed immeasurably to the success of this project, Miss F. Scheinis, who aided invaluably in computing and plotting the experimental results and preparing the final manuscript, and Messrs. C. Granneman and S. Roman who gave freely of their time and provided continued help and encouragement during the installation and testing of the model.

Acknowledgment is made to Miss N. Waldron and Mrs. G. Van Gieson for their aid in the preparation of the final manuscript, to the members of the Aeronautics Machine Shop, and in particular Mr. C. Bartsch, for the skilful construction of the test equipment, and to Messrs. N. Morishita and R. Destabelle for their help in developing the electronic balance components.

The author dedicates this thesis to his wife, Gretchen, without whose help and unshakable confidence this work could not have been completed.

ABSTRACT

A direct measurement of flat plate laminar local skin friction was undertaken at M = 5.8 in the GALCIT Hypersonic Wind Tunnel, Leg No. 1. A new balance particularly suited to the requirements of hypersonic experimentation was designed.

By means of the fluorescent lacquer technique for indicating boundary layer transition, unexpectedly high natural transition Reynolds numbers were observed. The several methods of forcing transition which were used were unsuccessful in producing transition at a Reynolds number of two million.

Observation of the leading edge shock wave and boundary layer by means of a schlieren system indicated that at M = 5.8 the shock wave and boundary layer are separated by appreciable distances wherever the boundary layer equations hold.

Skin friction force measurements were made at five Reynolds numbers in condensation-free flow. The discrepancies between the observed low values of $C_f\sqrt{Re}$ and existing laminar boundary layer calculations are reconciled by means of a qualitative analysis.

A theory describing the properties of the viscous boundary layer for flows with condensation in the free stream is presented. It is predicted that for a specified nozzle geometry and stagnation temperature, skin friction remains unchanged in the presence of moderate amounts of condensation, while heat transfer for a given wall temperature is affected by the presence of condensation which produces major changes in the adiabatic wall temperature.

TABLE OF CONTENTS

SYMBOLS AND NOTATION

a = speed of sound, ft/sec

A = nozzle cross sectional area

C = factor of proportionality in the equation $\frac{\mu}{\mu_\infty} = C(T/T_\infty)$

C_f = local skin friction coefficient, dimensionless

C_p = specific heat at constant pressure, Btu/lb/^oF

C_v = specific heat at constant volume, Btu/lb/^oF

e = internal energy per unit mass, Btu/lb

g = mass fraction of fluid condensed, dimensionless

h = enthalpy per unit mass, Btu/lb

h = local heat transfer coefficient, Btu/sq ft/hr/^oF

k = thermal conductivity, Btu/sq ft/hr/^oF/ft

L = latent heat of vaporization per unit mass, Btu/lb

M = Mach number in condensation-free flow, $\frac{u}{a}$, dimensionless

Nu = Nusselt number, hx/k, dimensionless

p = pressure, lbs/sq in

Pr = Prandtl number, $\mu Cp/k$, dimensionless

q = heat transfer rate, Btu/sq ft/hr

q = dynamic pressure, $\frac{1}{2}\rho U_\infty^2$, lb/sq in

q = mass velocity, ft/sec

Q = heat added per unit mass, Btu/lb

R = gas constant per unit mass, Btu/lb

Re = Reynolds number, $U_\infty X/\nu$, dimensionless

S = Sutherland's temperature, ^oR

t = time, sec

T = absolute temperature, ^oR

u,v = local velocity components in x and y directions, respectively, ft/sec

U_∞ = velocity outside the boundary layer, ft/sec

V = volts

x,y = coordinates parallel and perpendicular to surface, respectively, (with origin at leading edge), ft

X = characteristic length of body, ft

$\sim$ = cycles

δ = boundary layer thickness, ft

η = dimensionless independent variable occurring in the Blasius function $f(\eta)$

γ = ratio of specific heats, dimensionless

Θ = Sutherland's constant, dimensionless

θ = characteristic angle, degrees

μ = absolute viscosity, lb sec/sq ft

ν = kinematic viscosity, sq ft/sec

ρ = mass density, lb sec^2/ft^4

τ = shear stress, lb/sq ft

Φ = dissipation function

Ψ = stream function

ω = exponent in the equation $\frac{\mu}{\mu_\infty} = (T/T_\infty)^\omega$

Superscripts

( )* dimensionless quantities

( )* conditions at the throat, used only in A*

( )' ordinary differentiation

Subscripts

$( )_\delta$ conditions outside of the boundary layer

$( )_s$ conditions on the surface bounding the condensation free sub-layer

$( )_w$ conditions at the wall or surface of the body

$( )_e$ equilibrium conditions of an insulated surface

$( )_o$ stagnation or reservoir conditions

$( )_o$ properties of condensation free flow

$( )_c$ properties of two phase flow

$( )_L$ properties of liquid component

$( )_V$ properties of vapor component

$( )$ (without subscript) properties of mixture of vapor and droplets

$( )_B$ conditions at which Sutherland's constant is evaluated

Several other symbols and notations are defined in the text, for use only in the immediate vicinity of their definition.

TABLE OF FIGURES

I. INTRODUCTION

In discussing flow phenomena occurring at speeds which are large compared to the local speed of sound, it has become the accepted practice to refer to such speeds as "hypersonic". In the mathematical sense, the hypersonic regime is that in which terms of the order of $1/M^2$ are small compared to one and can often be neglected.

In a field as new as hypersonic fluid mechanics, it is inevitable that new phenomenological discoveries be made concurrently but independently by means of theoretical and experimental studies, and that there should be some time lag in verifying and correlating results. Two examples outstandingly typify the state of present knowledge, or lack of it, of the field. The first is the important hypersonic boundary layer transition problem which has been examined to some extent experimentally but has not yet been attacked by theoretical methods to any appreciable degree. The second is the hypersonic leading edge shock wave-boundary layer interaction problem which already has been extensively studied theoretically (Refs. 1, 2, 3, and 4) and is only now being investigated experimentally.

At the present stage of development in the field of hypersonic fluid mechanics, not only are known anomalous phenomena inadequately explained or verified, but the process of discovering new phenomena has just barely begun. It is important to note, however, that phenomenological anomalies should not, in general, be expected to occur solely due to the high ratio of ordered to random molecular energy characteristic of the hypersonic regime. Thus, for example, the pressure distribution on the surface of bodies in hypersonic flow, at high

Reynolds numbers where viscous effects are small, can be reliably predicted by means of considerations usually applicable for purely supersonic flows.

Unfortunately, experimentation at high Mach numbers is immensely more difficult than comparable work in the low supersonic Mach number regime due to the inevitable existence of extremes of temperature and pressure. During recent years much thought has been given to the design of several types of experimental installations capable of producing uniform and steady regions of hypersonic flow. The relative advantages of wind tunnels of the continuous and of the blow down type, several types of shock tubes, and ballistic ranges were examined, and design and construction of several such facilities were undertaken. To date, construction of at least three wind tunnels (5 in. and larger) capable of reaching Mach numbers of the order of ten has been completed (NACA Langley Aeronautical Laboratory, NOL, and GALCIT) and at least three hypersonic shock tubes have been designed (Polytechnic Institute of Brooklyn, Cornell University, and GALCIT).

Design, construction, and operation of high Mach number wind tunnels offer many specialized and difficult problems not generally encountered in low speed wind tunnel work, which very significantly influence its operational limitations. If air is expanded from a supply which is kept at room temperature and at several atmospheres pressure, the air vapor - liquid equilibrium saturation point is reached at a Mach number of the order of 4.5. Thus, if thermodynamic equilibrium is assumed to exist in the flow, the supply air must be heated for testing in condensation-free flow at Mach numbers higher than 4.5. The successively higher supply temperatures necessary for condensation-

free flow at higher Mach numbers, and the accompanying higher supply pressures usually necessary to obtain the required compression ratio across the nozzle, test section, and diffuser system, introduce increasingly severe wind tunnel structural design conditions.

In view of the difficulties outlined above, it is of great interest to examine the possibility of obtaining useful experimental results from tests performed in the presence of condensed air. It is, therefore, desirable to pursue experimental research at high Mach numbers in two parallel directions:

(1) Investigation of hypersonic effects.

(2) Investigation of the effect of the presence of condensation on hypersonic phenomena, or, in other words, the extent to which wind tunnel tests performed in the presence of condensation can still reliably be used to predict or verify hypersonic phenomena

The present need for operating high Mach number wind tunnels with and without air condensation introduces complications which will, of course, be avoided, or at least minimized, when it is clearly established in which regime specified research programs must be carried out. The severity of this requirement can be demonstrated, for example, by considering that the flat plate recovery temperature may, at a Mach number of ten (based on $\overline{q}/p_o$), vary from -160°F (with no supersaturation) to 800°F for reservoir temperatures varying from room temperature (80°F) to 1000°F, a temperature range readily attainable in the GALCIT Hypersonic Wind Tunnel Leg No. 2.

In the summer of 1951, work in progress or completed had already provided a qualitative experimental and theoretical description of the

phenomenon of air condensation in high Mach number wind tunnels (Refs. 5, 6, 7, and 8), and investigations leading to quantitative results were planned. At that time, condensation-free operation of the GALCIT 5 x 5 in. Hypersonic Wind Tunnel, Leg No. 1, was not yet possible at Mach numbers above five at pressures of the order of seven atmospheres, even considering the observed degree of supersaturation, since the supply air heater installation had not yet been completed. Due to these limitations in the facilities for experimentation, theoreticians and experimenters concerned themselves primarily with the condensation problem and only secondarily undertook predictions of anomalies to be expected in the field of hypersonic fluid mechanics. The decision was made at that time that the first extensive investigation to be undertaken upon the completion of the condensation-free hypersonic facility (Leg No. 1, with supply air heater, Cf. Appendix A) should concern itself with the viscous boundary layer. This decision was made with little knowledge of any unusual hypersonic effects.

It was planned that measurements of viscous drag would be undertaken at the condensation-free Mach numbers attainable in Leg No. 1 as soon as heater construction and shakedown allowed and at the higher Mach numbers of the planned Leg No. 2 when that became a useful facility for experimentation. Measurements were to be made on a flat plate in the presence of laminar and turbulent boundary layers with and without condensation. A similar program for flat plate heat transfer work to be carried out at the completion of the first phases of the drag investigations was also planned. The present author undertook the measurement of viscous skin friction, the first experimental program to be carried out principally in condensation-free flow.

A Mach number of at least eight in the test section could be attained with the Leg No. 1 heater installation. However, for testing contemplated to clarify condensation problems, the need for nozzle blocks in which condensation was absent for a comparatively long distance downstream of the nozzle throat dictated design and construction of a set of Mach six nozzle blocks. It was planned that, by means of suitable test section surveys and by making slight changes in the throat height to vary the Mach number in the test section, a Mach number and model location would be selected which was optimum in that existing pressure gradients were at a minimum.

From the point of view of the over-all requirements of hypersonic research at GALCIT, it was considered essential that new techniques of boundary layer research be developed which were applicable to the much more severe requirements of the higher Mach number Leg No. 2 operation. Existing techniques of skin friction measurements were, therefore, examined as to applicability under the conditions of forces, pressures, and temperatures which would be encountered at high Mach numbers with the extremes of stagnation temperature discussed above.

The problem of the experimental verification of theoretical predictions of viscous drag on bodies in motion at high speeds has until comparatively recent times remained unsatisfactorily solved, although it has long been of considerable interest. Dhawan (Ref. 9), under the guidance of Dr. H. W. Liepmann, carried out a systematic evaluation of experimental methods for determining skin friction in high subsonic and low supersonic flow, which included:

(1) Determination of skin friction from velocity profile measurements obtained by:

(a) Pitot (or total head) tubes

(b) Stanton tubes

(c) Hot-wire anemometers

(d) Interferometers

(2) Determination of skin friction by direct measurement of:

(a) Heat transfer

(b) Viscous shear force

As a result of extensive research, Dhawan concluded that a device could be built by means of which the local skin friction force could be directly measured to a greater degree of accuracy and reliability than is possible with the other methods. Dhawan designed and used a balance system which utilized a "floating" element, carefully aligned with the surface of a flat plate and supported by a three-bar linkage which assured the maintenance of the parallel alignment between the element and plate surfaces. The restraining force was supplied by a system of four flexure links which were part of the parallelogram support mechanism. The mechanical sensitivity of the instrument, that is, the amount of element deflection per unit force, could be varied by utilizing flexures of various stiffnesses. The position of the element was sensed by means of a differential transformer operating with an input frequency of twenty kilocycles. Damping was provided by an oil dash-pot.

As a result of the highly satisfactory performance of Dhawan's balance, demonstrating that accurate direct measurement of local skin friction was possible, a number of local skin friction balances were

developed (Refs. 10, 11, 12, etc.). To the best knowledge of the author, all of these balances were very similar in principle to that developed by Dhawan except that return force mechanisms were added in some cases to make them of the null-reading type.

The present author critically reexamined and reevaluated the various methods of skin friction measurement discussed in Ref. 9, and concluded that all of these methods, except that involving the direct measurement of local skin friction, are even more unreliable in the hypersonic range than in the subsonic and low supersonic range considered by Dhawan. Reasons for the unreliability differ in the present case only in degree. It was, therefore, concluded that local viscous skin friction would be determined by direct force measurement.

The above general considerations were completed during the summer of 1951, and a test program for experimentation in the GALCIT 5 x 5 in. Hypersonic Wind Tunnel was planned. On the basis of data available at that time it was believed possible to force a boundary layer transition at Reynolds numbers less than one million. It was also believed that the turbulent contamination of the laminar boundary layer would follow its usual behavior. The maximum downstream location of the floating element was thus fixed by the requirement that it be in a region which could be kept purely laminar. In this manner, the floating element location was established to be five inches from the plate leading edge. To avoid measurable effects of the plate trailing edge, a plate length of ten inches was decided upon.

Although flat plates of considerable thickness ($< 2/3$ in.) can be tested in the GALCIT 5 x 5 in. tunnel, a maximum plate thickness of 3/16 in. was established to facilitate the comparison between the techniques

employed in the present tests and those used in transonic investigations. To verify the feasibility of these size limitations, a roughly constructed plate was installed and wind tunnel starting characteristics and minimum running pressures established. Although no evidence of flow breakdown could be noted even with the supply air at atmospheric pressure, it was believed unjustifiable to undertake the considerably more complicated tunnel operation corresponding to total pressures less than atmospheric. Therefore, for ease of operation and plant safety the supply pressure operating range for a Mach number of about six was limited to a range from 16 psia to 100 psia.

A detailed evaluation of experimental methods useful for the present purposes was undertaken in which the use of existing techniques was heavily favored.

It was decided that flat plate static pressures were to be measured with respect to a known vacuum by means of static pressure orifices suitably distributed over the plate surface and connected to an oil manometer. Boundary layer pitot pressures were to be measured by means of a probe, having a slit 0.002 inch high and walls sharpened to a fine edge, connected to mercury and oil manometers.

The use of a new and powerful technique of surface temperature measurement, generally referred to as "thermography" (Ref. 13), was very extensively examined but finally discarded since the required development could not be completed without severe detraction from the principal purposes of this investigation. It was, therefore, decided that surface temperature measurements were to be made by means of thermocouples welded to the plate at points less than 0.010 inch below the aerodynamic surface.

The existing schlieren system was believed to be adequate for a qualitative examination of the test section wave pattern and the plate boundary layer.

A systematic evaluation of methods for indicating boundary layer transition was carried out, as a result of which it was concluded that methods based on the large differences between evaporation rates in regions of laminar and turbulent flow yielded the greatest amount of information for given expenditures of time and effort. Stalder and Slack (Ref. 14) obtained excellent results by means of a method of transition indication in which a lacquer was employed which fluoresces only when dry. A brief experiment in the GALCIT 5 x 5 in. Hypersonic Wind Tunnel indicated that the formulas suggested in Ref. 14 were inapplicable for the conditions existing in the test section at Mach six even with the supply air at room temperature. It was, therefore, planned that a program of extending the method of Ref. 14 to higher Mach numbers would be undertaken. Results of this investigation are discussed in Appendix C.

The most important, and, therefore, the most critical, evaluation made was that of the existing techniques of direct measurement of skin friction force. Since it was the purpose of the present investigation to develop techniques applicable at plate surface temperatures varying from $-160^{\circ}F$ to $800^{\circ}F$, the three-bar linkage balance systems, patterned after that of Dhawan, were examined critically with respect to the maximum allowable balance chamber temperature and the necessary accuracy of force measurement and of element and plate alignment. The following was concluded:

(1) A balance system utilizing electronic components in regions

of high temperature was infeasible.

(2) Major redesign of existing balances would be required to avoid apparent element deflections due to differential expansion of the linkage components and the differential transformer support mechanism.

(3) A nulling force mechanism must be supplied to allow measurement of skin friction at given nozzle geometries without sacrifice of accuracy under the wide range of Reynolds numbers possible in Leg No. 2 of the Hypersonic Wind Tunnel Facility.

(4) A mechanism for adjusting the relative vertical position of the floating element and the flat plate would be required to account for the inevitable excessive differential expansion of the plate and element support systems.

Thus, it was decided with considerable regret that the three-bar linkage system is inherently not adaptable to the stringent requirements of high Mach number, high temperature operation. A completely new balance system suited to the severities of hypersonic wind tunnel operation was, therefore, designed, constructed, and successfully operated. Pertinent details of this new balance design are discussed in Section II.

Since it was believed difficult to construct a single plate which incorporated the large number of pressure orifices and thermocouples required to obtain adequate surface pressure and temperature distributions in addition to the floating element and balance system, it was decided to construct two flat plates. The first of these plates, the survey plate, was to contain a large number of pressure orifices and thermocouples, while the second, or the balance plate, was to contain,

in addition to the floating element, only two plate surface pressure orifices for correlation with the first plate. Design details of both plates are discussed in Section II.

The experimental program was, thus, to consist of surface pressure and temperature measurements on the survey plate with a given nozzle configuration, at five values of reservoir pressure, and at values of reservoir temperature corresponding to various amounts of air condensation in the free stream. Skin friction force measurements and boundary layer pitot pressures were to be obtained on the balance plate under the same conditions of pressure and temperature. Boundary layer transition measurements were to be undertaken on either plate as required. Experimental procedures are further discussed in Section III. A discussion of skin friction results will be found in Section IV.

As briefly mentioned above, investigation of the effect of the presence of condensation on hypersonic phenomena is, at the present time, still an important part of hypersonic research. Thus, in addition to the experiments mentioned above, a theoretical investigation of the effect of condensation on skin friction and heat transfer was undertaken. Theoretical results obtained in these studies are discussed in Section V.

II. DESCRIPTION OF MODELS AND TEST EQUIPMENT

In a field as relatively unexplored as hypersonic fluid mechanics, it is a fundamental precept of experimental research that measurements should be directed not only toward the resolution of specified phenomena but also toward the discovery of new phenomena. During the present investigation, in addition to the measurement of skin friction force, schlieren photographs were taken, boundary layer transition studies and extensive flat plate surface pressure and temperature surveys were made, and boundary layer pitot pressure surveys were planned.

In addition to the known severities of the wind tunnel test conditions determined by the operating Mach number, total temperature, and total pressure, problems associated with the particular wind tunnel design employed in the GALCIT 5 x 5 in. Hypersonic Wind Tunnel (Cf. Appendix A) had to be considered. The manner in which these considerations directed the design of the models will be discussed below.

A. The Survey Plate

The known existence of flow non-uniformities in the test section made it imperative that extensive surveys be made of those pressure distributions which could measurably affect the skin friction force on the balance plate. The magnitude of these flow imperfections, principally due to waves originating on the side walls near the nozzle block inflection points, at first was found difficult to repeat.

Since attempts to include an adequate number of surface pressure orifices and thermocouples in the balance plate would greatly complicate its design and possibly introduce errors in the force readings due to

the effects of the presence of the orifices, it was believed necessary to use a survey plate specifically instrumented for pressure and temperature surveys. If data from the survey and balance plates were to be correlated, it was believed necessary that only models which could be installed without opening the wind tunnel doors should be utilized in the present investigations.

When the design requirements for the present investigation were established, it was also thought necessary to be able to vary the plate angle of attack to permit corrections for flow asymmetries and to assure attachment of the boundary layer over the complete plate. An angle of attack adjustment mechanism with a range of six degrees was, therefore, specified.

In observance of the precept that techniques were to be developed which were applicable at the conditions of high temperature possible in Leg No. 2 of the Hypersonic Wind Tunnel Facility, components of the survey and balance plates were constructed from materials capable of withstanding, for limited periods of time, temperatures as high as 1000°F. On the basis of its resistance to corrosion at high temperatures, hardness, dimensional stability during machining, and sufficient magnetic permeability for being held in a magnetic grinding chuck, a type 440C stainless steel was selected for use in the actual survey and balance plates. As a result of development work undertaken for this purpose, it was believed that the thermocouples could be attached closest to the aerodynamic surface by machining indentations into the lower plate surface to within less than .010 in. of the aerodynamic surface and welding the thermocouples directly to the plate. The stainless steel tubes used to lead the plate static pressures out of the model were silver

soldered to the plate.

A photograph of the survey plate configuration derived from the above general considerations is shown in Fig. 4. The location of the 16 static pressure orifices and 8 thermocouples is shown on Fig. 5. To minimize the blockage area, a requirement imposed only to develop more generally applicable techniques, the thermocouples and pressure leads were imbedded in the plate and covered with a stainless steel sheet (Type 302). The thermocouple wires were brought out of the model through the windshield and connected to one of the Brown potentiometers (Cf. Appendix A). The pressure leads were brought out of the tunnel by means of standard fittings located in the upper diffuser block and connected to the right hand two banks of the silicone manometer shown in Fig. 1b.

The windshield on which both plates were interchangeably mounted was made of Invar to minimize the differential expansion problem so important in the balance plate. To permit the angle of attack adjustments discussed above, the windshield was fastened to a circular cylinder which was free to rotate in the test section insert block (Fig. 18a).

B. The Skin Friction Balance and Plate

1. Balance Design Requirements

On the basis of careful analysis of existing skin friction balances, it was concluded that existing balance mechanisms were not adaptable to the requirements of high temperature wind tunnel operation. Design of the new mechanism described below was undertaken only after the need for a device capable of directly measuring the skin friction

force under high temperature conditions was clearly established.

If skin friction is to be measured on a plate without heat transfer, it is intolerable that portions of the mechanism close to the plate surface, particularly the members supporting the plate, be cooled. Temperature sensitive components cannot be housed in these supporting members since such members must,of necessity, be allowed to reach temperatures of the same order as that of the plate surface.

2. Selection of Displacement-Sensing Device

Of the possible types of strain or displacement-sensitive electrical devices, the strain gauge dependent on changes in electrical resistance is affected most by temperature changes, and gauges sensitive to changes in capacitance are the least commercially developed. The selection of a position-sensing device which fundamentally responds to changes in magnetic reluctance can, therefore, be justified on the basis of availability and comparative insensitivity to temperature changes (Ref. 15). Since differential transformers manufactured by the Schaevitz Engineering Company have been successfully used in several of the existing skin friction measuring devices, it was only natural that use of these devices should be considered in the present case. It was concluded, however, that these and all other presently available reluctance gauges cannot be exposed to temperatures above 450°F. If gauges of this type were nevertheless to be used,it was necessary to utilize a mechanism in which they could be located sufficiently far from the plate surface to remain within the allowable temperature range.

3. Comparison of Possible Balance Mechanisms

The three-bar linkage system used by Dhawan (Ref. 9) and others is not adaptable to the transmission of forces and deflections over large distances since long and cumbersome components would be required and the mechanical advantage of distance is always less than one. On the other hand, a very common mechanism which can readily amplify deflections and indicate them some distance away from the primary deflecting component is that used in ordinary chemical balances, where the pointer indicating the unbalance magnifies and remotely indicates the position of the balance pans.

In the three-bar linkage, the sensitivity (deflection per unit force) and natural frequency are both largely dependent on the stiffness of the flexures and cannot be independently altered. The natural frequencies corresponding to practical flexure stiffnesses are usually comparatively high. In general, the interchanging of flexures is cumbersome and requires realignment of the floating element.

In a chemical balance type of mechanism, the sensitivity and period of oscillation can be easily changed independently, without the need for floating element realignment, by changing the distribution of weight above and below the pivot point.

Hypersonic wind tunnels can operate over wide ranges of Reynolds numbers and dynamic pressures even with fixed nozzle blocks and, thus, almost invariant Mach numbers. Consequently, large variations in aerodynamic forces are possible. In balance systems not of the null type, a gap width greater than the product of sensitivity and maximum aerodynamic force must be used, where the required sensitivity is the

ratio of the minimum detectable displacement to the minimum force increment to be measured. To minimize the error introduced by the effect of a discontinuity in the plate surface, the gap around the element should be made as small as possible, consistent with the minimum allowable sensitivity.

A null balance system has the advantages of having almost unlimited sensitivity and of permitting the use of extremely small gaps between the element and the plate, but it has the disadvantage of usually requiring a movable mechanical connection with regions outside of the wind tunnel. Note that mechanisms of the chemical balance type are inherently of the null type.

In view of the above considerations, the decision was made that, for the present purposes, a nulling balance patterned after existing chemical balances was far superior to the three-bar linkage mechanism and that design of such a device should be undertaken.

4. Comparison of Possible Pivoting Methods

In studying the design details of existing balances, it was found that, in general, only five principal methods of providing frictionless pivot points are used. The rolling types of bearings (ball, roller, and journal) are the most suitable for large loads. Torsion strips and jewel bearings, while adaptable to small loads, introduce severe design problems. Thus, detailed consideration of practical pivoting methods was limited to flexure links and knife edges.

Without exception, the chemical balances examined utilized knife edges, which, for comparatively small loads, unquestionably provide

the most accurate and most frictionless pivoting mechanism. Knife edges, however, have the comparative disadvantage that two separable mating parts are involved. The required sharpness of knife edges is principally determined by the allowable friction and the amount of uncertainty in vertical position which can be tolerated. Excessive additional dulling of the edge due to chattering under non-steady loads and brinelling due to occasional overloads may seriously impair both the accuracy of pivot location and increase the contact friction. Examples of wind tunnel balances utilizing knife edge pivots are the GALCIT 10 ft. Wind Tunnel and the University of California Low Density Wind Tunnel.

Flexure links have the considerable advantage that all components are fastened together and relative sliding motion is not possible, but they have the disadvantage of having definite, and in the present case necessarily appreciable, spring constants and somewhat uncertain behavior at elevated temperatures. Examples of wind tunnel balances utilizing flexure links as pivot points are those at the Southern California Cooperative Wind Tunnel and the JPL 20" Wind Tunnel.

Although the choice was difficult to make, the uncertainty of high temperature flexure properties was responsible for the decision to use a knife edge pivot in the present case.

5. Comparison of Possible Nulling Methods

Three methods of applying a nulling force were considered in detail and dummy mechanisms constructed. Since for the present purposes the balance chamber must be kept at tunnel static pressure, it must be possible to increase or decrease the nulling force by remote control.

Some chemical balances are equipped with mechanisms which permit adding or removing individual weights remotely, but such devices are invariably complicated. However, the Chainomatic principle used in many accurate chemical balances, which permits continuous variation in load by changing the length of a fine-linked metal chain hanging from the balance arm, is readily adaptable to remote control.

The principal advantage of using a chain for the present purposes lies in its simplicity. It was found, however, that chains of the type under discussion are very susceptible to vibrations, which are difficult to damp out. The specific gravity of damping oils varies considerably with changes in temperature ($\approx .05\%/^{o}F$) and thus may introduce measurable errors in the calibrated chain weight due to changes in oil level and buoyancy force. An additional and even more severe disadvantage of using chain loading is that chains, fine linked enough to weigh with sufficient accuracy the minimum force, corresponding to the lowest Reynolds number and laminar flow, must be comparatively long to balance the maximum force corresponding to turbulent flow. The required long chain and well are particularly susceptible to the vibration and buoyancy effects mentioned above.

A mechanism sometimes used in metallurgical balances utilizes a soft iron core oriented at 45^{o} with the balance arm and at 45^{o} with a magnetic field. By changing the strength of the magnetic field, a nulling force of predictable strength can be supplied. This variable magnetic field mechanism has the considerable advantage of requiring a minimum of mechanical parts and the disadvantage of bulkiness since a very large volume of coiled wire is required to obtain a sufficiently

strong magnetic field.

Accelerometer studies of the wind tunnel vibration problem were undertaken to determine the most troublesome frequency components and the maximum amplitudes of deflection. On the basis of these studies in which, due to faulty equipment, the deflection amplitudes were underestimated and the most troublesome frequencies appeared higher than they subsequently turned out to be, it was believed that extensive damping of the mechanical parts would be required. The nulling force mechanism used in the final design (Fig. 17a and Fig. 18a) is believed to have none of the disadvantages of the other two systems given detailed consideration and has the tremendous additional advantage that it is readily adaptable to several methods of damping.

The final nulling force mechanism consists principally of an internal balance beam fastened to the main counterweight, which carries two permanent magnets, and an external balance beam, which also carries two permanent magnets. The external beam is pivoted on a knife edge and balanced by a pendulum which moves in damping oil. The internal beam is separated from the external beam by a brass plate which provides a vacuum tight seal for the balance chamber. By adding weights to the external balance pan, the external balance beam is rotated and a force transmitted to the internal beam which produces a moment about the main internal knife edge. The sensitivity of the nulling force mechanism can be varied by adjusting both the spacing between the balance beams and the position and magnitude of the pendulum weight.

6. Element Alignment Adjusting Mechanism

It is difficult and probably impossible to prevent excessive

differential temperature expansion of the members carrying the plate and those carrying the floating element. For example, with total temperatures of the order of 1000°F, differential temperatures of the order of 100°F must certainly be considered possible, and correspondingly, differential expansions of the order of 5×10^{-4} in. could be encountered between components 5 in. long. A mechanism for adjusting the vertical position of the element was therefore provided (shown in detail in Fig. 17c), which could be operated during actual tunnel operation or preset to align the element with the plate surface (or with a calibrated position above or below the plate to compensate for existing differential expansions). The plate and element alignment was, for the present purposes, made by observing interference fringes produced by a monochromatic light and an optically flat piece of quartz. In future work the element alignment can be made during tunnel operation by means of an interferometer whose general design was considered but not undertaken in detail.

To account for the fact that manufacturing and assembly tolerances inevitably could not be limited to sufficiently small values, an element tilt adjusting mechanism (shown in detail in Fig. 17b) which could be operated before tunnel operation was provided.

7. Electronic Components for Position-Sensing

A block diagram of the final arrangement of the electronic components of the balance position-sensing system is shown in Fig. 19a and the location of the two Schaevitz coils with respect to the mechanical components of the balance system is shown in Fig. 18a. Details of the circuitry are shown in Figs. 19b, 19c, and 19d, and the numerical values

of the circuit elements are tabulated in Fig. 19f.

Note that, by using two coils, changes in the output voltage due to differential temperature expansion of the balance components holding the coils and cores were minimized or even eliminated. A 100 kc input signal was used, rather than the more common 20 kc, because of the somewhat greater change in electrical output per unit core deflection obtainable. Simplification of system component construction is also possible by using such a comparatively high frequency. With the amplifier set at maximum gain ($\approx$ 500,000), a noise signal of 10 v and a change in output of 7 volts per milligram of aerodynamic force was obtained. The final electronic balance position-sensing system was used with complete success.

8. Calibrating Mechanism

The calibrating balance shown in Fig. 17a was designed to provide equal moments about the pivot point for equal loads on the calibrating balance pan and on the floating element. The permanent magnet spacing and the external counterweight position were adjusted to also provide equal moments about the pivot point for equal loads on the external balance pan and the floating element.

III. EXPERIMENTAL PROCEDURES

A. Selection of Flat Plate Location

As a first step in selecting the optimum model location, extensive pitot pressure surveys of the horizontal centerplane were made. In addition, flow inclination distributions were obtained by means of a wedge. On the basis of these nozzle calibrations, it was decided to test the models near the downstream end of the test rhombus and thus minimize the effects of the sidewall waves found to exist in the nozzle.

The survey plate, installed in this location, is shown in Fig. 4. The pressure orifice and thermocouple locations are shown in Fig. 5.

B. Selection of Reservoir Pressures and Temperatures

For ease of plant operation, maximum and minimum stagnation pressures of 94.4 psia and 16.0 psia, respectively, were selected with intermediate test pressures of 74.4, 46.9, and 23.4 psia.

From the pitot-static pressure surveys of the flow, at various stagnation temperatures (Fig. 3), a minimum temperature of 190°F for condensation-free flow was established. This temperature is somewhat below that theoretically required for equilibrium saturation due to the occurrence of supersaturation. For the present condensation-free tests, a total temperature of 225°F. was selected to include an adequate factor of safety.

C. Measurement of Survey Plate Surface Pressure and Temperature Distributions

The survey plate was tested at the five test stagnation pressures, at T_o = 225°F and at room temperature. To determine the length of time

necessary for plate surface temperature and Mach number equilibrium, temperature and pressure readings were recorded at 20 minute intervals until temperature equilibrium was reached. Since the heat transfer decreases with mass flow, the length of time for temperature equilibrium at T_o = 225°F increased from approximately two hours at 94.4 psia to five hours at 16.0 psia.

The changes in surface pressures, which were found to occur until equilibrium was reached, were caused by changes in apparent nozzle contours due to the initially greater cooling of the walls and the correspondingly thinner boundary layer, and by the warpage of the structure supporting the nozzle blocks. The survey plate surface pressure and temperature distributions obtained during the hot runs are shown in Figs. 8 to 11, and the chordwise pressure distributions for the cold runs are shown in Fig. 12.

The chordwise pressure distributions plotted in Fig. 8 show the existence of a severe pressure gradient near the plate leading edge, which is unquestionably due to the effect of the boundary layer on the free stream. The pressure gradients observed on the remaining portions of the plate, which became progressively more severe with increasing stagnation pressure, are probably due to gradients existing in the free stream even in the absence of the plate.

The spanwise pressure distributions 2.5" and 5" from the plate leading edge, Figs. 9 and 10, show pressure gradients of opposite sign. These pressure gradients are most probably due to slightly non-parallel nozzle throat boundaries.

The surface temperature distributions for the hot runs are presented

in Fig. 11. The comparison with theoretical predictions, based on the calculations of Young and Janssen (Ref. 16) who obtained a recovery factor of approximately 0.85, shows the experimentally-obtained temperatures to be considerably below the predicted values. This result is somewhat surprising since surface temperature measurements on plates with laminar boundary layers on one surface, but in which heat flow between the two sides is possible, generally give high results due to the effect of the usually turbulent or separated boundary layer on the second side. Two effects which probably contributed to the lowering of surface temperature are losses of heat due to radiation and losses due to heat transfer through the wind shield.

Although a complete set of surface pressure and temperature distributions was taken with the supply air at room temperature, only the chordwise pressure distributions are shown (Fig. 12). Much more severe pressure gradients existed on the plate during the cold runs due to the correspondingly severe non-uniformities in the free stream flow. Large pressure gradients in the free stream are caused by the fact that the nozzle was designed to produce uniform flow when the expansion occurs isentropically. Since the expansion process in flow with condensation is more nearly isothermal than isentropic, nozzle contours designed for condensation free flow must be inappropriate for producing pressure-gradient-free flow with condensation.

It was observed that static pressures on the nozzle blocks and on the plate surface were much less steady in the cold runs than in the hot. It is a well known fact that the static pressure in a high Mach number flow with air condensation is affected, to the first order, by

the amount of condensed air. The observed pressure fluctuations, therefore, probably correspond to comparable fluctuations in the degree of supersaturation prior to the collapse of the isentropic state. The observed plate surface temperature fluctuations are probably due to a similar phenomenon, since plate surface temperatures can be shown also to depend on the amount of condensation (Cf. Section V).

D. Determination of Mach Number and Reynolds Number

The Mach number determined from the equilibrium pressure readings five inches from the plate leading edge are shown in Fig. 6 as a function of stagnation pressure in the reservoir.

Reynolds numbers 5 inches from the plate leading edge, computed from the above values of Mach number and the measured total temperatures, are shown in Fig. 7. The wall Reynolds number, Re_w, is defined by the relationship

$$Re_w = 5in \times \frac{U_\infty}{\nu_w}$$

where the subscripts $(\ )_\infty$ and $(\ )_w$ correspond to free stream and wall conditions, respectively. The free stream Reynolds number, Re_δ, is defined by the relationship

$$Re_\delta = 5in \times \frac{U_\infty}{\nu_\infty}$$

Note that in the following discussion the terms "Reynolds number" and "free stream Reynolds number" are used synonymously, that is,

$$Re = Re_\delta$$

The variation of Mach number with stagnation pressure evident in Fig. 6, which occurs at constant initial throat setting, is due to two principal causes. The predominating effect, which produces increasing Mach numbers with increasing pressures, is the decrease in boundary layer displacement thickness, and the corresponding increase in area ratio, $\frac{A}{A^*}$, with the increasing Reynolds number. This Reynolds number effect is, however, partially compensated for by the opening of the throat due to pressure loads and thermal effects on the nozzle blocks and their supporting structure.

E. Investigation of Boundary Layer Characteristics by Means of the Fluorescent Lacquer Technique

Upon completion of the above measurements of pressure and temperature distribution, the plate boundary layer was studied by means of the fluorescent lacquer technique whereby regions of laminar, turbulent, and separated flow can be distinguished. (Cf. Appendix C).

Two anomalies were observed which were possibly more significant than any other results obtained in this investigation. The first of these was the observed fact that the turbulent wind tunnel side wall boundary layer did not contaminate the laminar plate boundary layer. (Fig. 13a). The second, crudely demonstrated in Fig. 13b, was the fact that not only was the boundary layer still laminar at a Reynolds number of two million, the highest that could be obtained with the present plate, but it was impossible to produce transition even by the severest of the several common transition-producing devices used. The air injection method, which is presently thought to be the most efficient transition-producing

device, (Ref. 17) was not used since the necessary orifices and air manifold could not have been provided without introducing further complications in the plate design. Subsequent tests performed in the GALCIT 5 x 5 in. Hypersonic Wind Tunnel with a plate equipped with air injection orifices corroborated the result that transition of the laminar boundary layer could not be produced at M = 5.8 at Reynolds numbers below 2×10^6.

Existing theories of laminar boundary layer stability (Refs. 18, 19, etc) predict that instability begins at Reynolds numbers of the order of several hundred for insulated flat plates at M = 6. The observed great resistance to transition could be due to one or more of the following reasons:

(1) Error in the theory predicting the Reynolds number at which the boundary layer becomes unstable.

(2) Absence of disturbance frequencies which can be amplified when the instability Reynolds number is reached.

(3) Very long transition region due to the possible long wavelength of frequencies proper for amplification.

(4) Comparatively greater damping of disturbances at the higher Mach numbers.

F. Schlieren Studies of the Plate Leading Edge

To examine the characteristics of the boundary layer and shock wave near the plate leading edge, schlieren photographs were taken of the first half-inch of the plate at all test Reynolds numbers. Unfortunately, the excessive amounts of oil present in the air of the wind tunnel (Leg No. 1), some of which is deposited on the tunnel windows, made schlieren observations extremely difficult. Photographs obtained at stagnation

pressures of 46.9 psia and 94.4 psia are shown in Figs. 14a and 14b. The location of the leading edge of the plate is marked by the symbol "L.E.". (The dark region upstream of the plate leading edge is due to optical diffraction.) The ratio of the height of the dark line characterizing the boundary layer to the distance from the plate leading edge, $\frac{\delta}{x}$, is shown at three stations. Note that the boundary layer assumptions are valid only where $\left(\frac{\delta}{x}\right)^2 \ll 1$. Values of the hypersonic shock wave - boundary layer interaction parameter, $\frac{M^3}{\sqrt{R_e}}$ (Refs. 1, 2, 3, and 4), which is directly related to the hypersonic similarity parameter, $M\Theta$, are marked. For the present test Mach number, $M \approx 6$, note the fact that the shock wave and boundary layer appear definitely separated wherever the boundary layer assumptions hold. The point at which the parameter $\frac{M}{\sqrt{R_e}}$ has the value 1/10 is marked, since that point is considered to be the downstream limit of the region where slip on the plate may occur.

Although the above results can be considered only preliminary, indications are undeniably present that the assumption of the shock forming the outer boundary of the viscous layer (Refs. 1 and 2) is not physically correct at $M \approx 6$, wherever the boundary layer equations are valid. Subsequent more detailed measurements of the leading edge shock wave, boundary layer, and pressure gradient made in a not yet completed series of tests on another plate indicate that the pressure gradients assumed to exist in Refs. 3 and 4 may also be in error. Thus, the fundamental assumptions of both of the two major theories of hypersonic leading edge efforts existing at present cannot be supported by experiment.

G. Installation of the Skin Friction Balance and Plate

Although the plates were designed to be interchangeably mounted

on the windshield and installed without opening the doors, it was finally decided that use of such a complicated procedure was unwarranted. For ease of model installation and final machining of the plate surface, the advantages of opening the doors far outweighed the disadvantages of possible non-repeatability of pressure gradients.

The installation of the balance mechanism and plate proved more difficult than anticipated due to the inaccessibility of the mounting surface, errors in manufacturing, and the existence of leakage into the balance chamber and pressure leads. Considerable time and work were required to locate the source of these difficulties,and some remachining of parts was necessary.

Little difficulty was encountered in aligning the floating element with the plate surface. The original alignment was made within one wave length of green light by the use of an optical flat and a monochromatic light source. The tilt and vertical adjustments shown in Figs. 17b and 17c were used with complete satisfaction.

Photographs of the balance plate installed in the wind tunnel are shown in Fig. 15. The flat plate and skin friction balance in a simulated mounting and associated electronic equipment are shown in Fig. 16.

H. Discussion of Procedural Difficulties

In the initial efforts towards the taking of data three major experimental difficulties were encountered:

(1) The wind tunnel deflections under the existing pressure and thermal stresses were much greater than had been originally estimated. Since

the main internal knife edge allowed free rotation of the internal balance pendulum, and thus assured constant alignment with the terrestial gravitational field, a relative displacement of the element was produced by a slight tilting of sections of the wind tunnel structure. With the balance sensitivity used, motions corresponding to a skin friction force of the order of 100 mg. were possible. Had the magnitude of the wind tunnel motions been correctly anticipated, the magnitude of the equivalent skin friction force could have been easily reduced to an inappreciable value by decreasing or completely removing the main counterweight. Since the wind tunnel deflections were underestimated (on the basis of apparently erroneous accelerometer measurements), a counterweight had been chosen which was as heavy as was reconcilable with the sensitivity of the electronic sensing system and the desired final accuracy. It had been believed that a heavy counterweight was desirable to reduce the possibility of the balance being lifted off its knife edge by the initial pressure differences between the balance chamber and the wind tunnel test section when flow was first established. This occurrence was, however, easily avoided by evacuating the balance chamber during the initial moments of tunnel operation.

For the present experiments it was believed simpler to eliminate the effects of tunnel tilting by using a removable vacuum-tight cover to exclude aerodynamic loads from the element while zeroing the balance.

(2) Efforts, carried out in anticipation of possible difficulties, to reduce the oil content of the air to an inappreciable amount, proved inadequate. The problem of the oil being deposited on the plate surface and flowing into the gaps proved to be the major unsolved

difficulty during the entire period of experimentation. In many instances the oil deposits were so heavy as to make the taking of data impossible. Although the widening of the gaps was considered as an immediate remedy, it was concluded from careful observation of the formation and motion of the oil droplets that gaps larger than .010 in. would be required to appreciably reduce the difficulties caused by the deposited oil. These large gaps would be required because the oil was found to flow into the gaps not as a film but in the form of comparatively large droplets. It was believed that the required large gaps could measurably affect the skin friction force on the floating element and that the use of such gaps should be avoided.

The most satisfactory oil-removing procedure evolved was the simultaneous introduction of atmospheric air into the balance chamber, and utilization of the bow wave from the balance cover to "sweep" the oil off the plate by repeatedly moving the cover towards and away from the plate. The author believes that neither the method used nor the increasing of the gap widths is a satisfactory experimental procedure, and it is strongly recommended that no direct skin friction measurements be undertaken unless the wind tunnel air is sufficiently free from impurities to prevent appreciable deposits on the plate surface.

(3) Upon reduction of the data, it was noted that the pressure gradients obtained from the two static pressure orifices on the balance plate did not duplicate the pressure gradients obtained on the survey plate. Fortunately, the pressure gradients on the balance plate were always less than those obtained on the survey plate, and, in particular, no measurable spanwise pressure gradient appeared to exist. The entirely

different pressure gradients were unquestionably due to differences in nozzle throat height and the exact alignment of the nozzle blocks.

Since no correlation was possible between the pressure distributions on the survey plate and those on the balance plate, the estimation of existing pressure gradients had to be based solely on pressures measured at two stations, one inch from the plate center line, and in the balance chamber. Although spanwise pressure gradients existed on the survey plate, no appreciable pressure differences existed between the balance chamber pressure and the pressure one inch to the side of the element center line. Thus, the assumption that the chordwise pressure gradient along the plate center line was the same as that obtained from the two pressure orifices one inch to the side of the center line appears to be entirely justifiable. On the basis of this assumption, a correction to the measured skin friction coefficients was applied by the method of Ref. 20, which is based on considerations of the von Kármán momentum equation. The corrected and uncorrected skin friction coefficients are shown as a function of Reynolds number in Figs. 21 and 22, and as a function of Mach number in Fig. 23.

IV. DISCUSSION OF SKIN FRICTION RESULTS

The theory of the laminar boundary layer on an insulated flat plate without pressure gradient has been formulated in great detail and is reliable except at very high Mach numbers, at low Reynolds numbers, and whenever various combinations of these two parameters become large (Refs. 1 - 4, 21 - 23, etc.). Reviews of existing laminar theories are available in several sources (Refs. 24, 25, etc.) so that discussion of such general considerations is omitted here.

A summary of the existing theoretical predictions of local skin friction coefficients is shown in Fig. 23. (Refs. 16 and 26 - 32). Each of the authors cited in Fig. 23 carried out solutions of the well known compressible boundary layer equations:

$$\frac{\partial}{\partial x}(\rho u) + \frac{\partial}{\partial y}(\rho v) = 0 \tag{1}$$

$$\rho u \frac{\partial u}{\partial x} + \rho v \frac{\partial u}{\partial x} = \frac{\partial}{\partial y} \mu \frac{\partial u}{\partial y} \tag{2}$$

$$\rho u \frac{\partial}{\partial x} C_p T + \rho v \frac{\partial}{\partial v} C_p T = \frac{\partial}{\partial y}\left(k \frac{\partial T}{\partial y}\right) + \mu \left(\frac{\partial u}{\partial y}\right)^2 \tag{3}$$

All authors cited except Crown (Ref. 27) considered the specific heat to be constant, and all authors except Young and Janssen (Ref. 16) considered the Prandtl number to be constant, although several different numerical values were used.

Van Driest and Gollos (Ref. 32) and Crown (Ref. 27) made comparative calculations to determine the effect of various numerical values of Prandtl number on the laminar skin friction coefficient. The conclusion reached by both of these authors was that, within wide limits, the

choice of the numerical value of Prandtl number is of secondary importance. Thus, the complication of assuming a non-constant Prandtl number does not seem to be warranted if values of skin friction coefficient are to be determined. It is important to note that the choice of Prandtl number affects to a greater degree the heat transfer coefficients and that the use of variable Prandtl numbers may be warranted if calculation of those coefficients is to be carried out.

From results obtained by Crown, it can be concluded that the use of variable specific heats produces only very minor changes in skin friction even at M = 12 with a free stream temperature of 90°R and a change of only 3% at M = 8 with a free stream temperature of 540°R.

The very pronounced spread between the various theoretical predictions of skin friction shown in Fig. 23 must, thus, be principally due to the differences between the assumed variation of viscosity with temperature. A discussion of the relative merit of these various assumptions is presented in Appendix B. It must be noted here, however, that it is concluded that viscosities predicted by the method of Hirschfelder, Bird, and Spotz, (Refs. 33 and 34) are the most reliable at all temperatures. The viscosities of Keyes (Ref. 35) are reliable at temperatures above 270°R, the Sutherland formula is reliable above 360°R, and Crown's assumption, although inaccurate throughout most of the temperature range, leads to values of viscosity which do not deviate from the values predicted by Hirschfelder at temperatures below 200°R as severely as to those obtained by the Sutherland formula. The variation, as a function of temperature, of $\rho\mu$ normalized by the value at T_o = 89.3°R obtained by Hirschfelder, is shown in Fig. 24. To avoid

overcomplication of the presentation, the variation of $\rho\mu$ as predicted by the power law is shown only for two important cases where $\omega = 1$. If the value of $\rho\mu$ is normalized by its value at $T_\infty = 89.3^\circ R$ as predicted by the various methods, the great discrepancies which exist at that low temperature cause a very considerable spread in the values of $\rho\mu$ as functions of temperature.

Laminar skin friction is basically a local phenomenon and thus depends most importantly on the local gas properties. The work of Chapman and Rubesin (Ref. 26) is based principally on this point of view. Comparison between the work of Chapman and Rubesin, in which it is assumed that $\rho\mu$ is constant throughout the boundary layer and has a value determined by the wall conditions, and calculations using the Sutherland formula, in a temperature range where it accurately represents the viscosity-temperature relationship, shows close agreement. This is true even though the Chapman and Rubesin assumption becomes increasingly inaccurate at higher Mach numbers when the temperature range, throughout which the assumption is used, becomes increasingly great.

While it is generally true that in obtaining numerical values of $C_f\sqrt{Re}$ it is progressively more important at higher Mach numbers that the correct viscosity-temperature relationship is assumed, surprisingly great inaccuracies are permissible for comparatively accurate final results. However, if the value of skin friction is to be evaluated from the product $C_f\sqrt{Re}$, or if this product is to be determined from the coefficient C_f, it is, of course, of fundamental importance that the value of viscosity pertinent to the Reynolds number be known to sufficient accuracy. For the hypersonic wind tunnel case, it is, therefore, essential that the free stream viscosity used be that predicted by

Hirschfelder.

Of the nine curves presented in Fig. 23, only in the top three was a free stream temperature of the same order as that which occurred in the present experiments explicitly assumed. Chapman and Rubesin assumed that $\rho\mu = \rho_w\mu_w$. For the present case of no heat transfer of dissociation, Crown's assumption corresponds to

$$\rho\mu = \frac{C}{C_1 + T} \tag{4}$$

where C and C_1 are evaluated at the wall conditions. Young and Janssen used the well-known Sutherland formula.

It appears that the values of Young and Janssen for $T_\infty = 100^\circ R$ are higher, by comparison with those of Chapman and Rubesin and Crown, than can be reconciled by their use of the Sutherland formula (Fig. 24) and a variable Prandtl number. The fact that the zero Mach number value of $C_f\sqrt{Re}$ obtained by these authors differs by several per cent from its well-known value of 0.664 lends credence to the opinion that computational errors occurred in their calculations.

The values obtained by the methods of Chapman and Rubesin and of Crown are very similar at M = 6, since their prediction of $C_f\sqrt{Re}$ differs only by the factor $\left(\frac{\rho_w\mu_w}{\rho_\infty\mu_\infty}\right)^{1/10}$.

Since no calculations exist at the present time in which the compressible boundary layer equations were solved using a viscosity-temperature variation which corresponds to the hypersonic wind tunnel case, arrangements have been made with the REAC group at the Jet Propulsion Laboratory to integrate these equations using the viscosity-temperature relationship of Hirschfelder, Bird, and Spotz. Due to more

urgent requirements of the Jet Propulsion Laboratory, these calculations could not be carried out in time for presentation in this report. Therefore, comparison of the experimental results can, at this time, be made only with theoretical predictions in which viscosity-temperature relationships of various degrees of accuracy were used.

Figs. 21 and 22 show, at a Reynolds number of one million, a $C_f \sqrt{Re}$ of 0.525 and 0.52, respectively. In preparing these diagrams, the eight points believed to have been unaffected by the presence of oil were faired by the method of least squares. During the taking of data, the presence of oil in the gaps was usually evident only by its effect on the value of the skin friction force. Whenever this effect was sufficiently obvious to be indisputable, no data were taken until this condition was corrected.

The results of all force measurements actually carried out are presented in Figs. 21 and 22. The data shown were taken on different days within a total period of more than a month, during which time major components of the balance were removed and reassembled for inspection and repair. The scatter within the eight points used in fairing the curves was obviously of a different order of magnitude than that of the remaining six points. Thus, rejection of the six scattered points appears justifiable on the basis that scatter evidenced by these points can be readily explained by the presence of oil in the gaps.

Figs. 21 and 22 show a trend of increasing $C_f \sqrt{Re}$ with increasing Reynolds number. However, the magnitude of this trend is too slight to be conclusive evidence.

The agreement shown in Fig. 23 between the experimental value of

$C_f\sqrt{Re}$, corresponding to a Reynolds number of one million, and the prediction of Van Driest (Ref. 31) is believed to be a coincidence since the calculations were carried out with an assumption of the viscosity-temperature relationship which was inappropriate for the hypersonic wind tunnel case.

The experimental result, shown in Fig. 23, is approximately 16% below the values of Crown and of Chapman and Rubesin, who used inaccurate simplifying assumptions as to the viscosity-temperature relationship, and approximately 21% below the value of Young and Janssen, which is believed to contain computational errors in addition to the inaccuracies due to the use of the Sutherland equation.

Much thought was given to an estimation of $C_f\sqrt{Re}$ corresponding to a more exact representation of the gas properties. Although no quantitative results could be obtained, it is believed that integration of the boundary layer equations using the correct variation of viscosity with temperature would lead to results close to, and possibly even somewhat higher than, the results obtained by Chapman and Rubesin (Ref. 26) and Crown (Ref. 27).

To reconcile the discrepancies which exist between theoretical prediction and experimental results, the following two possibilities were carefully examined:

(1) Possible Errors in the Experimental Measurements

At the completion of the test program, the thermocouple and Brown potentiometer used to measure total temperature and the stagnation pressure gauge were recalibrated. It is believed that the values of total temperature adopted after the thermocouple recalibration may still

be in error, although this error is not believed to be sufficiently great to significantly affect the comparatively temperature-insensitive skin friction measurements. Evidence that an error in total temperature measurement may still exist is the discrepancy between the measured survey plate surface temperatures and those predicted by Young and Janssen.

The skin friction balance mechanism operated satisfactorily during the entire period of data-taking. An oscillograph record of a typical laminar skin friction measurement is shown in Fig. 20. Note the steadiness of the force readings and the comparatively small drift as a function of time. It is estimated that the balance reading accuracy was $\pm$ 2 mg. or $\pm$ 5.7% and $\pm$ 1.7% of the minimum and maximum force readings, respectively.

Although it is difficult to quantitatively estimate the effect of the presence of the gaps and the minute element and plate misalignments on the force measurements, these effects are believed to be comparatively small.

To determine the values of the skin friction coefficients from the measurements of skin friction force, it is necessary to compute values of the dynamic pressure, $\overline{q}$, from measurements of static pressure, p, and reservoir pressure, p_o. The maximum manometer reading error corresponds to errors in p of $\pm$ 3.6% and $\pm$ .8% for the lowest and highest test Reynolds numbers, respectively. The maximum error in stagnation pressure, principally due to instrument calibration error, is believed to be less than $\pm$ 1%. Due to the combined effects of errors in static and stagnation pressure, errors in dynamic pressure of approximately $\pm$ 3% and $\pm$ 1% are possible at the lowest and highest test Reynolds

numbers, respectively.

The errors in Mach number corresponding to the combined maximum possible errors in p and p_o are 0.5% and 0.25%, at the lowest and highest test Reynolds number, respectively.

In the present Mach number range, the errors in Reynolds number are due almost entirely to errors in viscosity. In the present temperature range the free stream viscosity varies as $T^{0.4}$ (Cf. Table I). For an uncertainty in T_o of 2%, the $\sqrt{Re}$, which is the important parameter in the present case, varies by only 0.4%.

Note that the combined effects of all of the possible instrument errors could change the computed values of $C_f \sqrt{Re}$ by $\pm$ 9% and $\pm$ 3%, at the lowest and highest Reynolds numbers, respectively. Therefore, neither the scatter in the data nor their low value with respect to the available theoretical predictions can, to any appreciable extent, be reconciled by instrument error.

It is believed that the widely-scattered data points were probably taken with oil present in the gaps and should be rejected on those grounds. It is further believed that the comparatively low values of $C_f \sqrt{Re}$ obtained can be reconciled in the manner discussed below.

(2) Possible Errors in the Theoretical Predictions

In addition to a careful estimation of the effects of using inexact physical constants, results of which were discussed above, the appropriateness of the usual solutions of the boundary layer equations was examined. The effects of slip flow (Refs. 21, 22, etc.) and of the shock wave - boundary layer interaction at the plate leading edge (Refs. 1, 2, 3, and 4) were considered on the bases of existing theories. With

respect to both phenomena, existing theories predict appreciable effects only for limited regions of the plate near the leading edge, that is, where $\frac{M}{\sqrt{Re}}$ and $\frac{M^3}{\sqrt{Re}}$ are of order one. The schlieren photographs of the first half-inch of the flat plate, shown in Fig. 14, indicate the comparatively small fraction of the plate which falls, in the present case, within the limits imposed by the theories mentioned.

The effect of shock wave - boundary layer interaction near the leading edge is to increase the local skin friction coefficient in the region where an appreciable pressure gradient is produced by the interaction. Although the magnitude of this increase differs in Refs. 1, 2, and 3, it is difficult to dispute the contention that such an increase exists. However, it appears that the assumed or implied assumption that at the end of the interaction region the skin friction coefficient reaches the value predicted by classical theory is open to question.

It is unquestionably true that the increased skin friction at the leading edge necessitates, by the von Kármán momentum theorem, an increased mass flow into the viscous layer and a corresponding thickening of the boundary layer. Thus, the "normal" boundary layer, which is to start at the end of the shock wave - boundary layer interaction region, starts with an initially greater thickness than that predicted by classical theory. If the very plausible assumption is now made that the velocity distribution within the boundary layer very quickly approaches the classical distribution, then it is evident that at a given station the similarity parameter $C_f \sqrt{Re_{\delta^*}}$, where Re_{δ^*} is the Reynolds number based on the displacement thickness, requires that the value of C_f, and correspondingly $C_f \sqrt{Re}$, be lower than that predicted

from classical theory.

It is believed that the above qualitative justification of the experimentally obtained low skin friction coefficient is entirely plausible and warrants further careful theoretical and experimental verification.

V. THE BOUNDARY LAYER IN A TWO-PHASE FLUID

It would be of considerable practical interest if experimental data obtained in hypersonic wind tunnels with two-phase flow could be used to predict the properties of the hypersonic boundary layer in condensation-free flow. The extent to which correlation is possible is discussed below.

Note that it has been shown in Refs. 5, 6, 7, and 8 that severe deviations from the isentropic, Prandtl-Meyer type of flow occur even with the presence of only a slight amount of condensed air, and it is thus questionable whether experimental studies, in a two-phase fluid, of the important hypersonic shock wave-boundary layer interaction problems can be directly correlated with the corresponding condensation-free case. In the following analysis it will be assumed that in the region under consideration $\frac{M^3}{\sqrt{Re}} \ll 1$, so that the effect of the self-induced pressure gradient can be neglected.

It is immediately apparent that if ρ is defined to be the fluid density and if it is assumed that the condensed particles move with the mass velocity $\vec{q}$, then the continuity and momentum equations take the same form in the two-phase case as in the case without condensation.

To derive the applicable energy equation, note that the proper equations of state are

$$p = \rho_v RT \tag{1a}$$

or

$$p = \rho(1-g)RT \tag{1b}$$

and the enthalpy of fluid and vapor can be written as

$$h = h_L g + h_v (1-g) \tag{2a}$$

But

$$h_L = (h_v - L) \tag{3}$$

so that

$$h = C_p T - Lg \tag{2b}$$

The internal energy is, in terms of the enthalpy,

$$e = h - \frac{p}{\rho} \tag{4a}$$

so that

$$e = C_v T - g(L + RT) \tag{4b}$$

In the above equations, the subscript $(\ )_v$ denotes the properties of the vapor, L is the latent heat of vaporization per unit mass, g is the mass fraction of fluid condensed, and p, R, T, C_p, and C_v are the thermodynamic properties of the vapor.

The effect of the presence of condensed air on the viscosity of the droplet-vapor mixture can be evaluated by means of the Brownian movement law of Einstein and von Smoluchowski.

Einstein deduced the equation

$$\frac{\mu}{\mu_v} = 1 + 2.5n\left(\frac{4}{3}\pi a^3\right) \tag{5}$$

where n is the number of droplets per unit volume and a is the droplet radius. (This equation in conjunction with that for the diffusion coefficient can be used to determine Avogardo's number.) But n is of the order of

$$\frac{gN}{\left(\frac{a}{r}\right)^3}$$

where N is the number of molecules per cubic centimeter and r the molecular radius. Thus, under the worst practical conditions of test section pressure and temperature

$$2.5n\left(\tfrac{4}{3}\pi a^3\right) = O\left(10^{-3}\right)$$

so that the assumption that the viscosity depends on the state of the vapor only introduces, at worst, an error of 1/10 of 1%. It is of interest to note that in Einstein's equation the correction of viscosity due to the presence of condensed air droplets is proportional to the volume fraction of condensed air and is, therefore, small even for comparatively large values of the mass fraction of condensed air, g. Since the mechanisms of molecular momentum transfer and of molecular energy transfer are very similar, it can be assumed by analogy that the heat transfer coefficient, k, which represents the molecular energy transfer, is also only slightly affected by the presence of condensation. On making the further assumption that the transport properties μ and k are independent of fluid density, it can be concluded that the viscosity and heat transfer coefficients of the mixture of vapor and droplets are, to the present accuracy, only functions of the vapor temperature.

The general energy equation can now be written by analogy with the uncondensed case:

$$\rho\frac{Dh}{Dt} - \rho\frac{D(Lg)}{Dt} - \frac{Dp}{Dt} = \operatorname{div}(k\,\operatorname{grad} T) + \Phi + \rho Q \qquad (6)$$

where Φ is the dissipation as generally defined and Q the heat added per unit mass.

For the case of steady flow without pressure gradient, the usual boundary layer assumptions lead to the following equations of motion:

$$\frac{\partial}{\partial x}(\rho u) + \frac{\partial}{\partial Y}(\rho v) = 0 \tag{7}$$

$$\rho u \frac{\partial u}{\partial x} + \rho v \frac{\partial u}{\partial Y} = \frac{\partial}{\partial Y}\left(\mu \frac{\partial u}{\partial Y}\right) \tag{8}$$

$$\rho u \frac{\partial}{\partial x}(C_p T - Lg) + \rho v \frac{\partial}{\partial Y}(C_p T - Lg) = \frac{\partial}{\partial Y}\left(k \frac{\partial T}{\partial Y}\right) + \mu\left(\frac{\partial u}{\partial Y}\right)^2 \tag{9}$$

The relationship between viscosity and temperature which best represents the physical situation without introducing great computational difficulties is that suggested by Chapman and Rubesin (Ref. 26)

$$\frac{\mu}{\mu_\infty} = C \frac{T}{T_\infty} \tag{10}$$

where C is selected to give the correct value of μ_w. Since the viscosity of a two-phase fluid is very closely approximated by the viscosity of the vapor component, no more severe assumption is made in the present case than is usual. A similar assumption about the heat transfer coefficients and the usual assumption of constant C_p imply that Prandtl number is constant.

Unfortunately, however, the assumed temperature-viscosity relationship is not sufficient to allow the derivation of a momentum equation independent of the energy equation unless in the case of a two-phase fluid, it is instead assumed that the product of density and viscosity remains constant.

$$\rho\mu = C\rho_\infty \mu_\infty \tag{11a}$$

The comparative validity of this assumption for the present case can be evaluated in the following manner. The assumption

$$\frac{\mu}{\mu_\infty} = C\frac{T}{T_\infty} \tag{10}$$

in the two-phase case leads to

$$\frac{\rho\mu}{\rho_\infty\mu_\infty} = C\left[\frac{1-g_\infty}{1-g}\right] \tag{12}$$

so that the assumption $\rho\mu = C\rho_\infty\mu_\infty$ may be more severe in the present case by the factor g_∞ . Note, however, that at area ratios corresponding to Mach number six (and $T_o = 540^\circ R$), the temperature range throughout which the assumption $\rho\mu$ = constant is required to hold is considerably smaller in the case with condensation than without. This fact more than compensates for the comparative error of possible magnitude g_∞ .

By introducing the Von Mises transformation

$$u = \frac{\rho_\infty}{\rho}\frac{\partial\psi}{\partial y} \quad , \quad v = -\frac{\rho_\infty}{\rho}\frac{\partial\psi}{\partial x} \tag{13}$$

only the momentum and energy equations need be considered since the continuity equation is satisfied identically.

$$\frac{\partial u}{\partial x} = \frac{\mu_\infty}{\rho_\infty}\frac{\partial}{\partial\psi}\left(Cu\frac{\partial u}{\partial y}\right) \tag{14a}$$

$$\frac{\partial T}{\partial x} - \frac{L}{C_p}\frac{\partial g}{\partial x} = \frac{\mu_\infty}{Pr\,\rho_\infty}\frac{\partial}{\partial\psi}\left(Cu\frac{\partial T}{\partial\psi}\right) + \frac{\mu_\infty}{C_p\rho_\infty}Cu\left(\frac{\partial u}{\partial\psi}\right)^2 \tag{15a}$$

Note that the only term in the above two equations which differs from the usual case without condensation is that expressing the enthalpy change in the energy equation. For the sake of further simplification, dimensionless variables are now introduced.

$$u^* = \frac{u}{U_\infty} \qquad x^* = \frac{x}{X}$$

$$T_\infty = \frac{T}{T_\infty} \qquad \rho^* = \frac{\rho}{\rho_\infty} \tag{16a}$$

$$\mu^* = \frac{\mu}{\mu_\infty} \qquad \psi^* = \frac{\psi}{\sqrt{2\rho_\infty U_\infty X C}}$$

Using these variables, the equations of motion become

$$\frac{\partial u^*}{\partial x^*} = \frac{\partial}{\partial \psi^*}\left(u^* \frac{\partial u^*}{\partial \psi^*}\right) \tag{14b}$$

$$\frac{\partial T^*}{\partial x^*} - \frac{L}{C_p T_\infty}\frac{\partial g}{\partial x^*} = \frac{1}{P_r}\frac{\partial}{\partial \psi^*}\left(u^* \frac{\partial T^*}{\partial \psi^*}\right) + \frac{U_\infty^2}{C_p T_\infty} u^* \left(\frac{\partial u^*}{\partial \psi^*}\right)^2 \tag{15b}$$

The factor $\frac{U_\infty^{*2}}{C_p T_\infty}$ multiplying the viscous dissipation term which becomes $(\gamma-1)M_\infty^2$ in the case without condensation will not at this point be related to a Mach number, since the introduction of a speed of sound introduces unnecessary conceptual difficulties. The boundary conditions relevant to the above equations for the case without heat transfer at the wall are

$$u^* = 0 \quad \text{at} \quad \psi^* = 0 \quad (\gamma = 0)$$

$$u^* = 0 \quad \text{at} \quad \psi^* = \infty \quad (\gamma = \infty)$$

$$T^* = T_w^* \quad \text{at} \quad \psi^* = 0 \tag{16b}$$

$$T^* = 1 \quad \text{at} \quad \psi^* = \infty$$

$$g = g_\infty \quad \text{at} \quad \psi^* = \infty$$

Note that none of these boundary conditions is a function of x^* if it is assumed that g_∞ is constant. Following the procedure of Chapman and Rubesin, introducing

$$u^* = \frac{1}{2} f'(\eta) \tag{17}$$

where η is defined by

$$f(\eta) = \frac{\psi^*}{\sqrt{x^*}} \tag{18}$$

reduces the momentum equation to the well-known Blasius equation, with the boundary conditions

$$\begin{aligned} f'(\infty) &= 2 \\ f'(0) &= f(0) = 0 \end{aligned} \tag{19}$$

Since complete tables of the functions f, f', and f'' can be found in many references (Ref. 37, for example), the solution of the momentum equation is known as a function of $\frac{\psi^*}{\sqrt{x^*}}$.

Solution of the energy equation can now be undertaken by substituting

$$u^* = \frac{1}{2} f'(\eta) \tag{17}$$

and changing the independent variables from x^*, ψ^* to x^*, η. In this manner the energy equation becomes

$$\frac{\partial^2 T^*}{\partial \eta^2} + (P_r) f \frac{\partial T^*}{\partial \eta} - 2(P_r) f' x^* \frac{\partial T^*}{\partial x^*} + (P_r) f \frac{L}{C_p T_\infty} \frac{\partial g}{\partial \eta} \tag{20a}$$

$$- 2(P_r) f' x^* \frac{\partial g}{\partial x^*} \frac{L}{C_p T_\infty} = - \frac{P_r}{4} \frac{U_\infty^2}{C_p T_\infty} (f'')^2$$

with the boundary conditions

$$T^*(x^*,0) = T_w^*$$

$$T^*(x^*,\infty) = 1$$

$$g(x^*,\infty) = g_\infty \qquad (21a)$$

$$g(x^*,0) = 0$$

Since these boundary conditions are independent of x^*, solutions of the equation of the form $T^*(\eta)$ and $g(\eta)$ can be made to satisfy the boundary condition. Thus, only solutions of the equation

$$\frac{\partial^2 T^*}{\partial \eta^2} + (Pr) f \frac{\partial T^*}{\partial \eta} + (Pr) f \frac{L}{C_p T_\infty} \frac{\partial g}{\partial \eta} = -\frac{Pr}{4} \frac{U_\infty^2}{C_p T_\infty} (f'')^2 \qquad (20b)$$

need be considered.

Although no mention of the fact has to this point been made, it is obvious that the equations discussed so far are inadequate to provide a solution to the problem of the boundary layer in a two-phase fluid. Another equation involving the mass fraction of condensed air, g, as well as the space and state variables, must be supplied to solve the problem within the assumptions already made.

Unfortunately, however, derivation of an additional equation involving the mass fraction of condensed air, g, is difficult. The crux of the difficulties lies in the fact that while T* is a thermodynamic property which depends only on the state of the fluid and thus is a point function, the quantity, g, in addition to depending on the state of the fluid, depends on the thermodynamic process. The equation

$$p = (1-g)\rho RT \qquad (1b)$$

is therefore not an equation of state in the usual sense but really is

an equation combining the equation of state of the vapor

$$p = \rho_v RT \tag{1a}$$

with the equation describing the indestructibility of mass

$$\rho_v = (1-g)\rho \tag{22}$$

In all fluid mechanics problems involving two-phase fluids the most powerful simplifying assumption which can be made is that in which it is assumed that the process takes place at equilibrium. In the present case, the assumption of thermodynamic equilibrium leads immediately to a model in which the boundary layer consists of a sublayer defined by the nonexistence of condensation and a layer in which condensation is still present.

Since the assumption of thermodynamic equilibrium in general applies only to conditions "in the large" and does not rule out the occurrence of random deviations, the possibility of liquid air droplets impinging upon the plate surface must be considered. It is difficult to estimate quantitatively the probability of droplet collisions with the plate surface since this probability depends on two largely unknown phenomena, the degree of superheating possible and the distribution of random droplet velocities (which is a function of droplet size distribution). However, it is possible to judge intuitively that since equilibrium reevaporation occurs far from the plate surface in terms of the coordinate $\frac{\psi^*}{\sqrt{x^*}}$, only an extremely small number of unevaporated droplets can reach the plate.

The mean momentum of the droplets is the same as that of the vapor, so that collisions of droplets with the plate must leave the skin

friction unaffected. However, due to the great heat capacity of droplets, a relatively small number of droplets could measurably affect the heat transfer from the plate. The validity of neglecting droplet collisions with the plate in heat transfer calculations must be verified by experimentation.

It is apparent that in the condensation-free sublayer, the mass fraction of condensed air, g, and all its derivatives are zero so that the energy equation reduces to its usual form

$$\frac{\partial^2 T^*}{\partial \eta^2} + (Pr) f \frac{\partial T^*}{\partial \eta} = -\frac{Pr}{4} \frac{U_\infty^2}{C_p T_\infty} (f'')^2 \qquad (20c)$$

with the boundary conditions

$$\begin{aligned} T^*(x^*, 0) &= T_w^* \\ T^*(x^*, \eta_s) &= T_s^*(x^*, \eta_s) \end{aligned} \qquad (21b)$$

where the subscript $(\ )_s$ denotes the conditions on the surface of the condensation-free sublayer. However, the assumptions of similarity

$$\frac{\partial T^*}{\partial x^*} = \frac{\partial g}{\partial x^*} = 0 \qquad (23)$$

imply that the coordinates of the boundary are $\eta = \eta_s$ = constant, so that the boundary condition on that surface reduces to

$$T^*(x^*, \eta_s) = T^*(\eta_s) = T_s^* \qquad (21c)$$

The value of T_s^* must be matched with that obtained from a solution applicable in the layer with condensation.

In the condensation region the assumption of isothermal droplet reevaporation can be made with a high degree of accuracy, the errors being only those produced by differences between droplet and vapor

temperatures (surface tension effect) (Ref. 6). Thus, in this layer, the energy equation becomes

$$\frac{\partial g}{\partial \eta} = -\frac{U_\infty^2}{4L}\frac{(f'')^2}{f} \tag{20d}$$

with the boundary conditions

$$\begin{aligned} g(\eta) &= 0 \\ g(\infty) &= g_\infty \end{aligned} \tag{21d}$$

Fortunately, this energy equation can be integrated since f and f'' are known values of η.

$$g_\infty = \frac{U_\infty^2}{4L}\int_\infty^{\eta_s}\frac{(f'')^2}{f}\,d\eta = \frac{U_\infty^2}{4L}S(\eta_s) \tag{24}$$

Since the quantity $\frac{4L}{U_\infty^2}g_\infty$ is known, $S(\eta_s)$ and from it η_s can be determined. The boundary conditions on the surface $\eta_s, T_s = 1$, and the location of the surface are now determined as functions of the free stream conditions, and the solution of the energy equation for the condensation-free sublayer is readily obtainable.

The energy equation under consideration

$$\frac{\partial^2 T^*}{\partial \eta^2} + (P_r) f \frac{\partial T^*}{\partial \eta} = -\frac{P_r}{4}\frac{U_\infty^2}{C_p T_\infty}(f'')^2 \tag{20c}$$

is identical to that considered by Chapman and Rubesin except for the boundary conditions, and similar to one considered by Pohlhausen. By analogy with solutions obtained in Ref. 26 and Ref. 37 the solution to the present problem can be written

$$T^*(\eta) = a(\eta_s) + \frac{U_\infty^2}{2C_p T_\infty} r(\eta) + a_0 Y_0(\eta) \tag{25a}$$

where

$$r(\eta) = \frac{Pr}{2} \int_{\eta}^{\infty} [f''(\xi)]^{Pr} \int_{0}^{\xi} [f''(\theta)]^{2-Pr} d\theta \, d\xi \tag{26}$$

and $Y_o(\eta)$ is the solution of the homogeneous equation. The function was evaluated by numerical integration and has been plotted by Chapman and Rubesin. The constants a_o and $a(\eta_s)$ can be determined by simultaneous solution of the equations

$$\begin{aligned} T_w^* &= a(\eta_s) + \frac{U_\infty^2}{2C_p T_\infty} r(0) + a_o Y_o(0) \\ 1 &= a(\eta_s) + \frac{U_\infty^2}{2C_p T_\infty} r(\eta_s) + a_o Y_o(\eta_s) \end{aligned} \tag{25b}$$

where

$$Y_o(0) = 1$$

and

$$r(0) = 1$$

for Pr = 0.72. Thus, the adiabatic wall temperature is

$$T_{we}^* = a_e(\eta_s) + \frac{U_\infty^2}{2C_p T_\infty} 0.845 \qquad \text{for Pr = 0.72} \tag{25c}$$

Values of $a_e(\eta_s)$, for $T_o = 540^\circ R$, are shown in Fig. 26.

The skin friction and heat transfer for the case of a two-phase fluid can now be evaluated. The shear stress in the boundary layer is

$$\tau = \mu \frac{\partial u}{\partial y} \tag{27a}$$

or in terms of η,

$$\tau = \frac{\mu_\infty}{4} f''(\eta) U_\infty^2 \frac{C}{\sqrt{\nu U_\infty X}} \tag{27b}$$

Thus, at the wall, $\eta = 0$,

$$\tau_w = \frac{\mu_\infty}{4} f''(0) U_\infty^2 \sqrt{\frac{C_w}{\nu_\infty U_\infty X}} \tag{27c}$$

and

$$C_f = \frac{\tau_w}{q} = \frac{1}{2} f''(0) \sqrt{C_w} \frac{1}{\sqrt{\frac{U_\infty X}{\nu_\infty}}} \tag{28}$$

But since, $f''(0) = 1.328$, the relationship

$$C_f \sqrt{Re} = 0.664 \sqrt{C_w} \tag{29}$$

identical to that for the single-phase case is obtained. Note, however, that C_w must be evaluated from conditions given by the non-viscous saturated expansion relationships (Ref. 6) and a specified wall temperature.

The heat transferred from a unit area per unit time at a given point is given by

$$q = -k \left(\frac{\partial T}{\partial Y} \right)_w \tag{30a}$$

or in terms of the η coordinates, from Eq.

$$q = -\frac{k_\infty T_\infty}{2} C_w \sqrt{\frac{U_\infty}{\nu_\infty X C_w}} \left[\frac{U_\infty^2}{2 C_p T_\infty} r'(0) - a_0 Y_0'(0) \right] \tag{30b}$$

But,

$$r'(0) = 0$$

and from Ref. 26

$$Y_0'(0) = -0.5915$$

so that

$$q = -\frac{k_\infty T_\infty}{2}\sqrt{\frac{U_\infty C_w}{\nu_\infty X}}\,(0.5915) \tag{30c}$$

If the heat transfer coefficient is defined by the equation

$$h = -\frac{q}{T_w - T_{we}} \tag{31a}$$

then, by substituting for T_w , T_{we} , and q , the relationship

$$h = -0.5919\,\frac{k_\infty}{2}\sqrt{\frac{U_\infty C_w}{\nu_\infty X}} \tag{31b}$$

is obtained. If the local Nusselt number is defined to be

$$Nu = \frac{hX}{k_\infty} \tag{32a}$$

the relationship

$$Nu = -\frac{0.5915}{2}\sqrt{C_w}\sqrt{R_e} \tag{32b}$$

is obtained. Note that the expression for q, h, and Nu are identical in form for the cases with and without condensation. Again proper consideration must be taken of the free stream temperature and the value of for the condensation case.

The most important practical comparison between boundary layer properties with and without condensation is that which expresses the differences between the local skin friction, τ_w , and the differences between the local heat transfer, q, for specified values of $\frac{\overline{q}}{p_o}$, p_o , and T_o . Since $\frac{\overline{q}}{T_o}$, to the present approximation, depends only on the geometrical configuration $\frac{A}{A^*}$, such a comparison demonstrates the error introduced by assuming the expansion in a given wind tunnel nozzle to occur isentropically.

Thus, since the dynamic pressure, $\overline{q}$, is held constant, for the

insulated plate

$$\frac{\tau_c}{\tau_o} = \frac{C_{fc}}{C_{fo}} \tag{33a}$$

Substituting into the expression

$$C_f\sqrt{Re} = 0.664\sqrt{C_w} \tag{29}$$

the relationship

$$\frac{\tau_c}{\tau_o} = \frac{C_{fc}}{C_{fo}} = \sqrt{\frac{(C_w)_c}{(C_w)_o}} \tag{33b}$$

is obtained. But

$$C_w = \frac{\rho_w \mu_w}{\rho_\infty \mu_\infty} \tag{11b}$$

and

$$\frac{2q}{\rho_\infty} = U_\infty^2 \tag{34}$$

so that

$$\frac{\tau_c}{\tau_o} = \frac{C_{fc}}{C_{fo}} = \left[\frac{(\rho_\infty)_o}{(\rho_\infty)_c}\right]^{\frac{3}{4}} \sqrt{\frac{(\rho_w \mu_w)_c}{(\rho_w \mu_w)_o}} \tag{33c}$$

The ratio $\frac{C_{fc}}{C_{fo}}$ was computed for $T_o = 540^\circ R$ and Mach numbers, $M\left(\frac{A}{A^*}\right)$, from 5 to 10. It was found that within this Mach number range the present theory predicted an effect of less than 1% on the local skin friction coefficient. Thus, it is indicated that values of local skin friction coefficients obtained in flow with air condensation may be correlated directly with condensation-free values, whenever leading edge effects are negligible.

Direct measurements of the viscous shear force on the floating element were undertaken at a stagnation temperature of approximately $540^\circ R$, a Mach number (based on area ratio) of approximately 5.6, and

stagnation pressures of 94.4 psia and 46.9 psia. The experimental difficulties introduced by the presence of oil in the air stream were much more severe in these cold runs than had been previously encountered. Even the most drastic methods for cleaning the oil out of the gaps between the floating element and the plate proved to be only marginally effective due to the comparatively high viscosity of the oil at the low plate surface temperatures.

The measurements obtained resulted in local skin friction coefficients 6% and 11% higher than the values predicted by the present theory for the higher and lower Reynolds number, respectively, on the basis of the measurements made at stagnation temperatures of approximately 225°F (Fig. 21).

Although these experimental results are in closer agreement with the theoretical predictions of Chapman and Rubesin (Ref. 26) and Crown (Ref. 27) than the values presented in Figs. 21 and 22, this agreement is not believed to be significant since the theoretical predictions of Refs. 26 and 27 are believed to be inappropriate for the present range of Mach numbers and Reynolds numbers.

In addition to the inaccuracies of the present theory for skin friction in a two-phase fluid, three principal factors are believed to account for the differences between the results obtained from the cold and hot runs:

(1) A very severe pressure gradient existed on the plate during the cold runs (Fig. 12).

(2) Oil may have been present in the gaps while measurements were being taken.

(3) The effect of the thickening of the leading edge boundary believed to measurably affect the local skin friction coefficients was altered to an unpredicted extent by the presence of condensation.

For specified plate temperatures, the ratio of heat transfer with condensation heat transfer without condensation becomes, if the Prandtl number is assumed to be the same in the two cases,

$$\frac{q_c}{q_o} = \frac{(\mu_\infty T_\infty)_c}{(\mu_\infty T_\infty)_o} \frac{(C_w)_c}{(C_w)_o} \frac{(T_w - T_{w_e})_c}{(T_w - T_{w_e})_o} \frac{C_{f_o}}{C_{f_c}} \tag{35}$$

In the above expression (Eq. 35) the primary effect of the presence of condensation is the modification of the adiabatic wall temperature, T_{w_e}. Since $(T_{w_e})_c$ changes to the first order with changes in the amount of condensed air, g, the degree of supersaturation becomes of first order in importance in determining the heat transfer from a plate in two-phase flow. Since the degree of supersaturation cannot, in general, be predicted accurately enough for low temperature potentials, correlation between heat transfer coefficients obtained in two-phase flow cannot, in general, be made with condensation free values.

VI. CONCLUSION

In addition to the development of experimental techniques applicable to the study of boundary layer characteristics in hypersonic wind tunnels operating at high stagnation temperatures, the present investigation provided the following evidence as to the behavior of the laminar boundary layer at a Mach number of 5.8:

(1a) It was observed that the natural boundary layer transition occurred at much higher Reynolds numbers than had been anticipated. Further, even with the most severe methods used, transition could not be forced at a Reynolds number of two million. The present experiments give the first experimental indication of this vitally important phenomenon.

(1b) A significant property of the transition phenomenon is the observed inability of the wind tunnel sidewall turbulent boundary layer to contaminate the flat plate laminar boundary layer and produce transition in a region bounded by the usual contamination angle.

(2) Evidence was obtained that at M = 5.8 the assumption that the shock wave forms the boundary of the viscous layer does not correspond to the physical facts in regions sufficiently far from the plate leading edge for the boundary layer assumptions to hold.

(3) The measurements of the local laminar skin friction produced the extremely important result that existing theories considerably overestimate the magnitude of the local viscous shear force at Mach numbers and Reynolds numbers corresponding to those reached in the present investigation. A value of 0.52 was obtained for $C_f \sqrt{Re}$.

(4) A theory was developed for the laminar boundary layer in a

two-phase fluid, on the basis of which it was concluded that measurements of laminar skin friction can be correlated with condensation-free values (whenever leading edge effects are unimportant) and that heat transfer coefficients and recovery factors obtained in two-phase flow cannot be correlated reliably with condensation-free values due to the unpredictability of the degree of supersaturation.

REFERENCES

1. Shen, S. F., "Hypersonic Flow Over an Insulated Wedge with Viscosity Effects," Part I of an Sc. D. Dissertation, Department of Aeronautical Engineering, Massachusetts Institute of Technology, 1949.

2. Li, T. Y. and Nagamatsu, H. T., "Shock Wave Effects on the Laminar Skin Friction of an Insulated Flat Plate at Hypersonic Speeds," Contract No. DA-04-495-Ord-19, Memorandum No. 9 (GALCIT), July 1, 1952.

3. Lees, L. and Probstein, F., "Hypersonic Viscous Flow over a Flat Plate," April 20, 1952, Aeronautical Engineering Laboratory Report, Princeton University, No. 195.

4. Lees, L., "On the Boundary-Layer Equations in Hypersonic Flow and Their Approximate Solutions," Journal of the Aeronautical Sciences, Volume 20, No. 2, p. 143, February 1953.

5. Nagamatsu, H. T. and Willmarth, W. W., "Condensation of Nitrogen in a Hypersonic Nozzle," Memorandum No. 6, California Institute of Technology, Contract No. DA-04-495-Ord-19, Sponsored by Army Ordnance and Air Force, January 15, 1952.

6. Buhler, R. D., "Condensation of Air Components in Hypersonic Wind Tunnels -- Theoretical Calculations and Comparison with Experiment," Dissertation in Partial Fulfillment of the Requirements for the Degree of Doctor of Philosophy, California Institute of Technology, June 1952. Republished as Memorandum No. 13, Contract No. DA-04-495-Ord-19, Sponsored by Army Ordnance and Air Force, December 1, 1952.

7. Arthur, P. D., "Effect of Impurities on the Supersaturation of Nitrogen in a Hypersonic Nozzle," Dissertation in Partial Fulfillment of the Requirements for the Degree of Doctor of Philosophy, California Institute of Technology, June 1952. Republished as Memorandum No. 7, Contract No. DA-04-495-Ord-19, Sponsored by Army Ordnance and Air Force, February 15, 1952.

8. Grey, J., "The Effect of Air Condensation on Properties of Flow and Their Measurement in Hypersonic Wind Tunnels," Dissertation in Partial Fulfillment of the Requirements for the Degree of Doctor of Philosophy, California Institute of Technology, June 1952. Republished as Memorandum No. 8, Contract No. DA-04-495-Ord-19, Sponsored by Army Ordnance and Air Force, June 15, 1952.

9. Dhawan, S., "Direct Measurement of Skin Friction," Dissertation in Partial Fulfillment of the Requirements for the degree of Doctor of Philosophy, California Institute of Technology, June 1951. Republished as NACA TN 2567, January 1952.

10. Coles, D., "Measurements in the Boundary Layer on a Smooth Flat Plate in Supersonic Flow," Dissertation in Partial Fulfillment of the Requirements for the Degree of Doctor of Philosophy, California Institute of Technology, June 1953.

11. Häkkinen, R. J., "Measurements of Skin Friction in Turbulent Boundary Layers at Transonic Speeds," Dissertation in Partial Fulfillment of the Requirements of the Degree of Doctor of Philosophy, California Institute of Technology, June 1953.

12. Wilson, R. E., Young, E. C., and Thompson, M. J., "2nd Interim Report on Experimentally Determined Turbulent Boundary Layer Characteristics at Supersonic Speeds," DRI/JT Report CM-501, DRL-196, January 25, 1949.

13. Urbach, F., Nail, N. R., and Pearlman, D., "The Observation of Temperature Distributions and of Thermal Radiation by Means of Non-Linear Phosphors," Journal of the Optical Society of America, Volume 39, Number 12, p. 1011, December 1949.

14. Stalder, R. and Slack, G., "The Use of the Luminescent Lacquer for the Visual Indication of Boundary Layer Transition," NACA TN 2263, 1951.

15. Schaevitz, H., "The Linear Variable Differential Transformer," Proceedings of the Society for Experimental Stress Analysis, Vol. 4, No. 2, p. 79, 1947.

16. Young, B. W. and Janssen, E., "The Compressible Boundary Layer," The RAND Corporation, p. 214, June 1, 1951.

17. Fage, A. and Sargent, R. F., "An Air-Injection Method of Fixing Transition from Laminar to Turbulent Flow in a Boundary Layer," ARC, R & M 2106, June 1944.

18. Lin, C. C., "On the Stability of Two-Dimensional Parallel Flows," Part I - General Theory, Quarterly of Applied Mathematics, Vol. III, No. 2, July 1945, Part II - Stability in an Inviscid Fluid, Quarterly of Applied Mathematics, Vol. III, No. 3, October 1945, Part III - Stability in a Viscous Fluid, Quarterly of Applied Mathematics, Vol. III, No. 4, January 1946.

19. Lees, L. and Lin, C. C., "Investigation of the Stability of the Laminar Boundary Layer in a Compressible Fluid," NACA TN No. 1115, 1946.

20. Bertram, M. H., "An Approximate Method for Determining the Displacement Effects and Viscous Drag of Laminar Boundary Layers in Two-Dimensional Hypersonic Flow," NACA TN 2773, September 1952.

21. Maslen, H., "Second Approximation to Laminar Compressible Boundary Layer on Flat Plate in Slip Flow," NACA TN 2818, November 1952.

22. Nonweiler, T., "The Laminar Boundary Layer in Slip Flow," The College of Aeronautics, Cranfield, Report No. 62, November 1952.

23. Tsien, H. S., "Superaerodynamics, Mechanics of Rarefied Gases," Journal of the Aeronautical Sciences, Volume 13, No. 12, p. 653, December 1946.

24. Kuerty, G., "The Laminar Boundary Layer in Compressible Fluids," Advances in Applied Mechanics, Vol. 11, Edited by Mises, R. von and Kármán, Th. von, 1951.

25. Lewis, J. A. (under the supervision of G. F. Carries), "Boundary Layer in Compressible Fluids," Tech. Dept. No. F-TR-1179-ND, 1948.

26. Chapman, D. R. and Rubesin, M. W., "Temperature and Velocity Profiles in the Compressible Laminar Boundary Layer with Arbitrary Distribution of Surface Temperature," Journal of the Aeronautical Sciences, Vol. 16, No. 9, p. 547, September 1949.

27. Crown, J. C., "The Laminar Boundary Layer at Hypersonic Speeds," United States Naval Ordnance Laboratory, White Oak, Maryland, NAVORD Report 2299, April 15, 1952.

28. Kármán , Th. von, "The Problem of Resistance in Compressible Fluids," V Convego della Foundazione Allessandro Volta (Tema: Le Alte Velocita in Aviazione), Reale Accademia D'Italia, Rome, 1935.

29. Hantzsche, W. and Wendt, H., "Die Laminare Grenzschicht der Ebenen Platte Mit und Ohne Wärmeübergang Unter Berücksichtigung der Kompressibilität," Jahrbuch der Deutschen Luftfahrtforschung, 1942.

30. Kármán, Th. von and Tsien, H. S., "Boundary Layer in Compressible Fluids," Journal of the Aeronautical Sciences, Vol. 5, No. 6, p. 227, April 1938.

31. Van Driest, E. R., "Investigation of the Laminar Boundary Layer in Compressible Fluids Using the Crocco Method," North American Aviation, Inc., Aerophysics Laboratory, Report AL-1183, January 9, 1951.

32. Van Driest, E. R. and Gollos, W. W., "On the Methods of Solution of the Laminar Boundary-Layer Equations," Project Bumblebee, North American Aviation, Inc., Aerophysics Laboratory, Report CM-614 (AL-1044), May 23, 1950.

33. Hirschfelder, J. O., Bird, R. B., and Spotz, E. L., "Viscosity and Other Physical Properties of Gases and Gas Mixtures," Transactions of the American Society of Mechanical Engineers, p. 921, November 1949.

34. Bromley, L. A. and Wilke, C. R., "Viscosity Behavior of Gases," Industrial and Engineering Chemistry, Vol. 43, p. 1641, July 1951.

35. Keyes, F. G., "The Heat Conductivity, Viscosity, Specific Heat, and Prandtl Numbers for Thirteen Gases," Massachusetts Institute of Technology, PROJECT SQUID Technical Report 37, April 1, 1952.

36. Pohlhausen, E., Der Wärmeaustausch Zwischen Festen Körpern und Flüssigkeiten mit Kleiner Reibung und Kleiner Wärmeleitung, Z.A.M.M., Bd. 1, p. 115, 1921.

37. Goetz, A., et al., "Early Detection of Bacterial Growth", Final Report to the Chemical Corps, U. S. Army, 1951.

Goetz, A., "Application of Molecular Filter Membranes to the Analysis of Aerosols", American Journal of Public Health, Vol. 43, No. 2, p. 150, February 1953.

38. Chapman, S. and Cowling, T. G., "Mathematical Theory of Non-Uniform Gases," Cambridge University Press, 1939.

APPENDIX A

EXPERIMENTAL FACILITIES

The GALCIT 5 x 5" Hypersonic Wind Tunnel is of the continuous type, that is, air is continually recirculated through the compressor plant and test section. The compressor plant employed to operate the wind tunnel consists of eleven positive displacement pumps driven by seven electric motors (Fig. 2). The nine compressors employed in the lower stages of compression are of the rotary type (Fuller Company). In the final stage of compression two double acting reciprocating compressors (Ingersoll-Rand Company) may be used. The rotary compressors were selected because of their immediate availability and because of their ability to operate at the necessary high compression ratios.

The intricate system of piping and valves interconnecting the various pumps permits operation under a wide variety of conditions of total compression ratio and mass flow. By the aligning of all the compressors into a single stage of compression, sufficient mass flow is available for operation at Mach numbers below two, while the arrangement into six stages can supply compression ratios greater than a thousand, permitting operation at Mach numbers greater than ten.

Since the nozzle block throat width cannot be varied, the test section Mach number, and, as a consequence thereof, the compression ratio necessary to maintain the specified Mach number flow are determined primarily by the throat height. The required compression ratio determines, in turn, the minimum number of stages necessary, while the required volume flow determines the maximum possible number of stages of compression. Selection of a

test section Mach number, therefore, implies definite limitations in reservoir pressure. It is important to note that model size and configuration play an important, and sometimes dominating, part in determining the minimum allowable supply air pressure.

The use of rotary pumps has the considerable advantage of providing increasing compression ratios with decreasing mass flow so that wind tunnel and compressor plant characteristics inherently have the same trend. Unfortunately, however, the liquid seal required between the floating vanes and the housing inevitably introduces oil into the air stream in considerable quantity and necessitates extensive oil removal methods. By far the largest amount of oil is removed by coagulation and settling in the piping and pressure vessels. In the second most effective method of oil removal centrifugal separators are employed, in which coagulation and settling are accelerated due to a centrifugal force field produced by a forced rotary motion of the air stream. The third, and not completely successful, method of oil removal employed in the original wind tunnel configuration utilizes eight high pressure cannisters containing approximately 250 pounds of activated charcoal (burnt cocoanut), which has little effect on removing oil in the form of droplets from the air stream.

Since these oil removal methods proved very inadequate, an extensive investigation of possible filtering methods was undertaken, as a result of which it was decided to utilize the 36-in. diameter settling tank for housing various filtering media. Partly for this purpose, the tank was moved from its location immediately upstream of the throat to a point upstream of the heat exchangers. The first, and

at present only, filtering equipment installed in the tank consists of two layers of one-inch thick sheets of sintered coke and a sheet of a "molecular" filter paper recently developed for bacteriological sampling (Ref. 37). Although these additional filtering methods reduced the amount of oil in the wind tunnel air stream, quantities which were prohibitive for some purposes continued to settle on the model surfaces and on the wind tunnel doors and windows. Concerted efforts are now being made to provide additional oil removal equipment.

The air is dried by continuously circulating it through a tank containing approximately two thousand pounds of silica gel. Under normal operation, the water content of the air can by this method be easily kept well below one part in a hundred-thousand (by volume). The dryer reactivation cycle takes less than 15 hours so that regular over-night reactivation is possible.

The Leg No. 1 wind tunnel air heating system consists of eight finned copper heat exchangers energized by saturated steam at $\approx 350^{\circ}F$ provided by the Institute's central boiler plant. Steam superheaters capable of increasing the steam temperature to $550^{\circ}F$ are also provided. However, since the maximum steam rate is at present determined by the feed water pumping system, the possible increased steam temperature produces a decrease in steam flow rate which almost nullifies the effectiveness of the superheating system. Installation of equipment assuring more efficient use of the existing steam superheaters has been undertaken.

A water-cooled heat exchanger is used to cool the wind tunnel air before it reenters the compressor system.

Two systems of suitably valved piping duct the air output from the compressor plant and heaters located in the sub-basement to the basement of the Guggenheim Aeronautical Laboratory Building in which the wind tunnel and its associated instrumentation are located. Sixteen-inch piping capable of withstanding pressures below 250 psi is used for comparatively large volume flow operations, while the much smaller high pressure piping can be used at pressures as high as 1000 psi. Two valves located, respectively, immediately upstream and downstream of the nozzle block-diffuser section permit channeling of all of the compressor air through suitable bypass piping and thus allow opening of the wind tunnel doors without interference with the operation of the compressor plant.

The supply air pressure is indicated on the Tate-Emery Load Indicator (Baldwin-Southwark) shown at the left of Fig. 1a. The supply air temperature is recorded by means of the "Speedomax" (Leeds and Northrup) two-range, 20-point recorder (Fig. 1a, upper right), which also records other pertinent temperatures throughout the installation as selected by means of the two patchboxes shown in the lower right corner of Fig. 1a. The supply air temperature is also indicated on the air-operated "Electronic" potentiometer controller (Minneapolis-Honeywell) which is used for supply air temperature control (Fig. 1a, center, right). The temperature controller determines the dome loading on two diaphragm valves which control, respectively, the fraction of air bypassed around the heat exchangers and the steam flow rate into the heat exchangers. By means of this controller, the temperature reading of the thermocouple closest to the nozzle throat can be maintained

constant to within less than $\frac{1}{2}^{\circ}$F. The supply air pressure is controlled by means of a "Air-o-line" flow controller (Minneapolis-Honeywell) with a sensitivity of 1/10-in. of water pressure, which determines the rate of high pressure air leakage through an exhaust valve (Fig. 1a, upper left of control console).

The dew point meter, shown near the center of Fig. 1a, utilizes a polished chromium plated brass button, the surface of which can be cooled by means of a jet of carbon dioxide. The dew point temperature is determined by measuring the temperature at which fogging of the polished button occurs.

In addition to the pressure controller and dew point meter already discussed, the console shown in Fig. 1a contains motor and motorized valve controls, compressor pressure and pressure-ratio gauges, controls for the pneumatic bypass, intake, and exhaust valves, and motor current and power meters.

The contour, downstream of the inflection point, of the M = 6 nozzle was designed by the Foelsch method. The throat region, which has a specified radius of curvature of .67 in., was connected to the inflection point by a quintic to obtain a continuous variation of curvature throughout the whole nozzle length. Both nozzle blocks are provided with 18 static pressure orifices located at integral inches from the throat along the center line. The downstream 16 orifices of the upper nozzle block are connected to the left hand pair of banks of the silicone oil* manometer shown at the right of Fig. 1b.

---

* DC 200 silicone oil with a kinematic viscosity of 10 centistokes and a specific gravity of approximately 0.94 is used.

Model pressures are indicated on the remaining two banks of the silicone manometer, on a single tube mercury micromanometer, or on a simple 20-tube mercury manometer (not shown). The reference vacuum pressure is measured by means of the "Alphatron" (National Research Corporation) shown at the bottom center of Fig. 1b. Model temperatures are indicated on the two Brown potentiometers shown at the left and in the center of Fig. 1b. Seventy-two thermocouples can be connected to these instruments at one time.

Model controls are provided which allow the model to be rotated about a line parallel to the tunnel axis, moved along the tunnel axis, moved vertically, or pitched. Remote model controls and position-indicating counters are provided.

The schlieren system consists of the following: an air-cooled, high pressure mercury arc light source (B-H6, General Electric Company); a two-lense collimating and focusing system; a light-masking slip; a small, flat, first-surface, folding mirror; two 8-in. diameter, 120-in. focal length, first-surface, spherical mirrors; two traversable 10-in. diameter, flat, first surface mirrors arranged in a "Z"; an "iris" shutter; a knife edge at the focal point of the second spherical mirror which can be used to cut off adjustable fractions of the light in the vertical or horizontal planes; a second small, flat, first-surface, folding mirror; and a ground glass viewing screen in front of which film holders can be introduced when desired. Any portion of the nozzle block - diffuser section located between the glass-ports can be brought into view by traversing the large flat mirrors. The location of the knife edge and image planes can be varied when required.

APPENDIX B

VISCOSITY-TEMPERATURE RELATIONSHIPS

In general, the viscosity of a gas is a point function of the state of the gas, so that knowledge of pressure, temperature, and density is necessary and sufficient for a precise determination of its value. However, since the state variables are related by an equation of state, knowledge of any two of the state variables uniquely determines the viscosity of a specified gas. Unfortunately, the exact functional relationships between viscosity and the state variables are extremely complicated. Thus, approximations to these exact relationships are necessary if solutions of differential equations involving both the viscosity and the state variables are to be obtained. Fortunately, the regimes of most frequent interest in fluid mechanics are those in which pressures which are high compared with the critical pressure (37.2 atmospheres for air) are accompanied by temperatures which are high compared with the critical temperature (238.1°R for air). Low temperatures usually occur with low pressures. In both of these instances, pressure effects on the coefficient of viscosity are negligible, and it is, therefore, usually possible to consider viscosity to be a function of temperature only. The additional assumptions as to the variation of viscosity with temperature usually employed in boundary layer theory will be discussed below in the order of decreasing accuracy.

The best available predictions of the coefficients of viscosity of gases as functions of temperature are those based on the theory of Hirschfelder, Bird, and Spotz (Refs. 33 and 34), in which it is assumed

that the gas consists of non-polar, smooth, spherical molecules. Chapman and Cowling (Ref. 38) developed an equation for the coefficient of viscosity of a single gas by means of a rigorous treatment of the kinetic theory of gases (based on the work of Chapman, Enskog, Pidduck, and others), which, in the notation of Ref. 34, becomes

$$\mu\left[\frac{\text{slugs}}{\text{ft sec}}\right] = 5.573\times10^{-6}\left[\frac{1}{(r_o)^2}\sqrt{\frac{M\epsilon}{k}}\right]\left[\left(\frac{5}{9}\,\frac{kT}{\epsilon}\right)^{\frac{1}{2}}\frac{V}{W^2(2)}\right] \quad \text{(B-1a)}$$

where M is the molecular weight, T is the temperature in degrees R, r_o is the low energy collision diameter expressed in angstroms, V and $W^2(2)$ are slowly varying functions of $(5/9\,\frac{k}{\epsilon}T)$, k is the Boltzmann constant in ergs/^oK, and ϵ is related to the interaction potential between two molecules, E(r), by the equation

$$E(r) = 4\epsilon\left[-\left(\frac{r_o}{r}\right)^6 + \left(\frac{r_o}{r}\right)^{12}\right] \quad \text{(B-2)}$$

in which r is the distance between molecules. The viscosity of a gas thus depends on only two parameters: (1) ϵ, the maximum energy of attraction (2) r_o, the low-velocity collision diameter, which must at the present time be determined from measurements of viscosity, second virial coefficients, or diffusion at two temperatures, or estimated from such properties as the critical temperature and density, the volume of the liquid, boiling point, etc. The above expression for the viscosity can, for convenience, be rewritten in a form in which the effects of the temperature and of the inherent gas properties are clearly separated.

$$\mu\left[\frac{\text{slugs}}{\text{ft sec}}\right] = 5.573\times10^{6}\left[\frac{1}{(r_o)^2}\sqrt{\frac{M\epsilon}{k}}\right] f\left(\frac{5}{9}\frac{kT}{\epsilon}\right) \qquad \text{(B-1b)}$$

where

$$f\left(\frac{5}{9}\frac{kT}{\epsilon}\right) = \left(\frac{5}{9}\frac{kT}{\epsilon}\right)^{1/2}\frac{V}{W^2(2)} \qquad \text{(B-3)}$$

and

$$\frac{1}{r_o^2}\sqrt{\frac{M\epsilon}{k}} = 97^\circ K \quad \text{for air}$$

For values of ϵ and r_o determined in Ref. 33, the values of $\frac{1}{r_o^2}\sqrt{\frac{M\epsilon}{k}}$ and $f\left(\frac{5}{9}\frac{kT}{\epsilon}\right)$ were determined and tabulated in Ref. 34. Note that the viscosities of a given gas at two temperatures are related by the equation

$$\frac{\mu_2}{\mu_1} = \frac{f\left(\frac{5}{9}\frac{kT_2}{\epsilon}\right)}{f\left(\frac{5}{9}\frac{kT_1}{\epsilon}\right)} \qquad \text{(B-4)}$$

An accurate and more convenient relationship between temperature and viscosity determined by Keyes (Ref. 35) has the following three constant emperical form:

$$\mu = \frac{a_o\sqrt{T}}{1 + \frac{a_1}{T}10^{-a_1/T}} \qquad \text{(B-5)}$$

The constants a, a_o, a_1 must be determined from experimental measurements of viscosity. For air, Keyes' equation becomes

$$\mu\left[\frac{\text{slugs}}{\text{ft sec}}\right] = 2.316\times10^{-10}\frac{\sqrt{T}}{1 + \frac{219.8}{T}10^{-\frac{219.8}{T}}} \qquad \text{(B-6)}$$

Although Keyes states that the above equation for the viscosity of air

is valid only above 142°R, it can be used with reasonable accuracy at lower temperatures. For example, at 90°R Keyes' equation predicts a viscosity which is only 2.7% higher than the more correct value predicted by Hirschfelder, Bird, and Spotz. It is of interest to note that for polar gases an empirical equation of the Keyes' type may actually be more reliable. For example, while Keyes' equation allows accurate extrapolation of values of the viscosity of CO_2 to temperatures of the order of 1800°R, extrapolation by the method of Hirschfelder, Bird, and Spotz leads to viscosity values 3% higher than the experimentally-determined ones.

The well-known Sutherland equation

$$\mu = k_s \frac{\sqrt{T}}{1 + \frac{S}{T}} \tag{B-7}$$

accurately predicts viscosity variation for limited temperature ranges. If the values of the viscosity and the rates of change of viscosity predicted by the Sutherland formula are equated to values obtained by Hirschfelder, Bird, and Spotz, values of the Sutherland temperature, S, appropriate at each base temperature can be determined. Values of S obtained in Ref. 33 and values of k_s and $\frac{k_s}{k_{s_{400°R}}}$ computed from these are tabulated in Table I. The Sutherland formula is often also written in the form:

$$\mu = \mu_B \left(\frac{T}{T_B}\right)^{\frac{1}{2}} \frac{1 + \Theta}{1 + \frac{\Theta}{T_B}} \tag{B-8a}$$

or

$$\mu = \frac{\mu_B}{\sqrt{T_B}} (1 + \Theta) \frac{\sqrt{T}}{1 + \frac{\Theta T_B}{T}} \tag{B-8b}$$

The quantities k_s and S are thus

$$k_s = \frac{\mu_B}{\sqrt{T_B}}(1+\Theta) \tag{B-9}$$

and

$$S = \Theta T_B \tag{B-10}$$

If a base temperature, T_B, is selected and k_s considered truly constant, it is possible only to equate values of viscosity or its derivative to those obtained by Hirschfelder, Bird, and Spotz. The values of the Sutherland constants, Θ , obtained by equating the viscosity for $T_B = 400^{\circ}R$ are also tabulated in Table I.

The similarity in form between Sutherland's and Keyes' equations is quite apparent since Keyes' equation can be written

$$\mu = a_o \frac{\sqrt{T}}{1 + \frac{\Sigma(T)}{T}} \tag{B-11}$$

where

$$\Sigma(T) = a 10^{-a/T} \tag{B-12}$$

Values of $\Sigma(T)$ are tabulated in Table I.

Crown (Ref. 27) proposed a relationship between the viscosity of the gas and the enthalpy in the viscous laminar boundary-layer involving conditions at the point of highest enthalpy. For the case of no heat transfer from the wall and no condensation or dissociation of the gas, the enthalpy is highest at the wall. Crown's relationship can then be stated to be

$$\mu = \frac{C_o}{1 + \frac{C_1}{T}} \tag{B-13}$$

where

$$C_0 = \mu_w \left[\frac{\frac{T_w}{T_\infty} - 1}{\frac{\mu_\infty}{\mu_w}\frac{T_w}{T_\infty} - 1} \right] \tag{B-14}$$

and

$$C_1 = T_\infty \left[\frac{\frac{T_w}{T_\infty} - 1}{\frac{\mu_\infty}{\mu_w}\frac{T_w}{T_\infty} - 1} - 1 \right] \tag{B-15}$$

This equation is generally less reliable than the Sutherland formula. By means of Crown's relationship, the boundary layer momentum equation can be made explicitly independent of the free stream Mach number, a result which can otherwise be obtained only by more inaccurate temperature viscosity relationships.

The viscosity-temperature relationship of most limited accuracy in the regimes of fluid mechanics which are of general interest can be written

$$\mu = s' T^{\omega'} \tag{B-16}$$

By matching the value of the coefficient of viscosity and its first derivative with respect to temperature obtained by means of the above relationship with that obtained by the method of Hirschfelder, Bird, and Spotz, the value of ω', correct at a specified temperature, can be obtained. Values of ω' computed in Ref. 33 are retabulated in Table I. By assuming $s' = s$ to be constant and to have the value determined for $T = 540^\circ R$, values of ω satisfying the equation

$$\mu = s T^{\omega} \tag{B-17}$$

can be obtained (Cf. Table I).

APPENDIX C

DETECTION OF BOUNDARY LAYER TRANSITION IN HYPERSONIC WIND TUNNELS

Stalder and Slack (Ref. 14) developed a method for distinguishing between regions of laminar and turbulent boundary layers by means of lacquers which fluoresce when dry. Due to the much faster drying of the lacquer in regions of turbulence, those regions can be readily distinguished from the laminar ones. The lacquers developed in Ref. 14 were found to dry much too fast to be useful at the conditions of high velocity, high temperature, and low pressure which occur in the GALCIT Hypersonic Wind Tunnel, Leg No. 1.

As a result of extensive efforts undertaken to extend the method of Stalder and Slack to conditions existing in the Hypersonic Wind Tunnel at $M \approx 6$ and $T_o \approx 225^{\circ}F$, two satisfactory lacquers were developed.

Lacquer base: 50% T - 1400 dye mixture (Vogel Luminescense Corp. San Francisco)

50% solvent:

10% ethanol

10% butanol

10% ethyl cellosolve

50% butyl carbitol

20% plasticizer

The following drying times, corresponding to the two plasticizers used, were observed:

Reservoir Pressure (psia)	Turbulent Drying Times (Minutes)	
	Dibutyl Phthalate	Dibutyl Sebacate
34.4	8 - 10	20
54.4	5 - 5	10 - 12
74.4	1 - 3	9 - 11
94.4		7 - 9

TABLE I

CONSTANTS APPEARING IN VISCOSITY EQUATIONS

50	26.0			145	.845		
75	59.6	.5651	.4082	166.5	.939	.07382	.3354
100	95.5	.6163	.4452	178.0	.993	.07216	.4222
125	132.9	.8310	.4631	186.2	1.018	.07609	.4845
150	165	.9306	.4710	191.2	1.018	.08753	.5319
175	177.1	.9649	.4747	195.1	1.003	.1063	.5689
200	183.6	.9818	.4767	198.4	.981	.1319	.5987
250	188.5	.9955	.4762	233.8	.935	.2007	.6442
300	190.5	1.000	.4754	210.0	.890	.2970	.6771
350	189.7	.9991	.4751	205.8	.852	.4161	.7023
400	190.0	1.000	.4748	207.2	.822	.5504	.7223
450	191.7	1.003	.4741	209.7	.797	.7006	.7388
500	192.0	1.004	.4736	211.0	.777	.8589	.7525
600	193.2	1.005	.4732	213.0	.743	1.222	.7744
700	196.7	1.009	.4714	213.5	.719	1.606	.7914
800	205.6	1.019	.4670	212.0	.703	1.977	.8050
900	217.8	1.031	.4619	207.0	.693	2.314	.8163

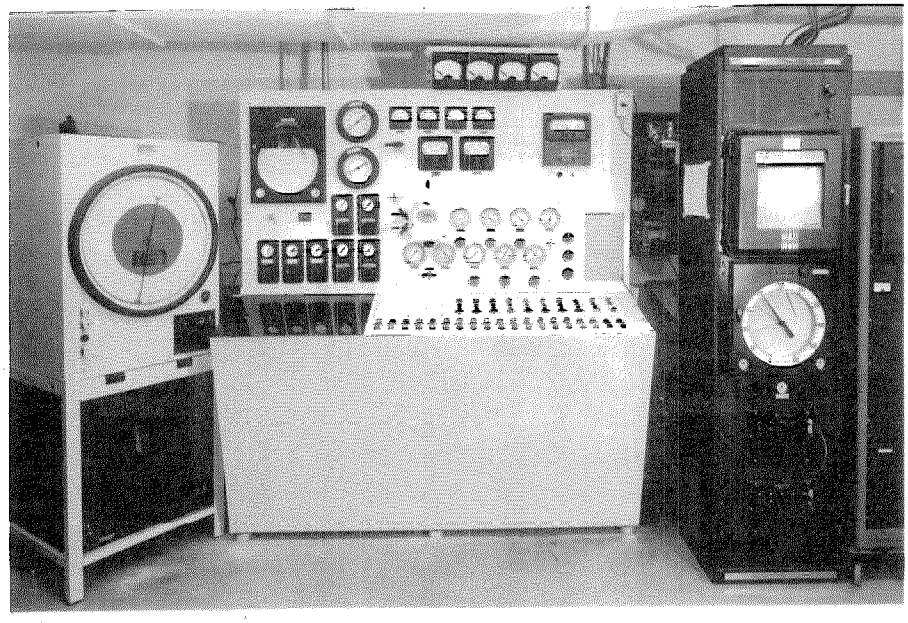

Compressor Plant Motor and Valve Controls
Reservoir Pressure and Temperature Regulators
Plant Pressure and Temperature Indicators

Fig. 1a

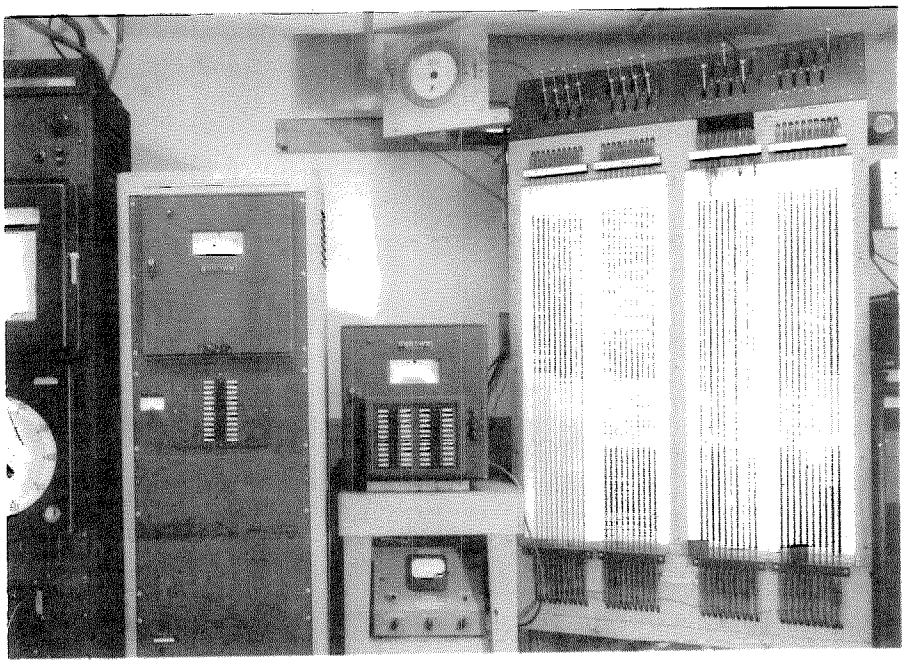

Test Section and Nozzle Block
Pressure and Temperature Instrumentation

Fig. 1b

GALCIT 5 x 5 IN. HYPERSONIC WIND TUNNEL
CONTROLS AND INSTRUMENTATION

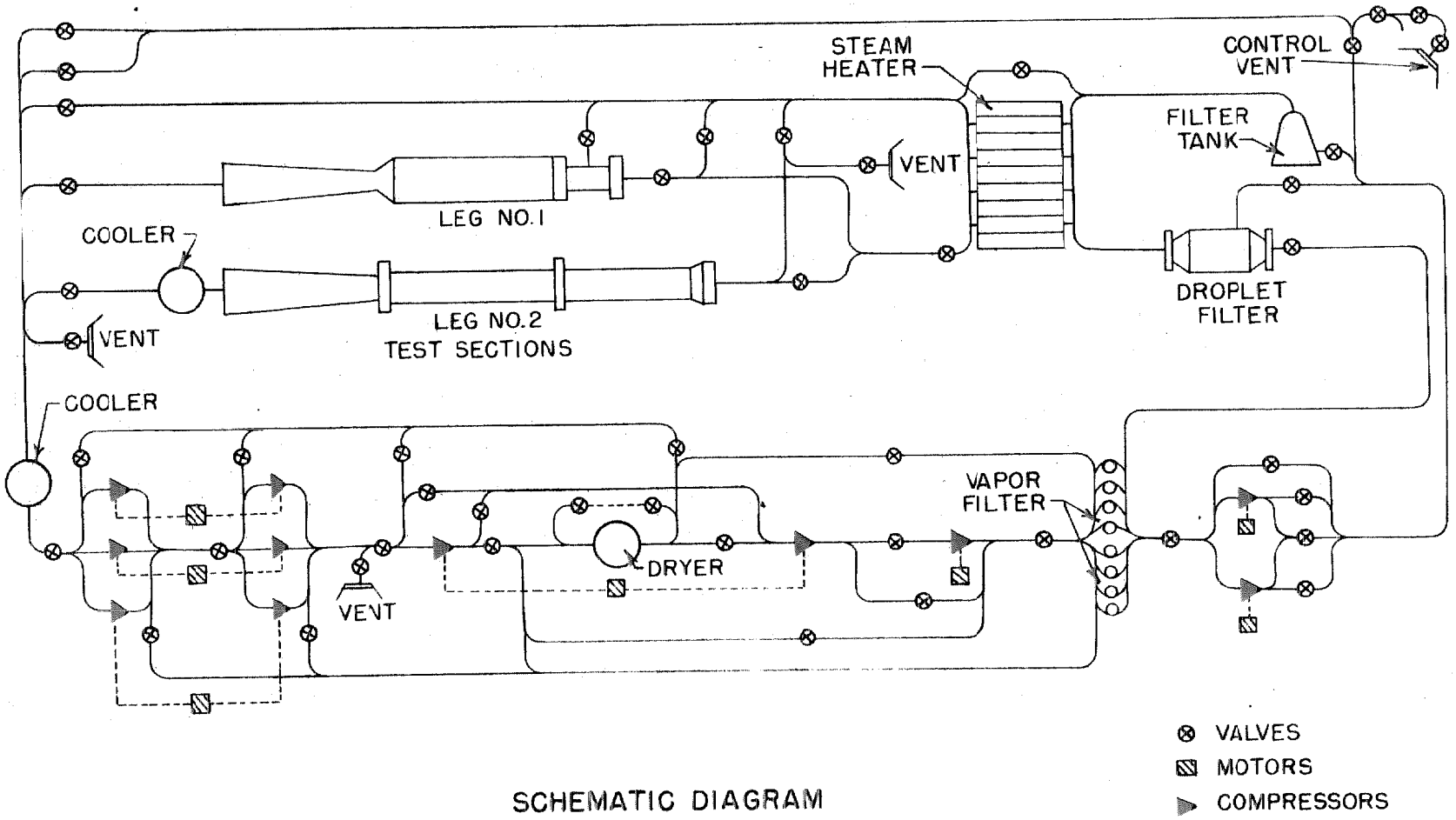

SCHEMATIC DIAGRAM

OF GALCIT 5x5in. HYPERSONIC WIND TUNNEL INSTALLATION

FIG.2

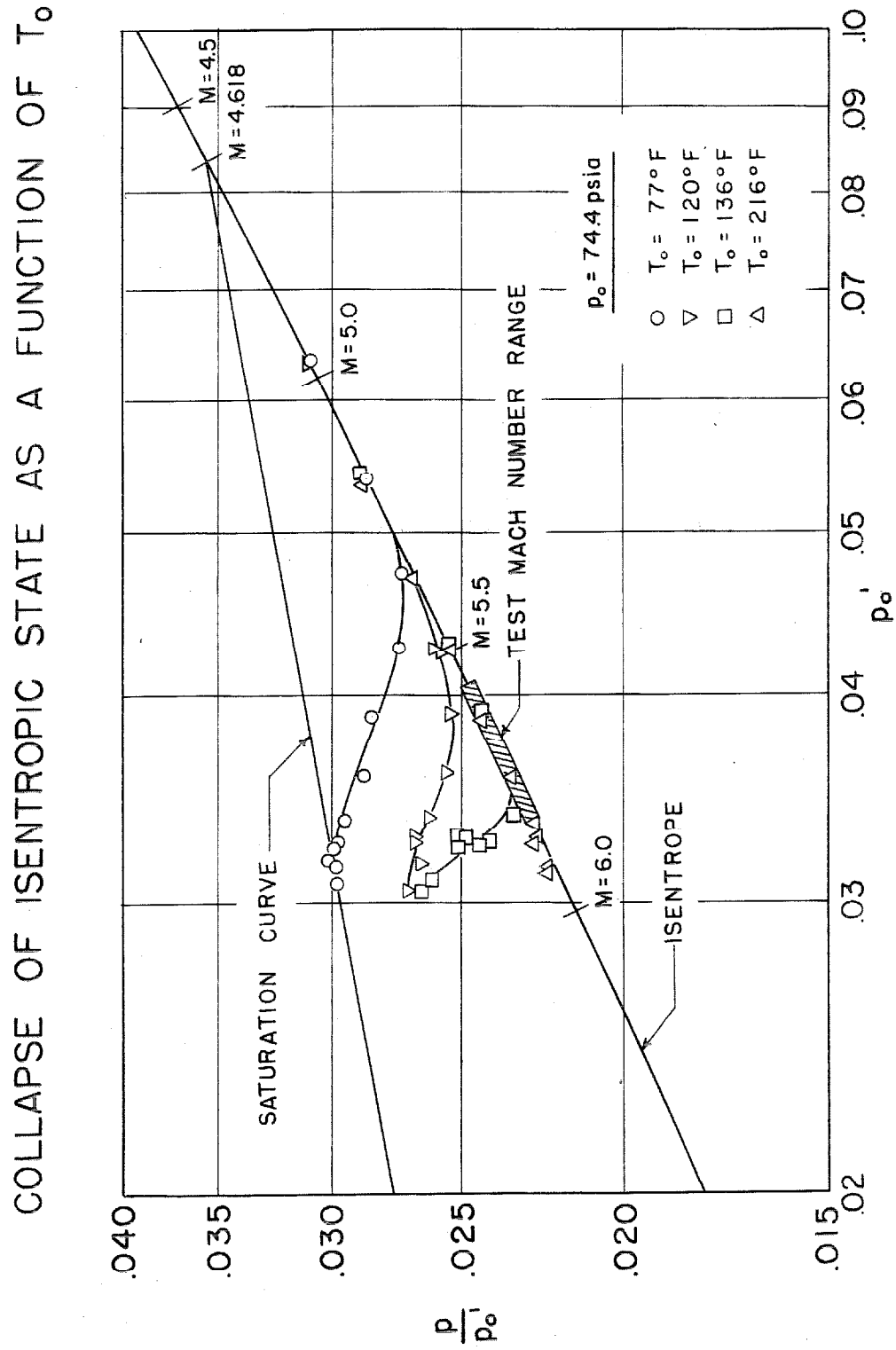
COLLAPSE OF ISENTROPIC STATE AS A FUNCTION OF T_o
$\frac{p}{p_o'}$
$\frac{p_o'}{p_o}$
.040
.035
.030
.025
.020
.015
.02
.03
.04
.05
.06
.07
.08
.09
.10
M=4.5
M=4.618
M=5.0
M=5.5
M=6.0
SATURATION CURVE
ISENTROPE
TEST MACH NUMBER RANGE
p_o = 74.4 psia
T_o = 77°F
T_o = 120°F
T_o = 136°F
T_o = 216°F

FIG. 3

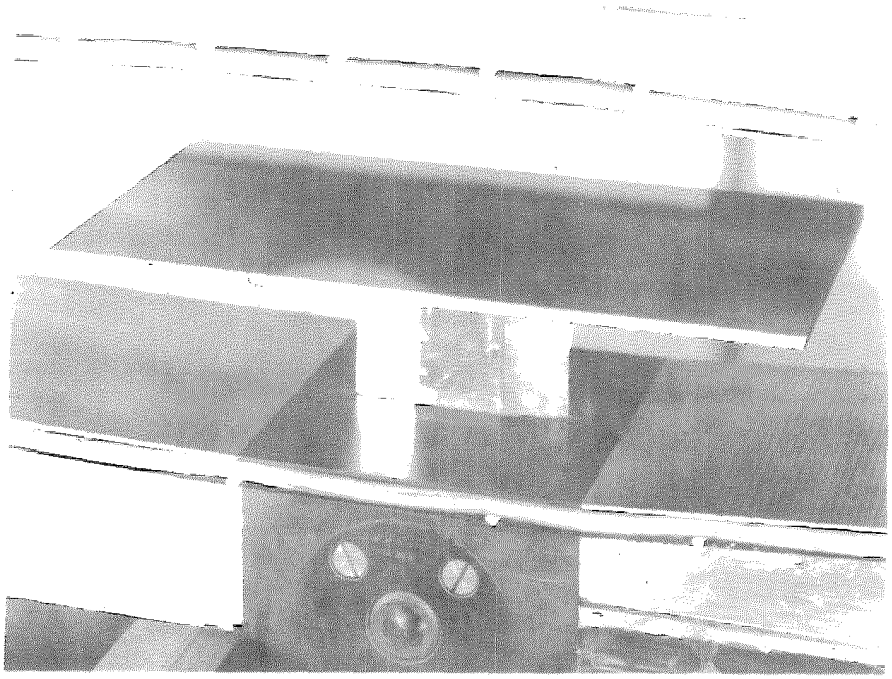

5 x 10in. Plate Used for Determination of
Pressure and Temperature Distribution
Installed in 5 x 5 in. Hypersonic Wind Tunnel

Fig. 4

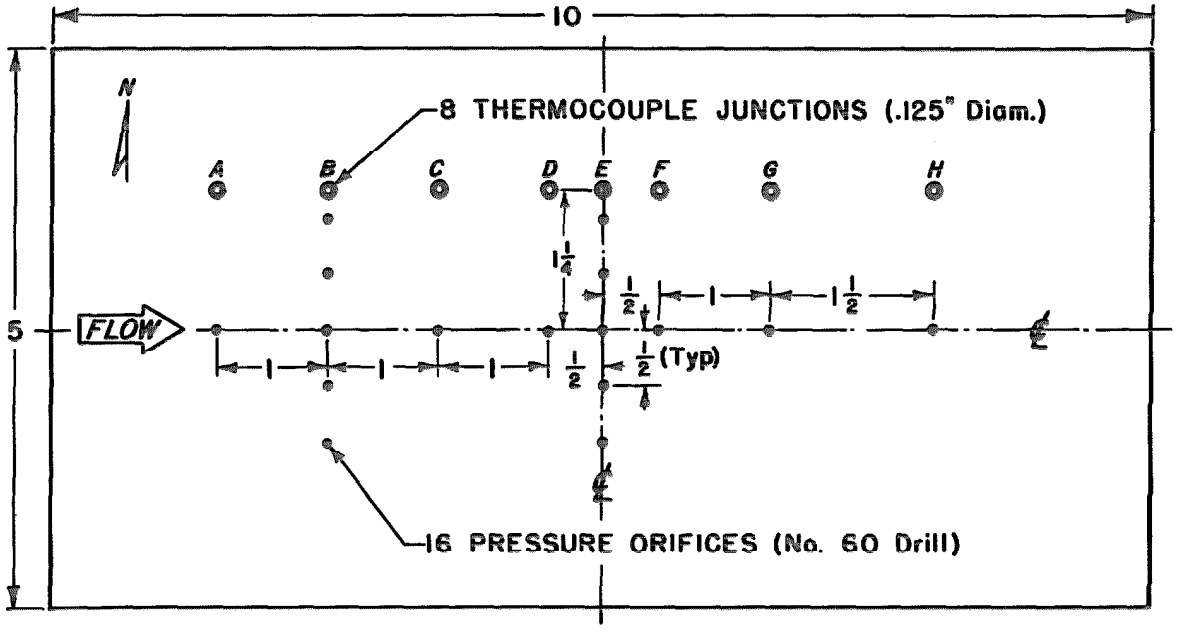

Schematic Sketch of Pressure and Temperature Distribution Survey Plate

Fig. 5

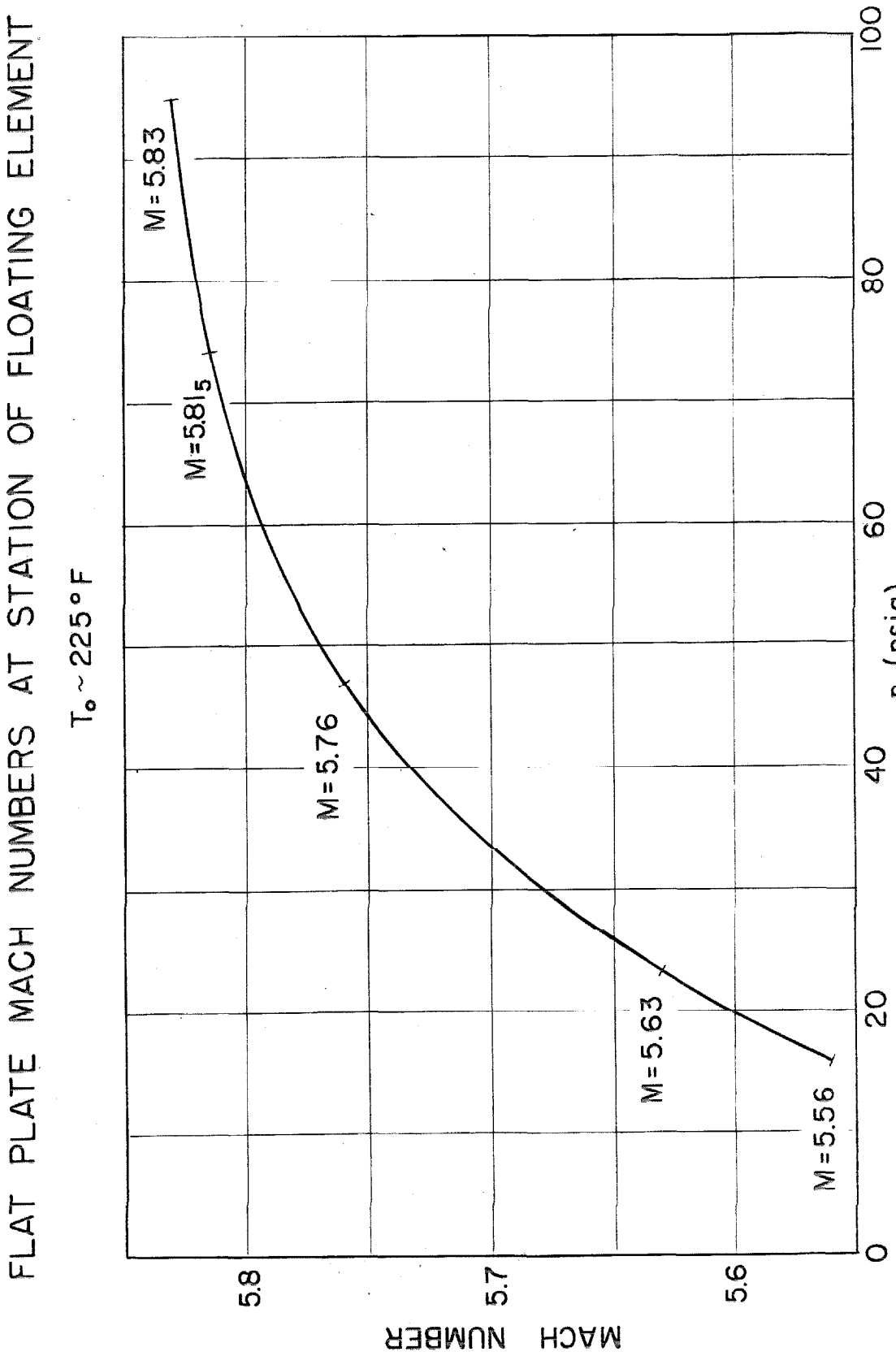
FLAT PLATE MACH NUMBERS AT STATION OF FLOATING ELEMENT
$T_o \sim 225°F$
M=5.83
M=5.81$_5$
M=5.76
M=5.63
M=5.56
MACH NUMBER
5.8
5.7
5.6
0
20
40
60
80
100
p_o (psia)

FIG. 6

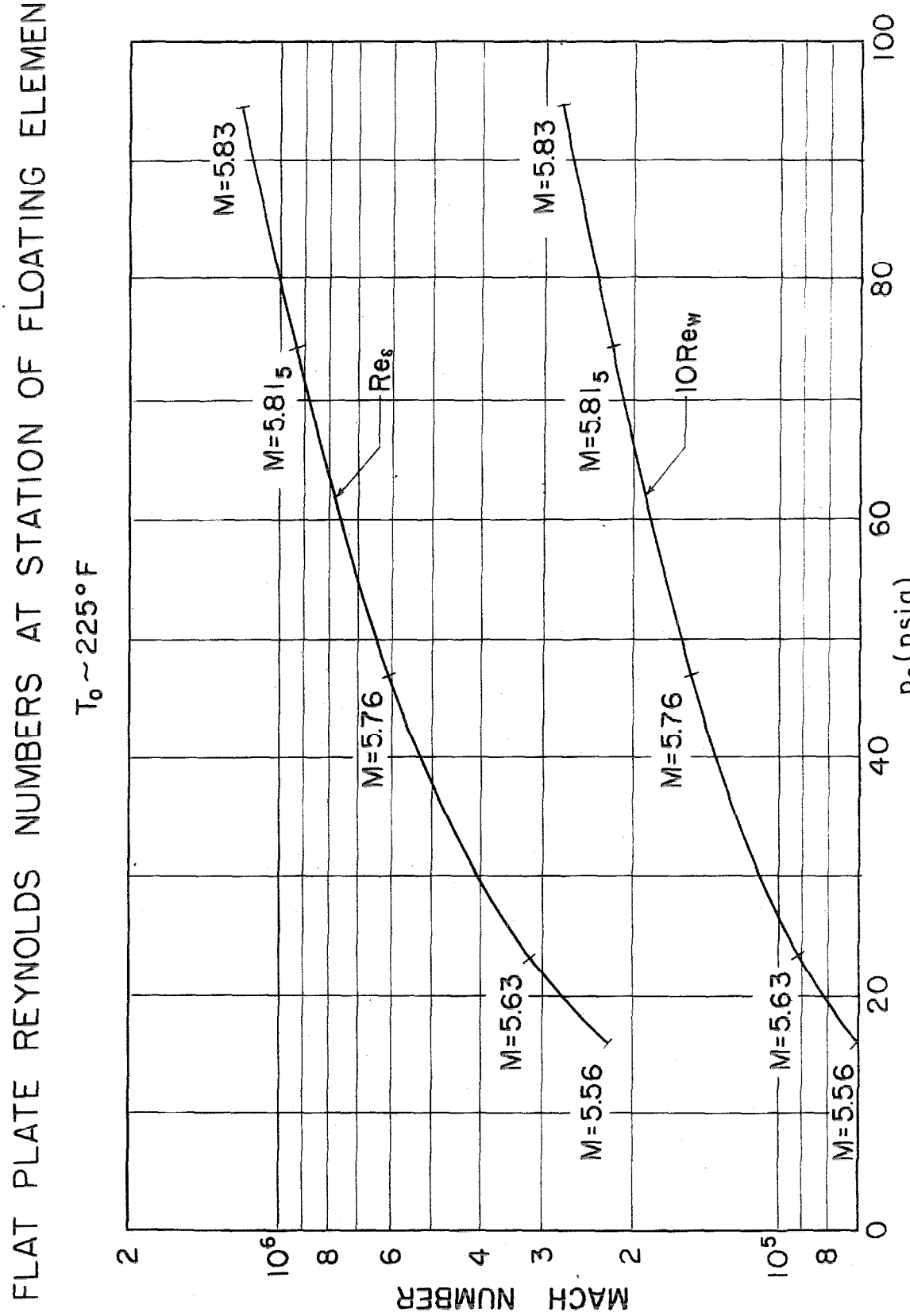
FLAT PLATE REYNOLDS NUMBERS AT STATION OF FLOATING ELEMENT
$T_o \sim 225°F$
MACH NUMBER
p_o (psia)
M=5.83
M=5.81$_5$
Re_δ
M=5.76
M=5.63
M=5.56
M=5.83
M=5.81$_5$
$10Re_w$
M=5.76
M=5.63
M=5.56
2
10^6
8
6
4
3
2
10^5
8
0
20
40
60
80
100

FIG. 7

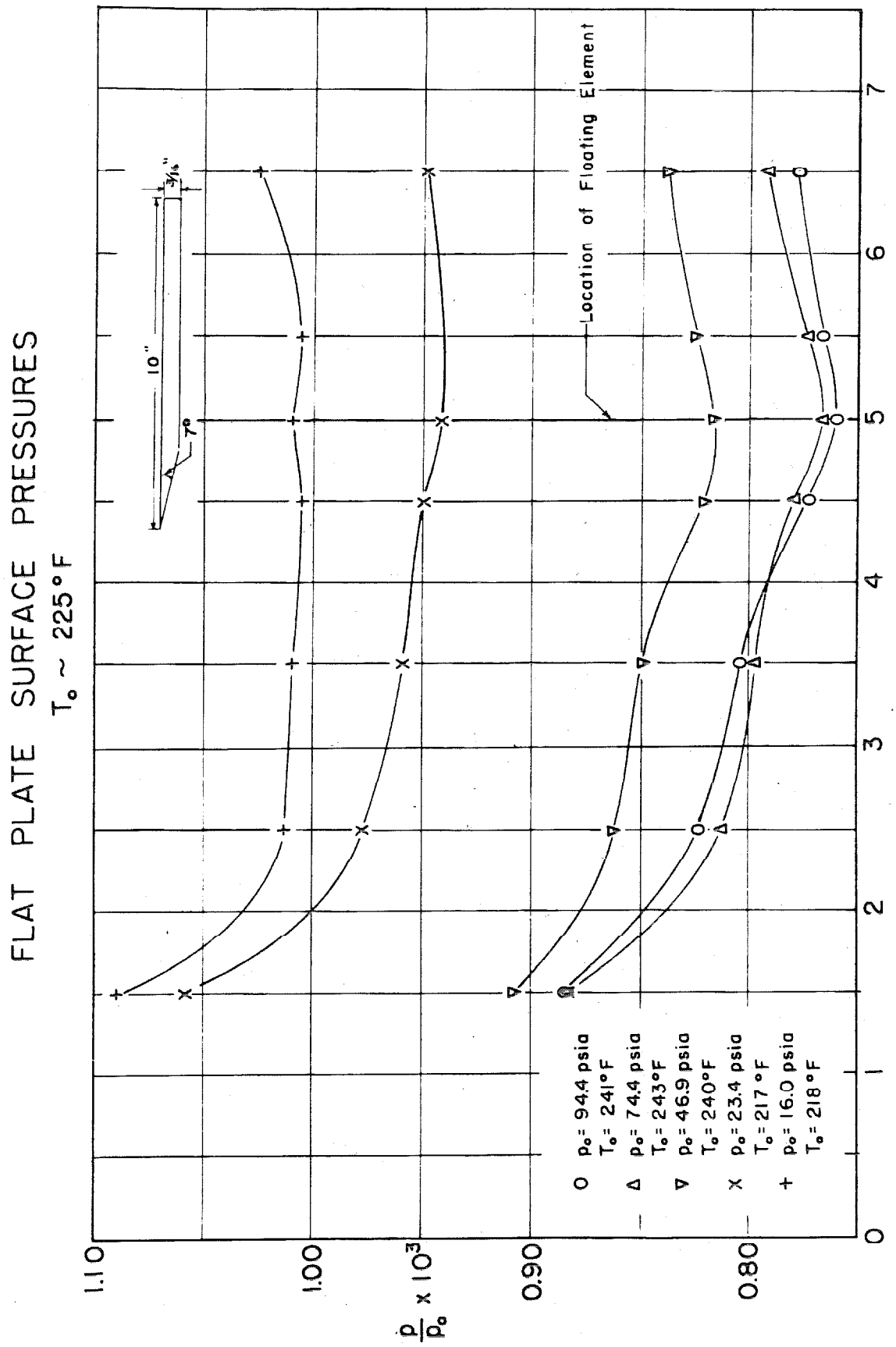
FLAT PLATE SURFACE PRESSURES
$T_o \sim 225°F$
$\frac{p}{p_o} \times 10^3$
1.10
1.00
0.90
0.80
0
1
2
3
4
5
6
7
x - DISTANCE FROM PLATE LEADING EDGE (in.)
Location of Floating Element
10"
7°
O p_o= 94.4 psia T_o= 241°F
Δ p_o= 74.4 psia T_o= 243°F
∇ p_o= 46.9 psia T_o= 240°F
X p_o= 23.4 psia T_o= 217°F
+ p_o= 16.0 psia T_o= 218°F

FIG. 8a

FLAT PLATE SURFACE PRESSURES
$T_o \sim 225°F$

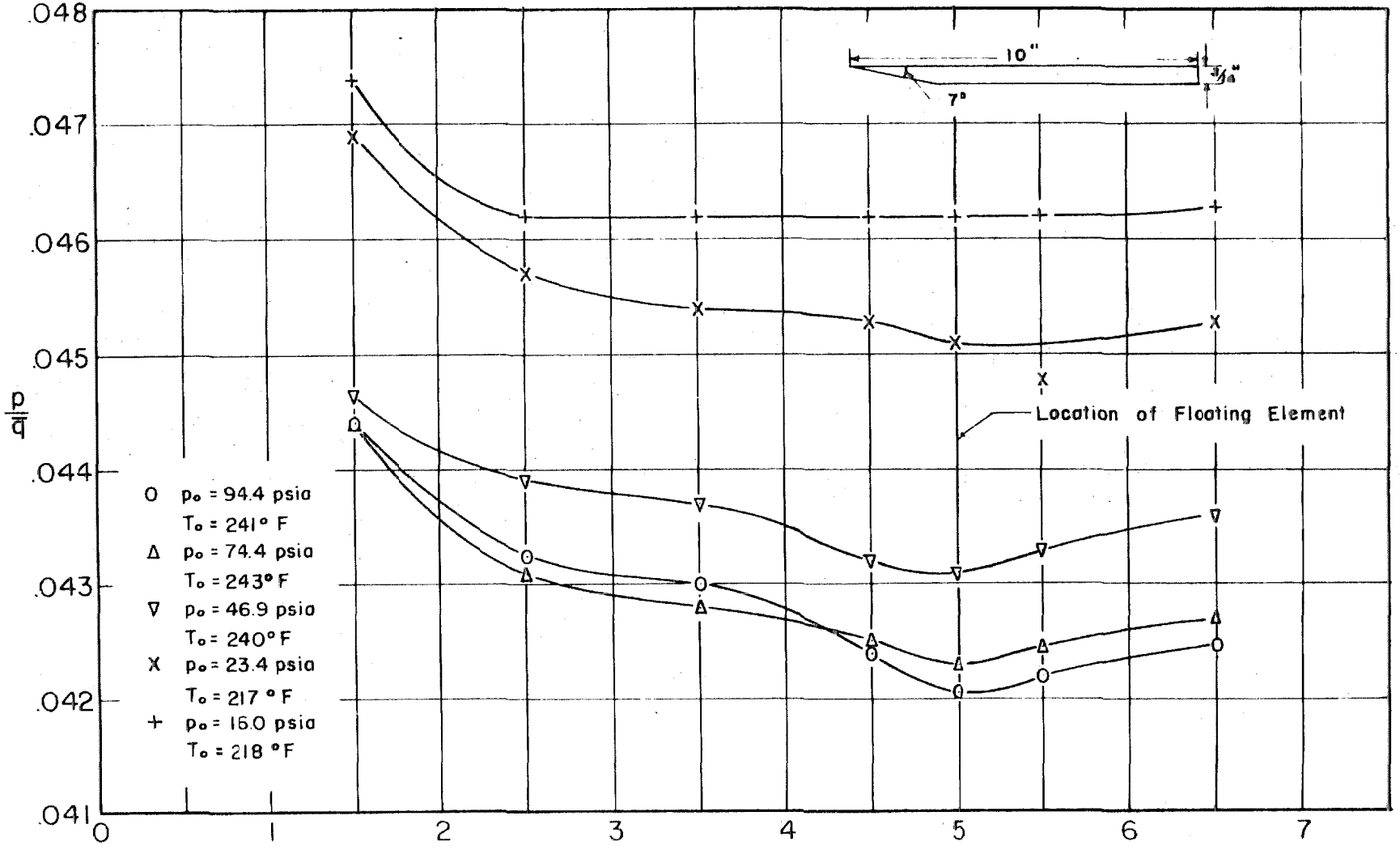

FIG. 8b

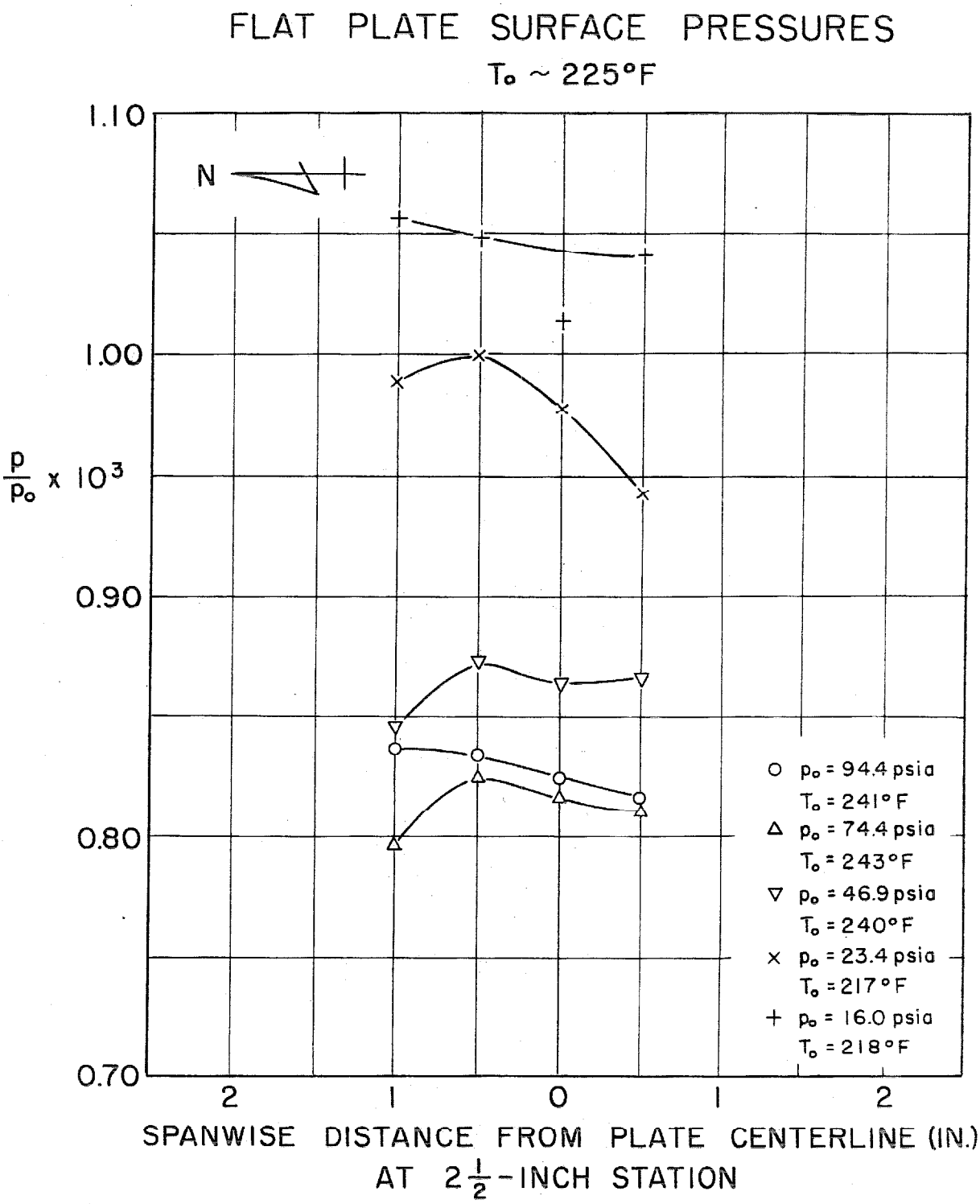
FLAT PLATE SURFACE PRESSURES
$T_o \sim 225°F$
1.10
1.00
0.90
0.80
0.70
$\frac{p}{p_o} \times 10^3$
N
p_o = 94.4 psia
T_o = 241°F
p_o = 74.4 psia
T_o = 243°F
p_o = 46.9 psia
T_o = 240°F
p_o = 23.4 psia
T_o = 217°F
p_o = 16.0 psia
T_o = 218°F
2
1
0
1
2
SPANWISE DISTANCE FROM PLATE CENTERLINE (IN.)
AT $2\frac{1}{2}$-INCH STATION

FIG. 9a

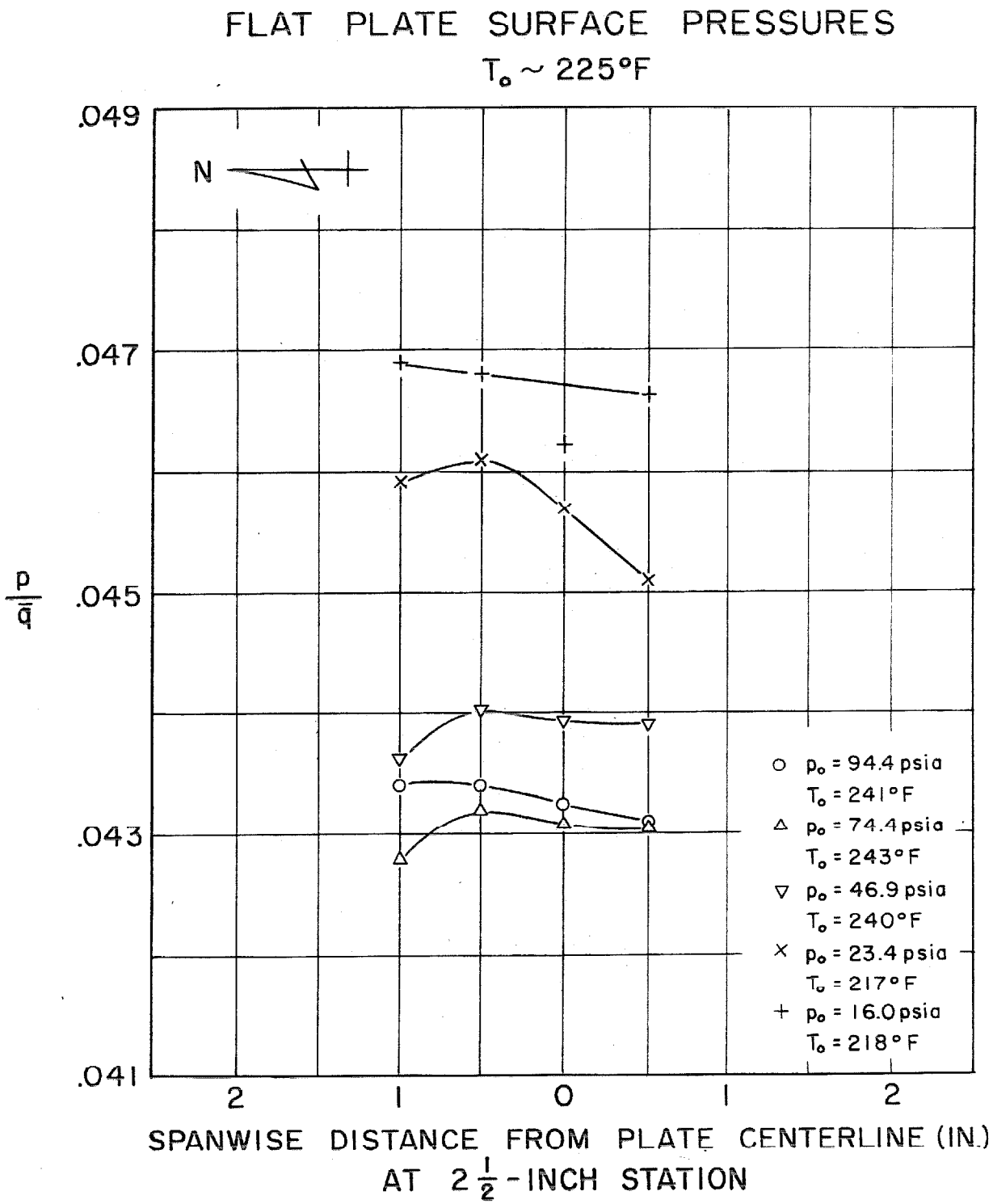
FLAT PLATE SURFACE PRESSURES
$T_o \sim 225°F$
.049
.047
.045
.043
.041
$\frac{p}{q}$
N
p_o = 94.4 psia
T_o = 241°F
p_o = 74.4 psia
T_o = 243°F
p_o = 46.9 psia
T_o = 240°F
p_o = 23.4 psia
T_o = 217°F
p_o = 16.0 psia
T_o = 218°F
2
1
0
1
2
SPANWISE DISTANCE FROM PLATE CENTERLINE (IN.)
AT $2\frac{1}{2}$-INCH STATION

FIG. 9b

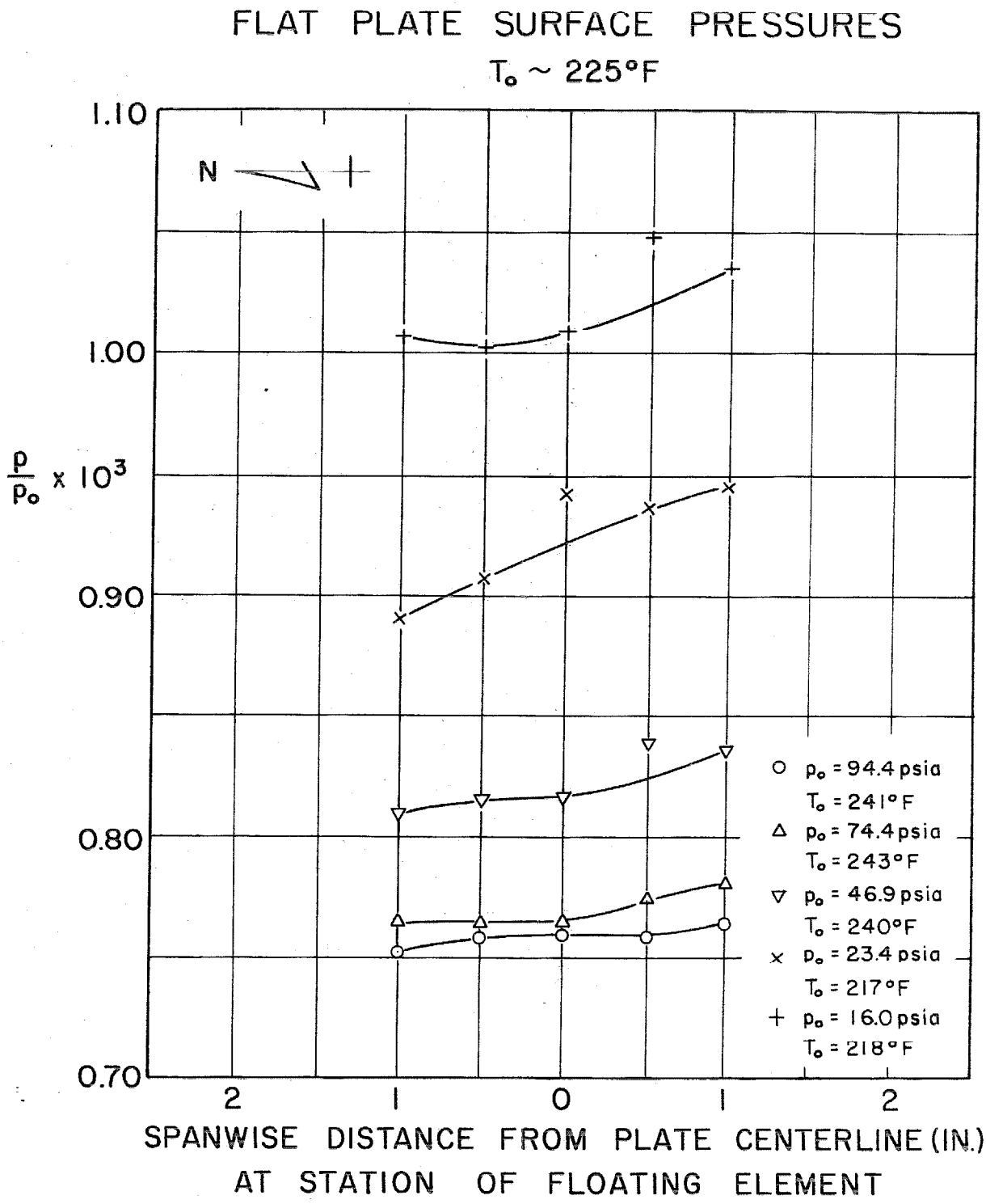
FLAT PLATE SURFACE PRESSURES
$T_o \sim 225°F$
1.10
1.00
0.90
0.80
0.70
$\frac{p}{p_o} \times 10^3$
N
p_o = 94.4 psia
T_o = 241°F
p_o = 74.4 psia
T_o = 243°F
p_o = 46.9 psia
T_o = 240°F
p_o = 23.4 psia
T_o = 217°F
p_o = 16.0 psia
T_o = 218°F
2
1
0
1
2
SPANWISE DISTANCE FROM PLATE CENTERLINE (IN.)
AT STATION OF FLOATING ELEMENT

FIG. 10a

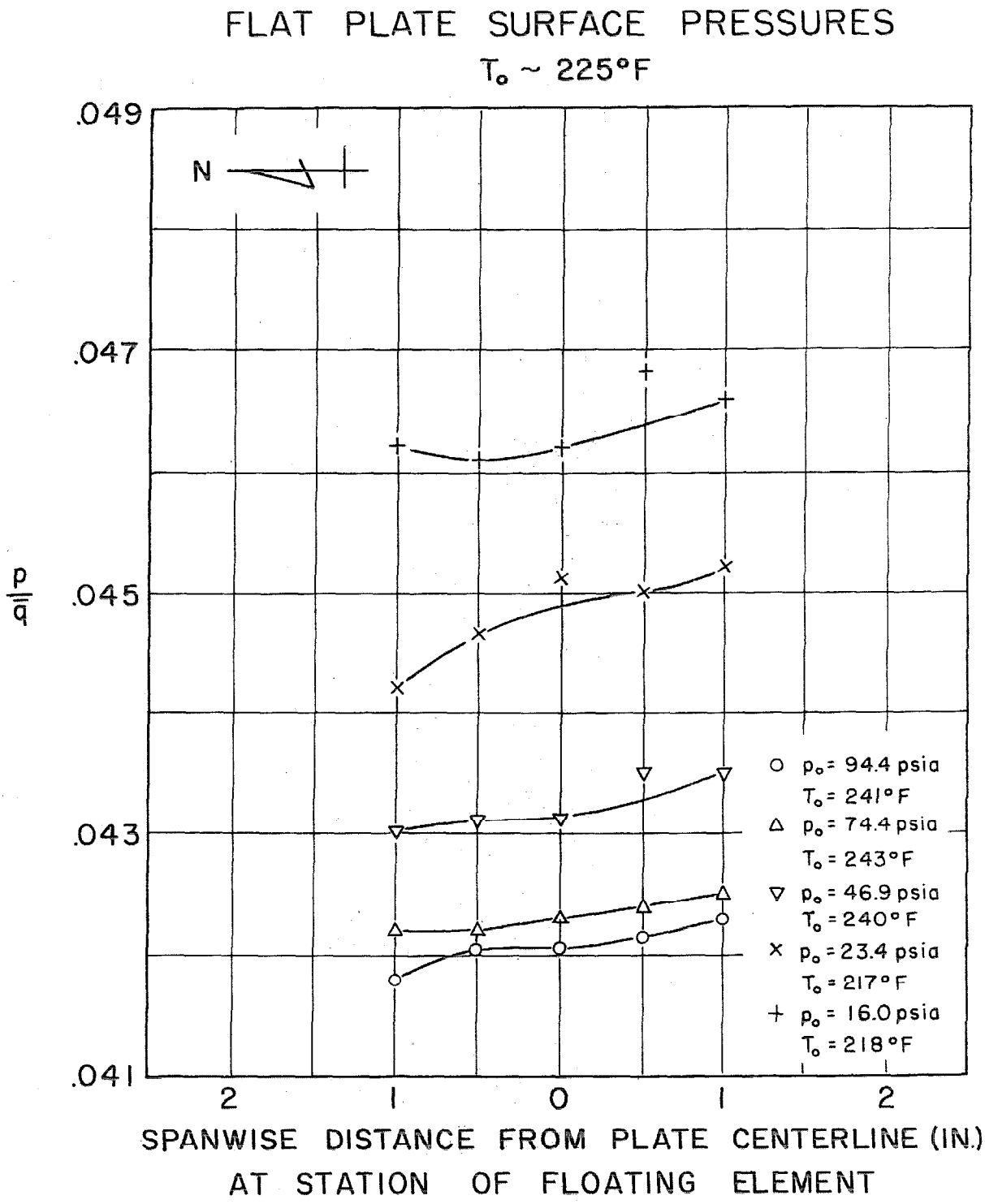
FLAT PLATE SURFACE PRESSURES
$T_o \sim 225°F$
.049
.047
.045
.043
.041
$\frac{p}{q}$
N
p_o = 94.4 psia
T_o = 241°F
p_o = 74.4 psia
T_o = 243°F
p_o = 46.9 psia
T_o = 240°F
p_o = 23.4 psia
T_o = 217°F
p_o = 16.0 psia
T_o = 218°F
2
1
0
1
2
SPANWISE DISTANCE FROM PLATE CENTERLINE (IN.)
AT STATION OF FLOATING ELEMENT

FIG. 10b

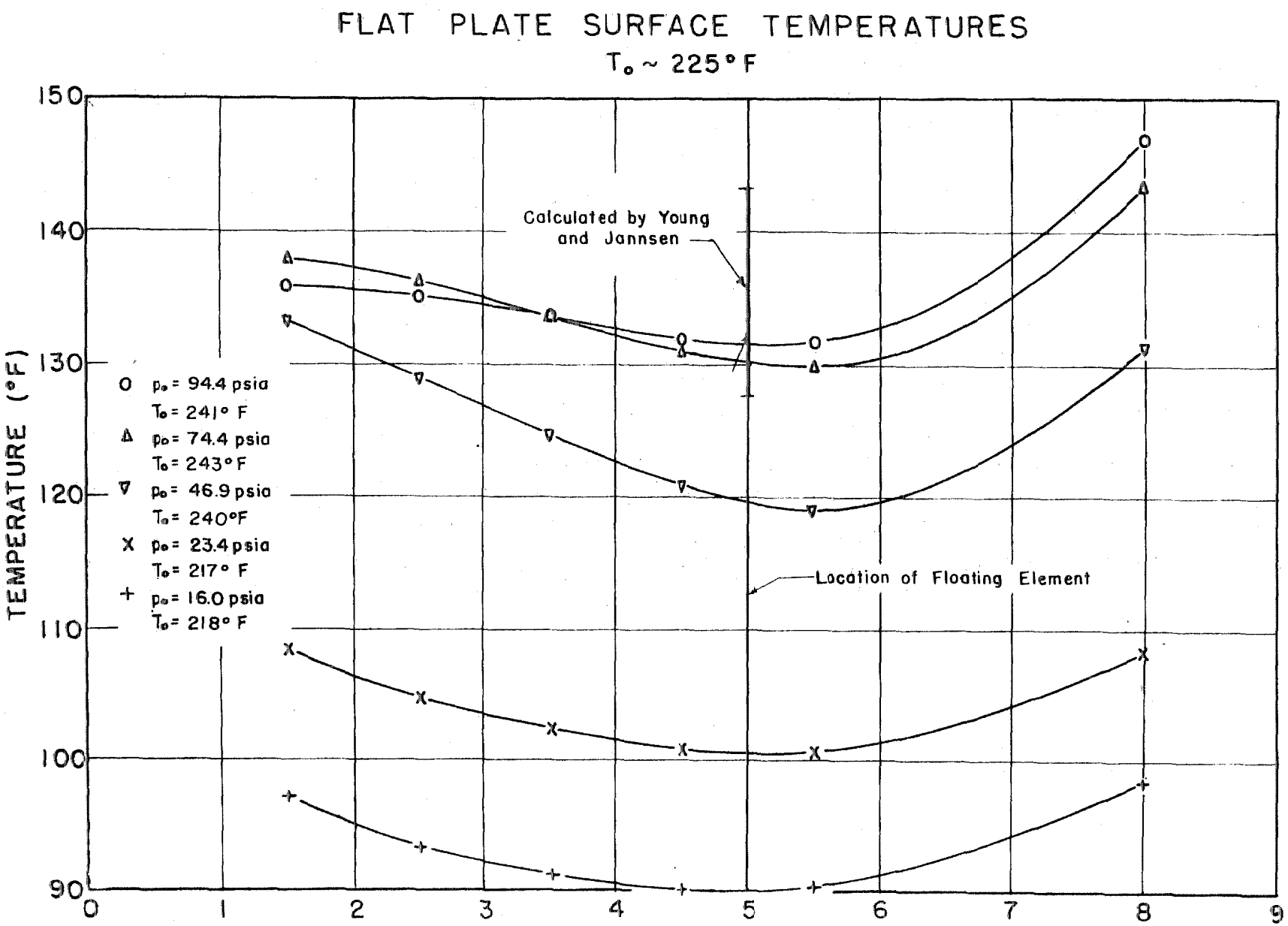
FLAT PLATE SURFACE TEMPERATURES
$T_o \sim 225°F$
TEMPERATURE (°F)
150
140
130
120
110
100
90
0
1
2
3
4
5
6
7
8
9
Calculated by Young and Jannsen
Location of Floating Element
O p_o = 94.4 psia
T_o = 241° F
Δ p_o = 74.4 psia
T_o = 243° F
∇ p_o = 46.9 psia
T_o = 240°F
X p_o = 23.4 psia
T_o = 217° F
+ p_o = 16.0 psia
T_o = 218° F
x - DISTANCE FROM PLATE LEADING EDGE (IN.)

FIG. 11

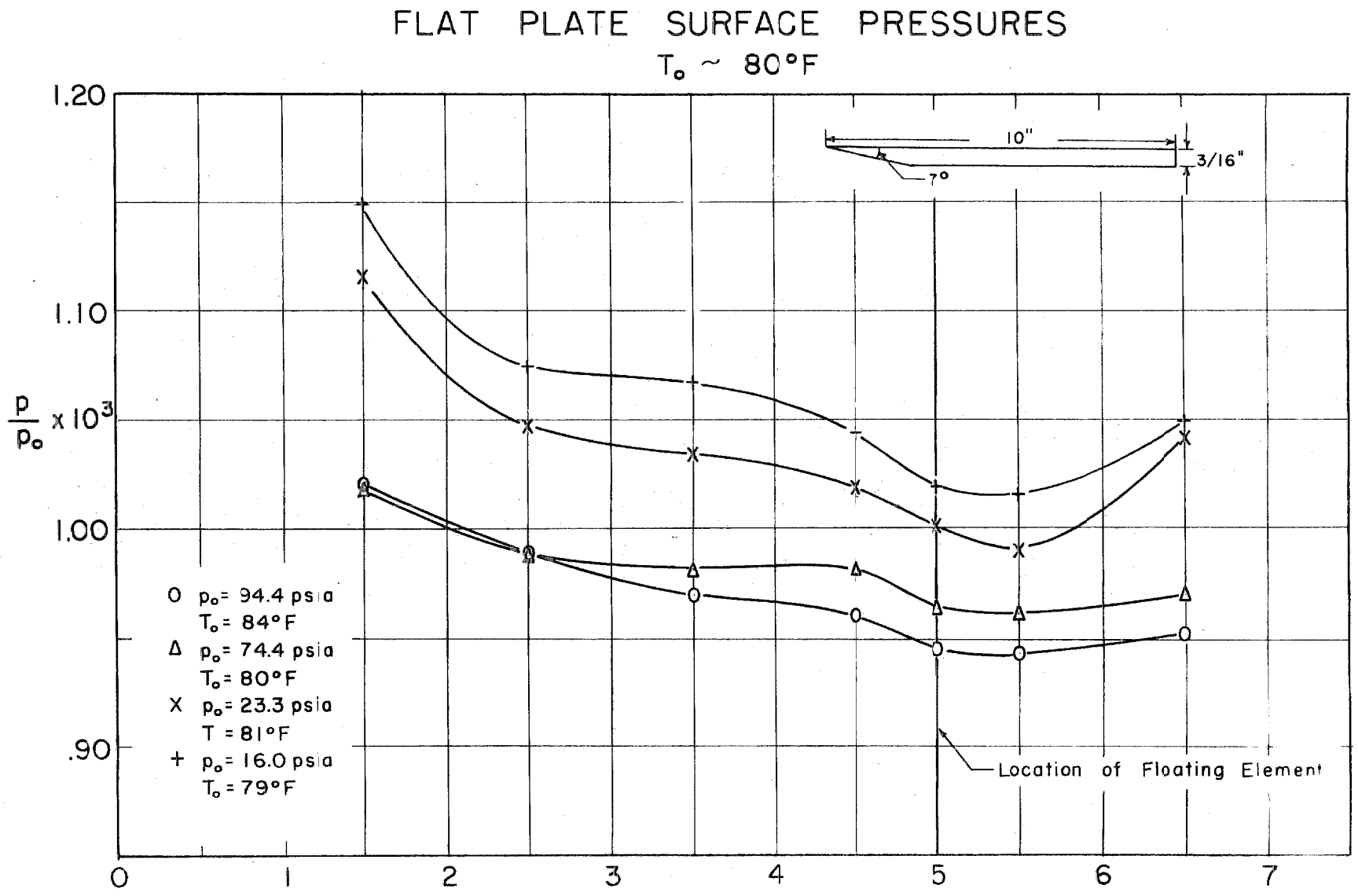
FLAT PLATE SURFACE PRESSURES
$T_o \sim 80°F$
1.20
1.10
1.00
.90
$\frac{p}{p_o} \times 10^3$
10"
3/16"
7°
O p_o= 94.4 psia
T_o= 84°F
Δ p_o= 74.4 psia
T_o= 80°F
X p_o= 23.3 psia
T = 81°F
+ p_o= 16.0 psia
T_o= 79°F
Location of Floating Element
0
1
2
3
4
5
6
7
x - DISTANCE FROM PLATE LEADING EDGE (in)

FIG. 12

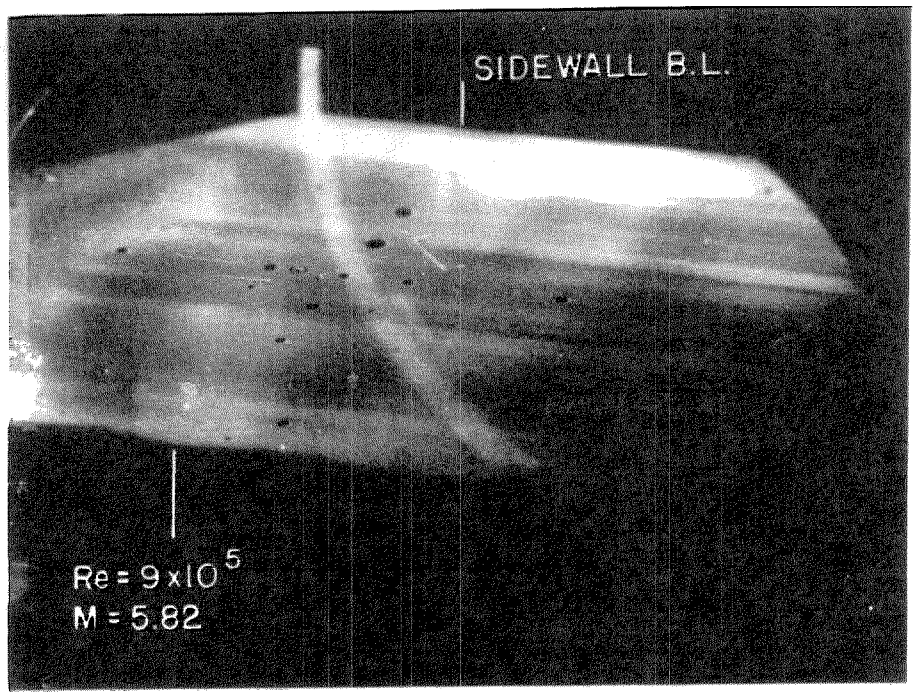

Plate Sprayed with Fluorescent Lacquer
No Artificial Disturbance

Fig. 13a

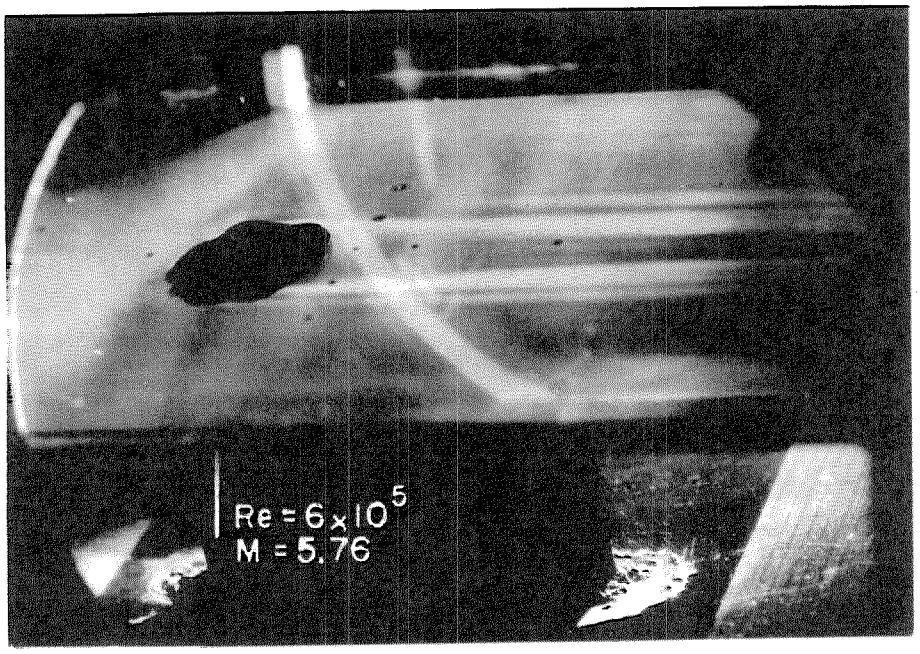

Plate Sprayed with Fluorescent Lacquer
Disturbance Produced by Irregular Bump 3/16 in. High,
Located 4 in. from Plate Leading Edge

Fig. 13b

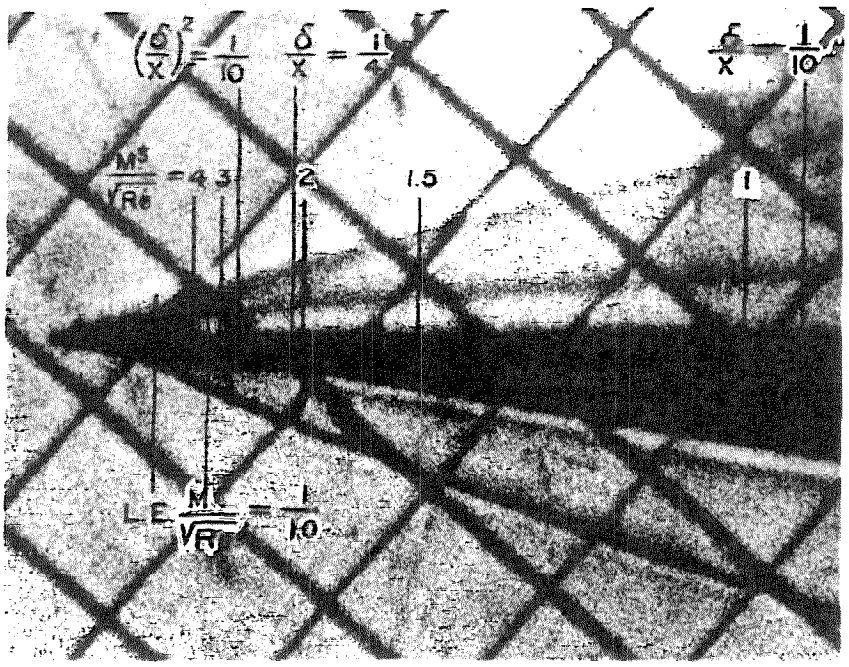

M = 5.76, Re/in = 1.2×10^5, T_o = 225°F, p_o = 46.9 psia

Fig. 14a

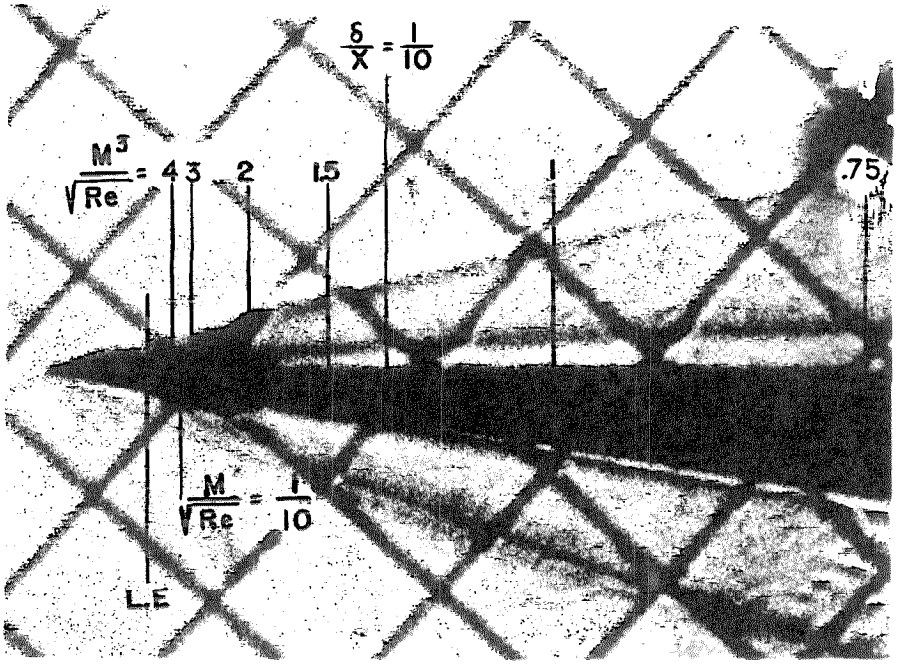

M = 5.83, Re/in = 2.5×10^5, T_o = 225°F, p_o = 94.4 psia

Fig. 14b

SCHLIEREN PHOTOGRAPHS OF FLAT PLATE LEADING EDGE

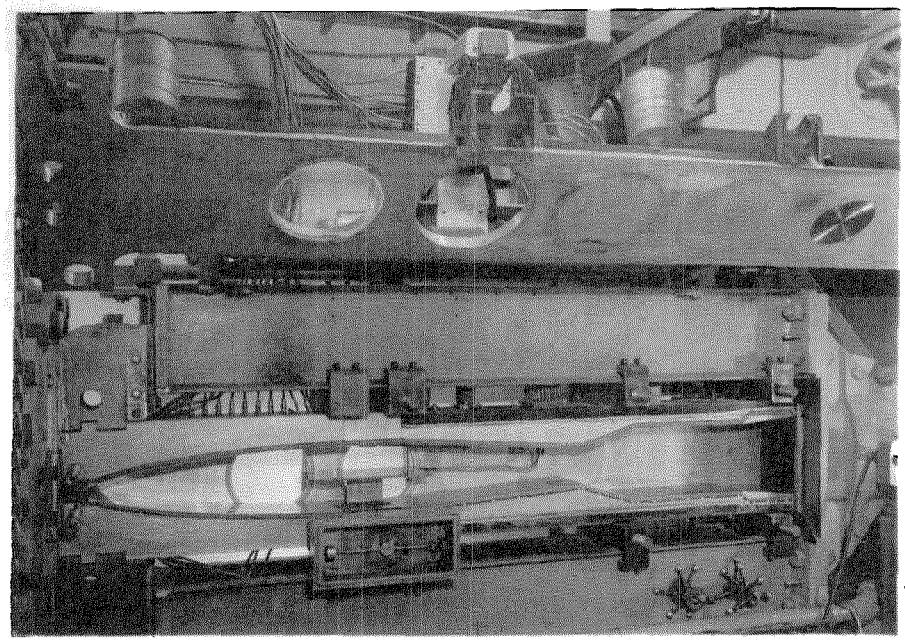

Fig. 15a

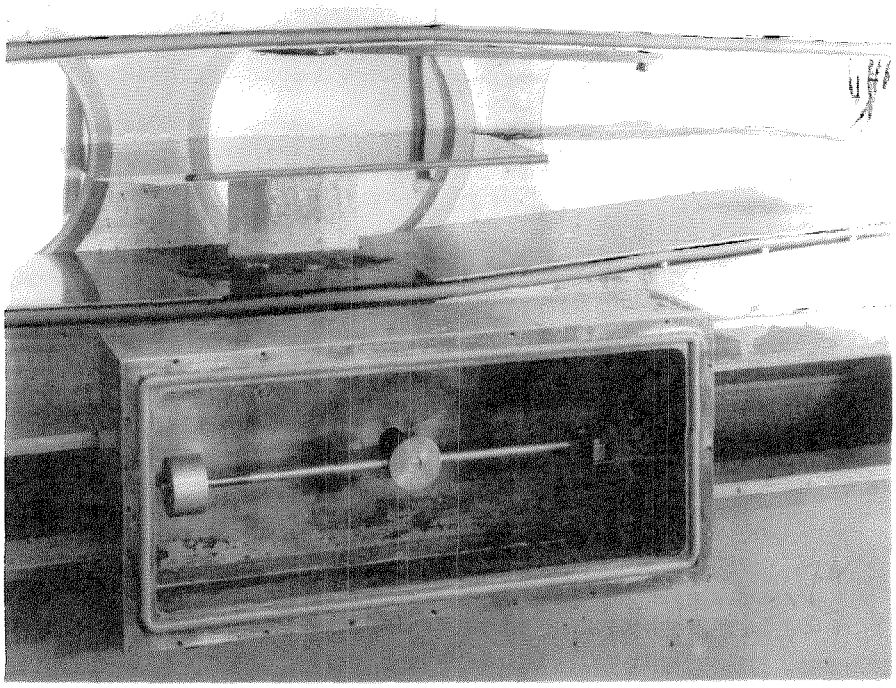

Fig. 15b

5 x 10 IN. FLAT PLATE USED IN SKIN FRICTION MEASUREMENTS INSTALLED IN GALCIT 5 x 5 IN. HYPERSONIC WIND TUNNEL

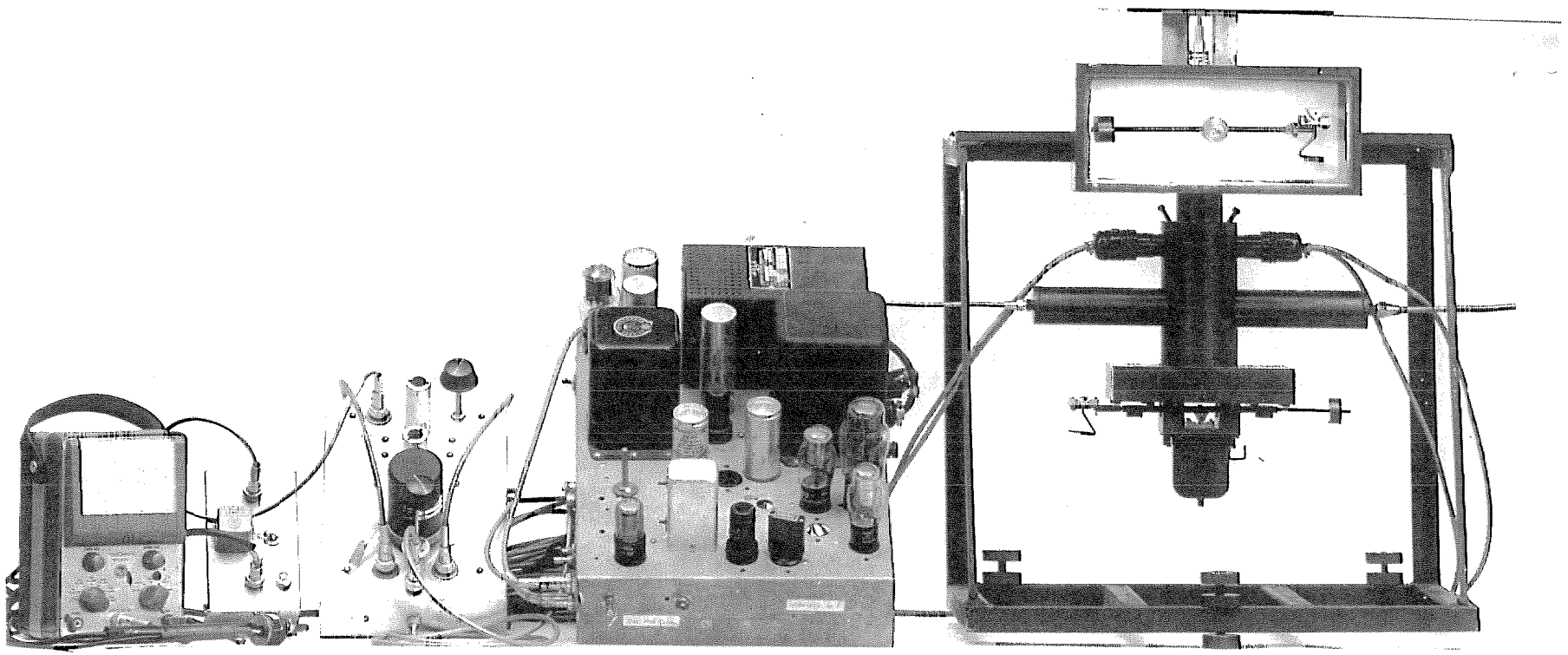

Flat Plate and Skin Friction Balance in Simulated Mounting,
Power Supply and 100kc Oscillator, High Gain Amplifier, Vibration Filter, and Voltmeter

Fig. 16

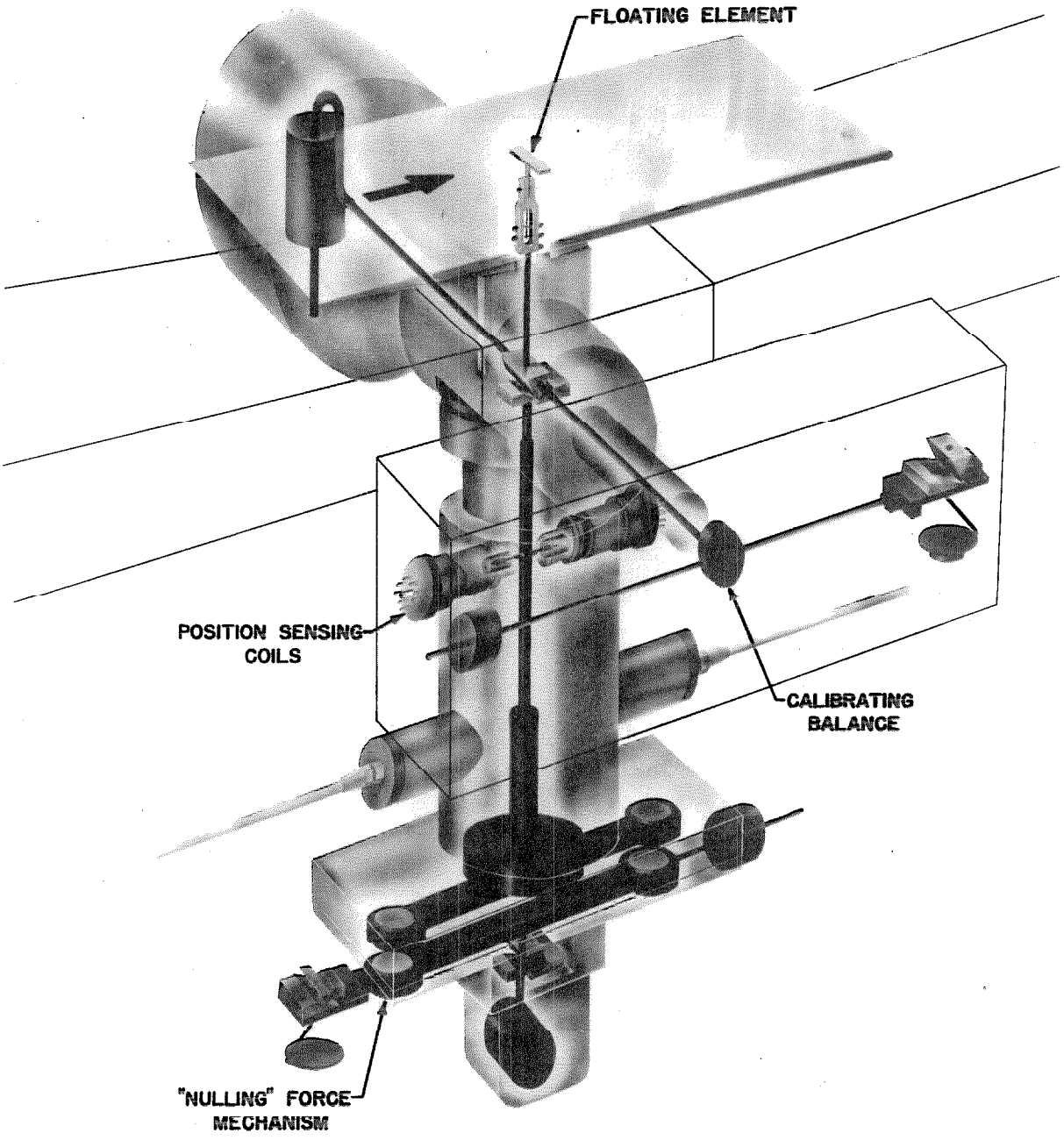

SKIN FRICTION BALANCE

FIG. 17a

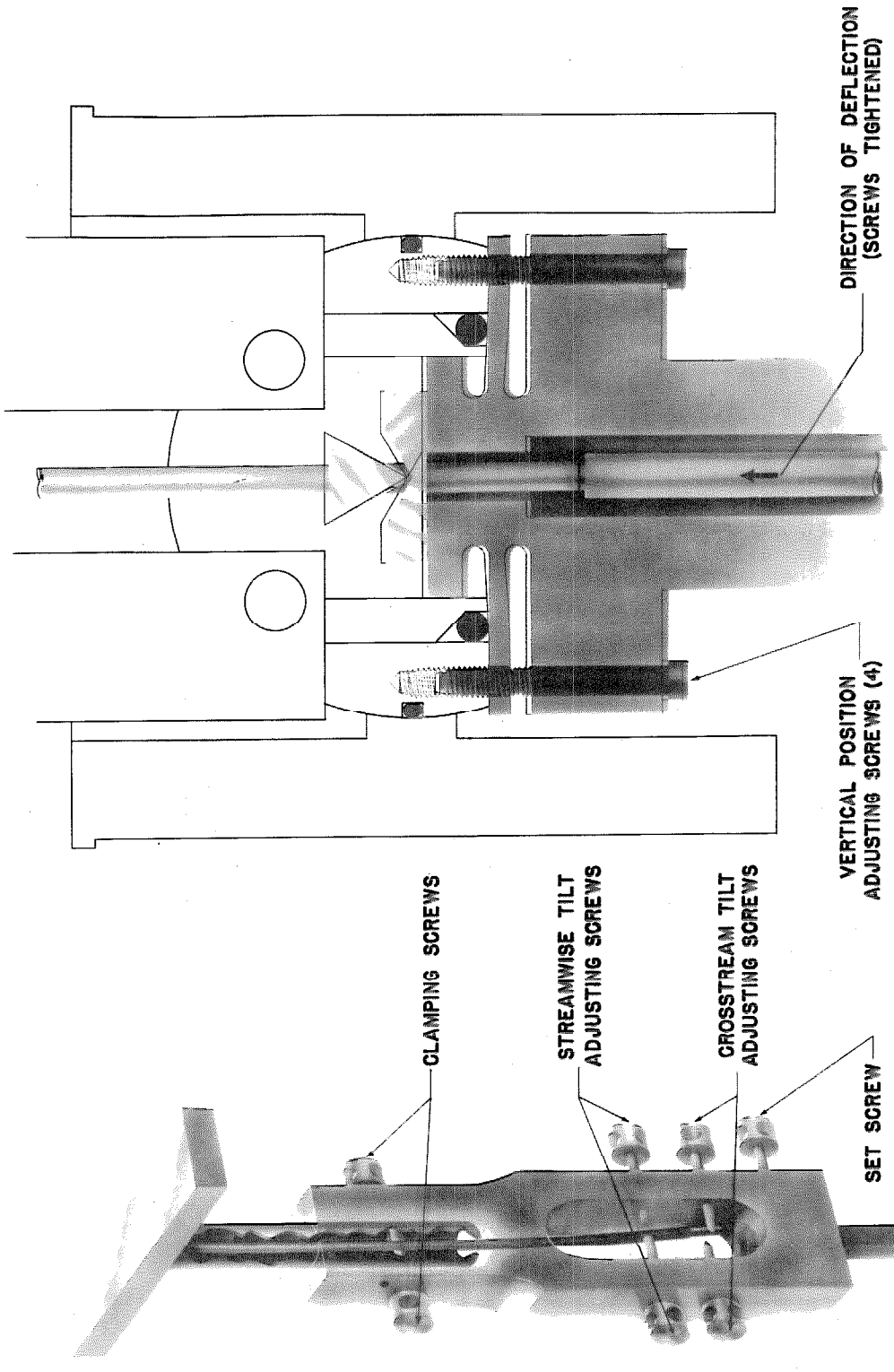

ELEMENT TILT ADJUSTING MECHANISM

FIG. 17b

ELEMENT VERTICAL ADJUSTING MECHANISM

FIG. 17c

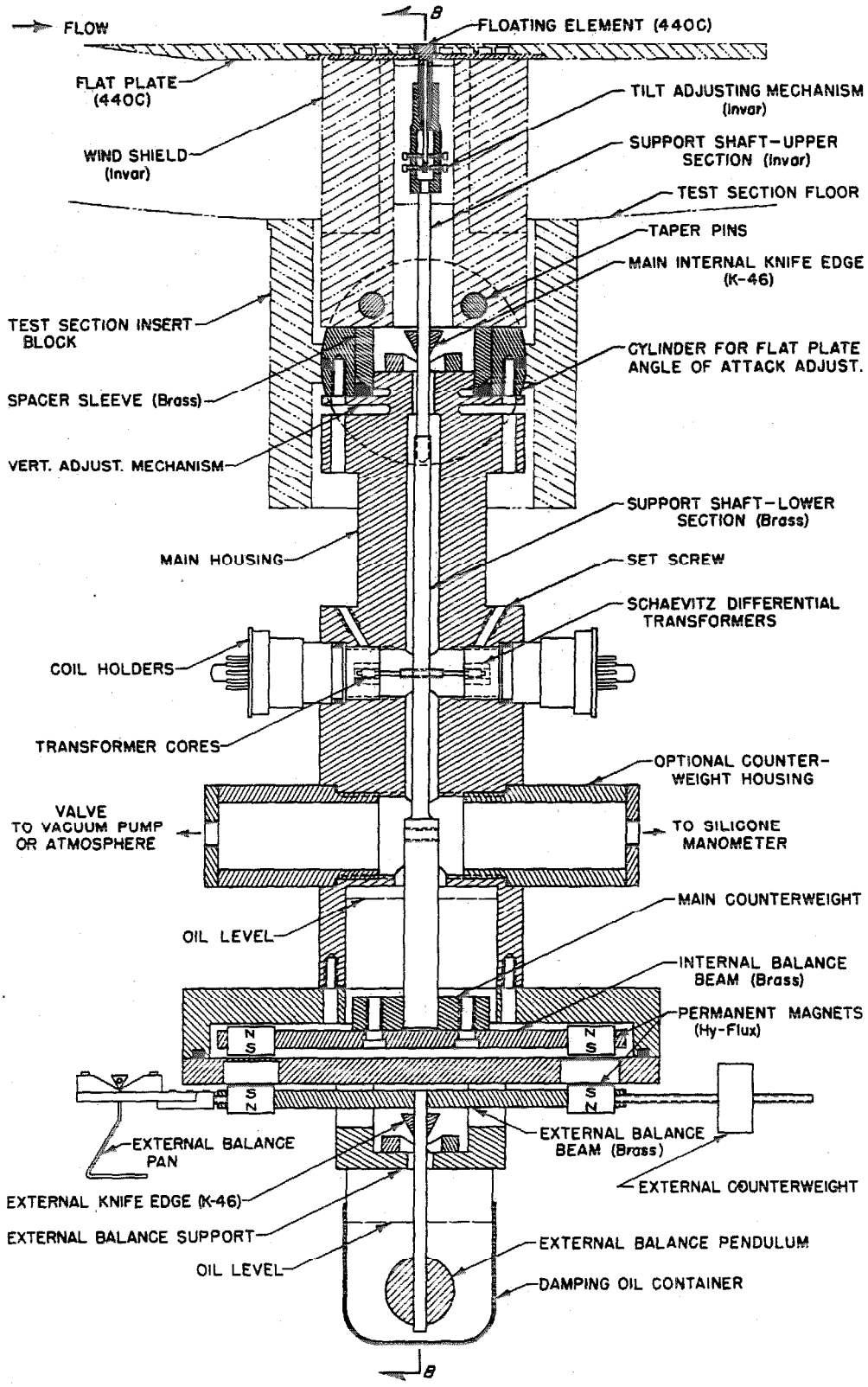

SKIN FRICTION BALANCE

SECTION A-A

FIG. 18a

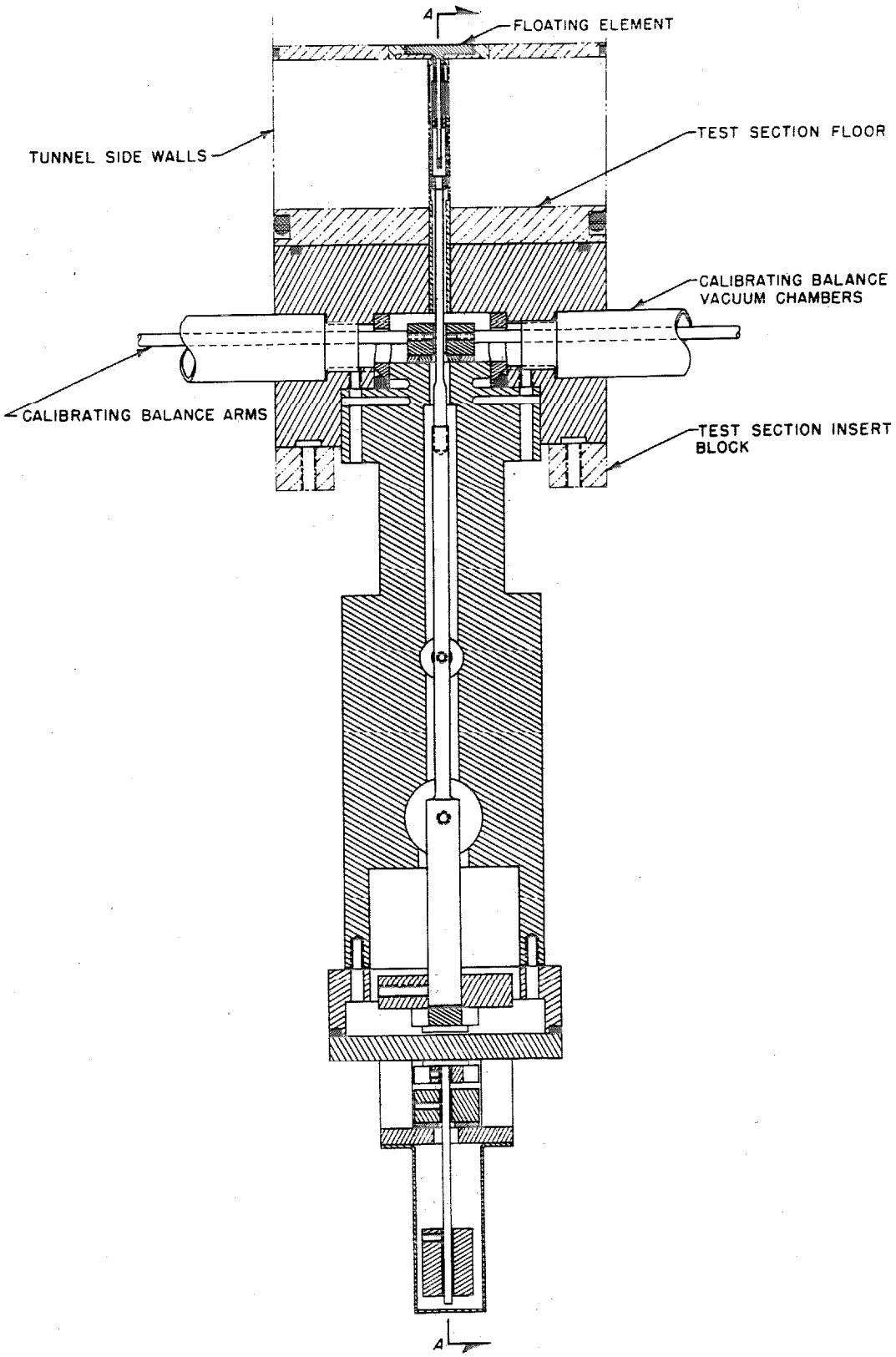

SKIN FRICTION BALANCE

SECTION B-B

FIG. 18b

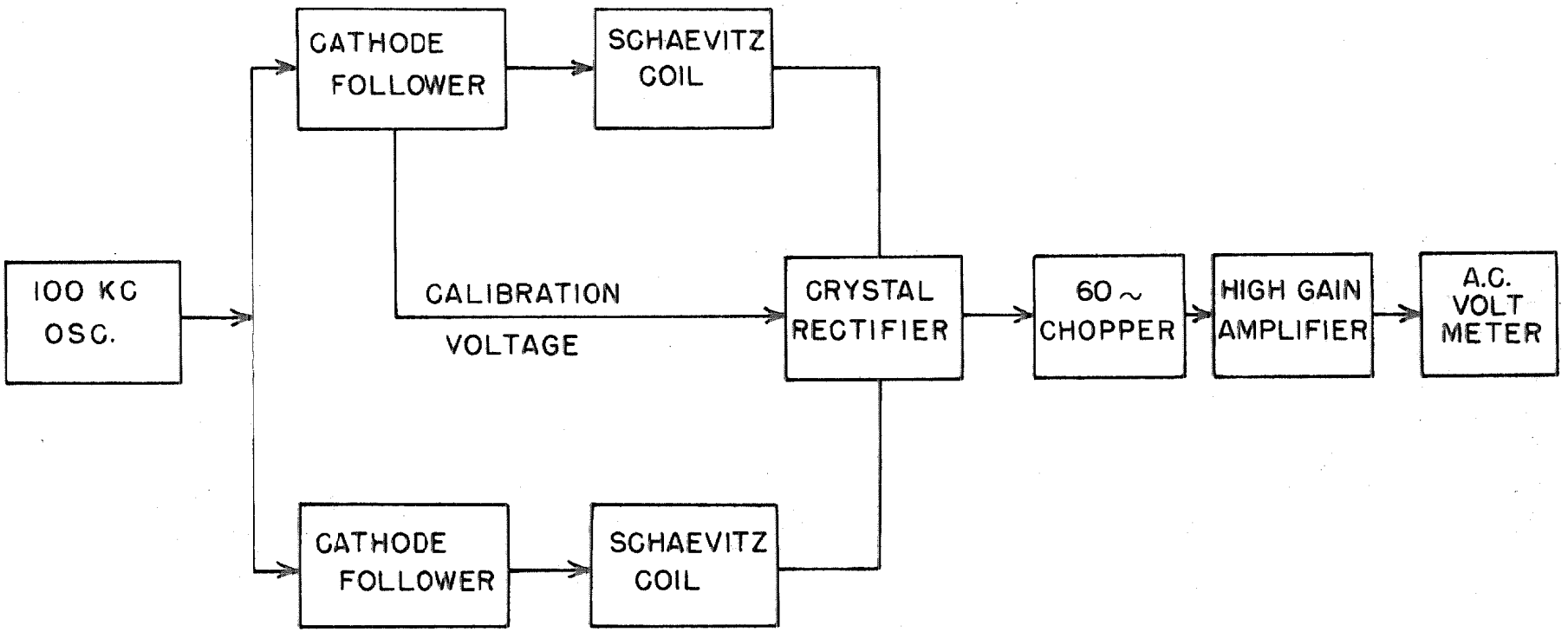

ELECTRONIC COMPONENTS FOR BALANCE POSITION SENSING

BLOCK DIAGRAM

FIG. 19a

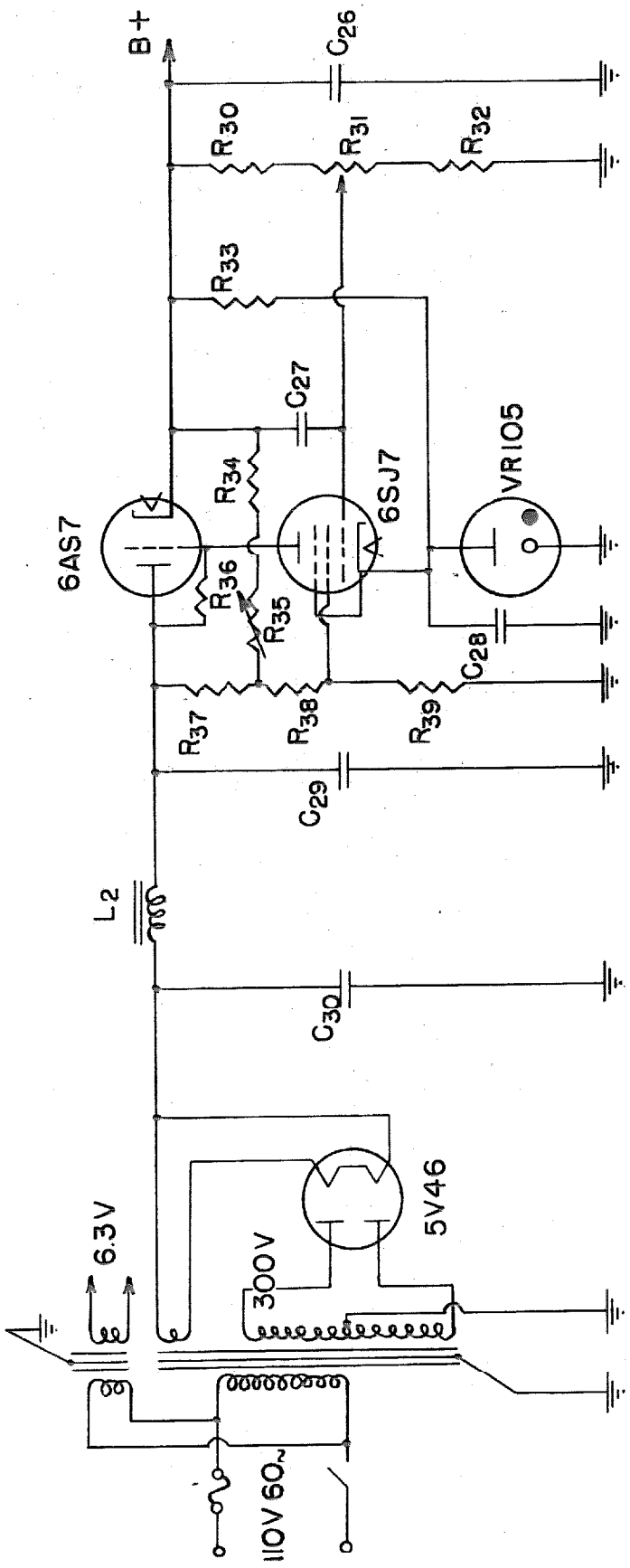

REGULATED POWER SUPPLY

FIG.19b

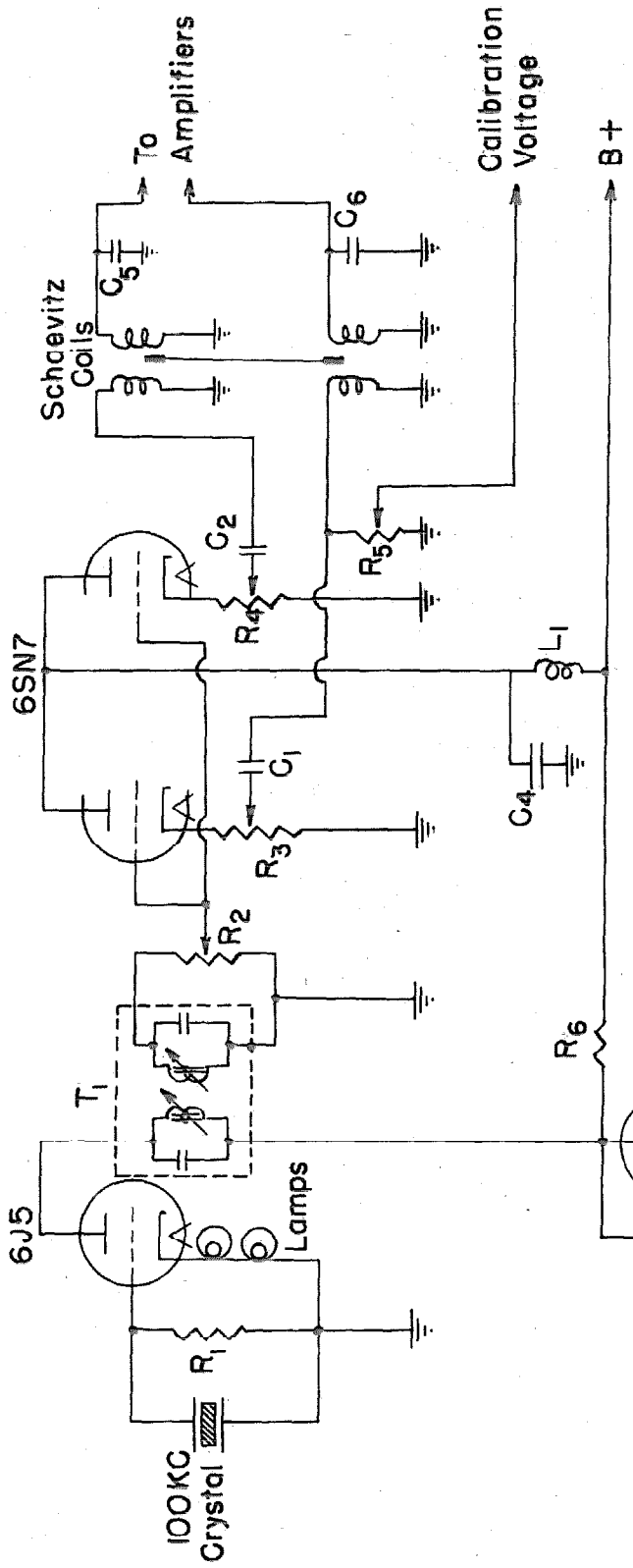

100 KC CRYSTAL CONTROLLED OSCILLATOR, CATHODE FOLLOWERS, AND SCHAEVITZ COILS

FIG. 19c

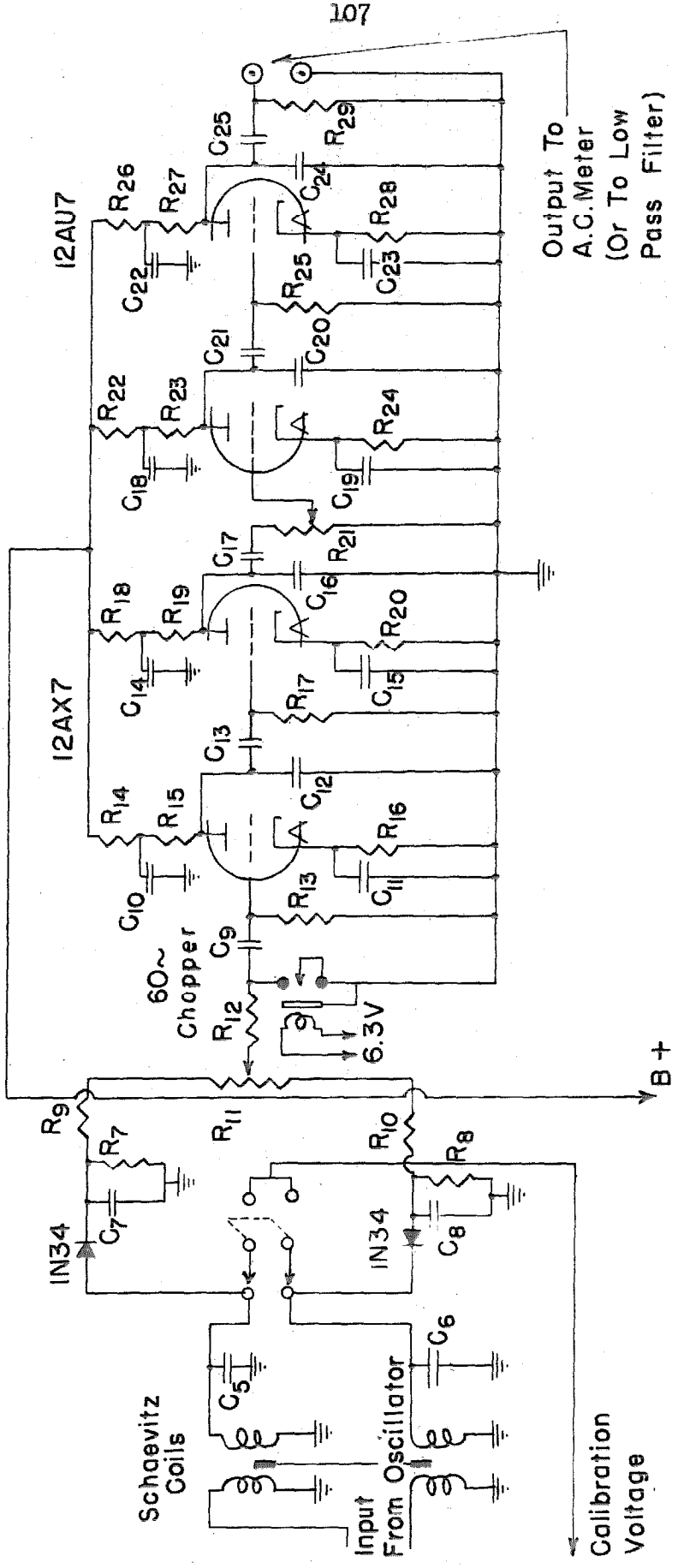

SCHAEVITZ COILS, CRYSTAL RECTIFIERS, AND HIGH GAIN AMPLIFIER

FIG. 19d

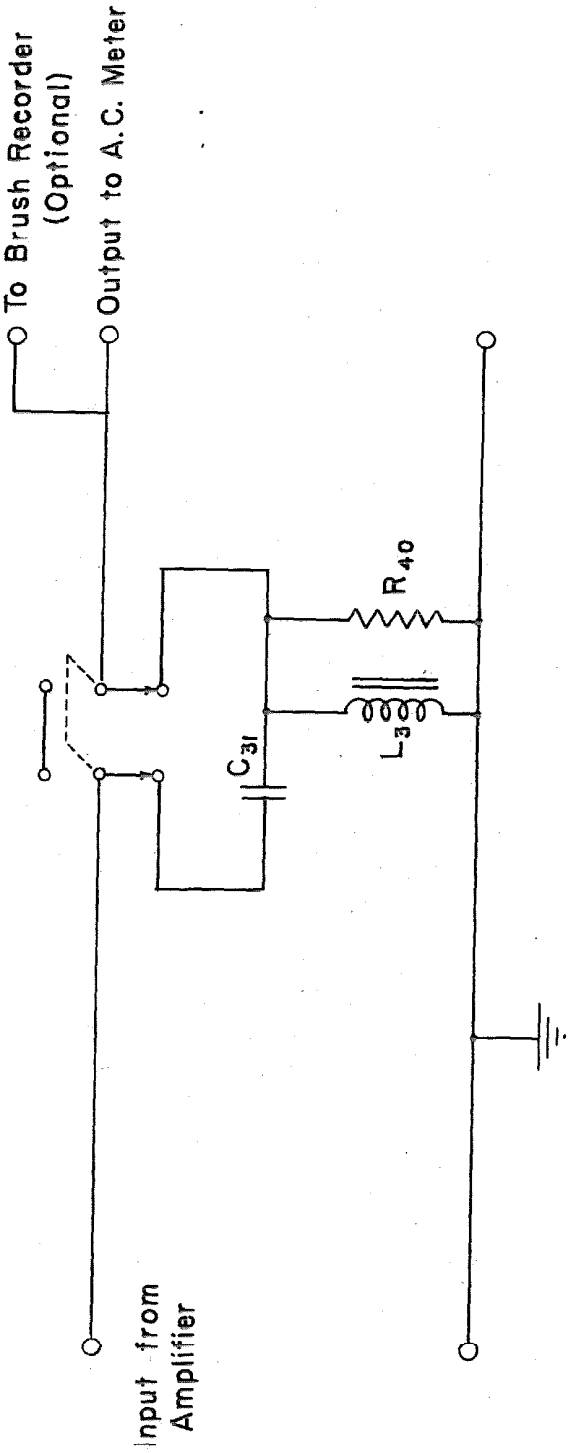

LOW PASS FILTER (OPTIONAL)

FIG. 19e

Resistances (Ohms)		Capacitances (Microfarads)		Inductances (Henrys)	
R_1	= 100K	C_1	= .05	L_1	= .05
R_2	= 50K	C_2	= .05	L_2	= 30
R_3	= 5K	C_3	= .1	L_3	= 150
R_4	= 5K	C_4	= .1		
R_5	= 1K	C_5	= .001		
R_6	= 8K	C_6	= .001		
R_7	= 27K	C_7	= .25		
R_8	= 27K	C_8	= .25		
R_9	= 27K	C_9	= .5		
R_{10}	= 27K	C_{10}	= 8		
R_{11}	= 10K	C_{11}	= 25		
R_{12}	= 56K	C_{12}	= .001		
R_{13}	= 1 Meg	C_{13}	= .1		
R_{14}	= 4.7K	C_{14}	= 8		
R_{15}	= 100K	C_{15}	= 25		
R_{16}	= 1.5K	C_{16}	= .001		
R_{17}	= 220K	C_{17}	= .1		
R_{18}	= 4.7K	C_{18}	= 8		
R_{19}	= 100K	C_{19}	= 25		
R_{20}	= 2.7K	C_{20}	= .001		
R_{21}	= 200K	C_{21}	= .1		
R_{22}	= 4.7K	C_{22}	= 8		
R_{23}	= 100K	C_{23}	= 25		
R_{24}	= 2.7K	C_{24}	= .001		
R_{25}	= 220K	C_{25}	= .1		
R_{26}	= 4.7K	C_{26}	= 8		
R_{27}	= 100K	C_{27}	= .1		
R_{28}	= 2.7K	C_{28}	= .1		
R_{29}	= 220K	C_{29}	= 8		
R_{30}	= 200K	C_{30}	= 8		
R_{31}	= 50K	C_{31}	= .016		
R_{32}	= 100K				
R_{33}	= 10K				
R_{34}	= 25K				
R_{35}	= 150K				
R_{36}	= 500K				
R_{37}	= 75K				
R_{38}	= 75K				
R_{39}	= 150K				
R_{40}	= 100K				

Circuit Values for Balance Position Sensing System

Fig. 19f

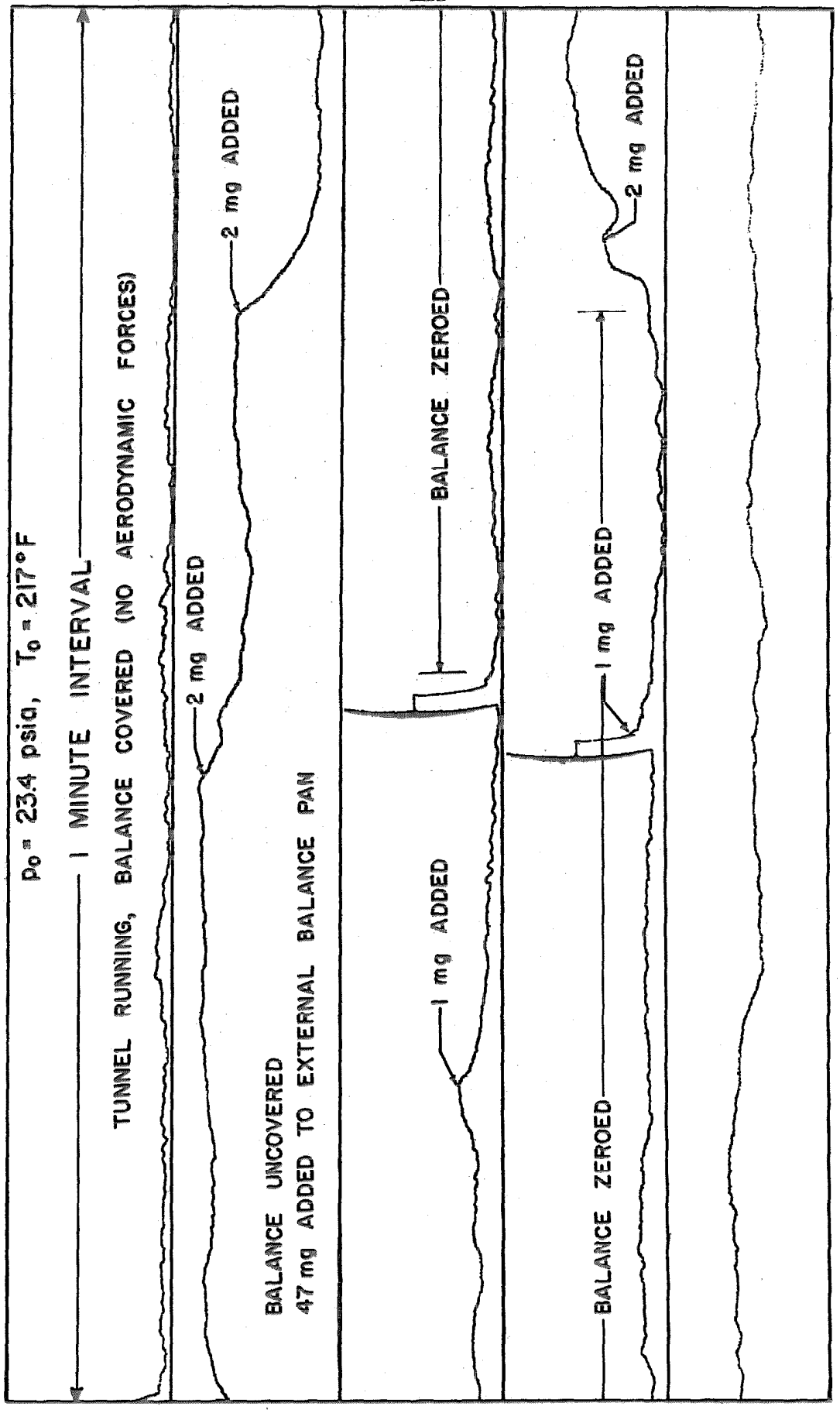

OUTPUT OF BALANCE POSITION SENSING SYSTEM AS A FUNCTION OF TIME

FIG. 20

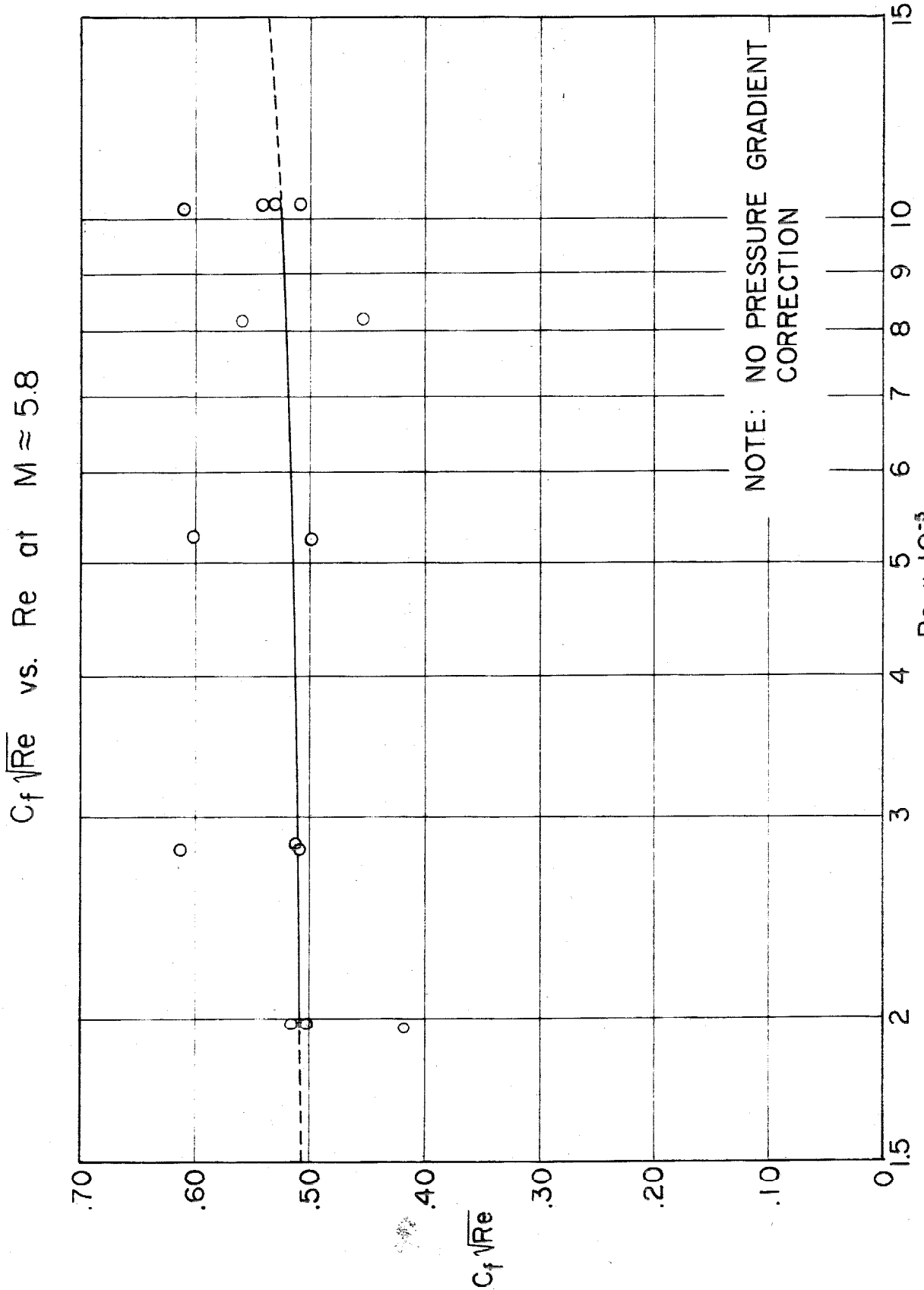
$C_f\sqrt{Re}$ vs. Re at M ≈ 5.8
NOTE: NO PRESSURE GRADIENT CORRECTION
$C_f\sqrt{Re}$
Re x 10^{-3}
0
.10
.20
.30
.40
.50
.60
.70
1.5
2
3
4
5
6
7
8
9
10
15

FIG. 21

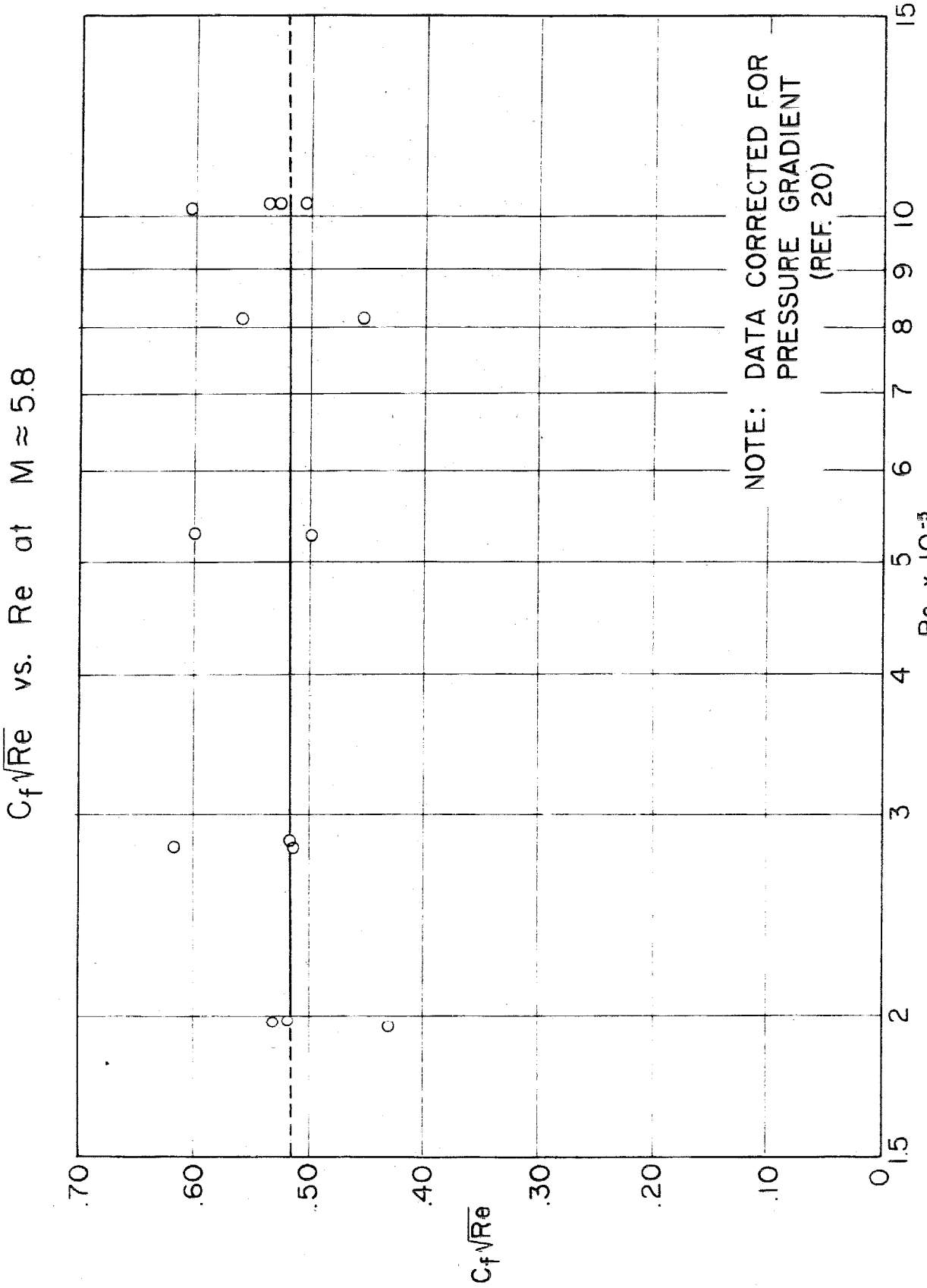
$C_f\sqrt{Re}$ vs. Re at $M \approx 5.8$
NOTE: DATA CORRECTED FOR PRESSURE GRADIENT (REF. 20)
$C_f\sqrt{Re}$
Re x 10^{-5}
.70
.60
.50
.40
.30
.20
.10
0
1.5
2
3
4
5
6
7
8
9
10
15

FIG. 22

PREDICTIONS OF LOCAL SKIN FRICTION COEFFICIENT AS A FUNCTION OF MACH NUMBER

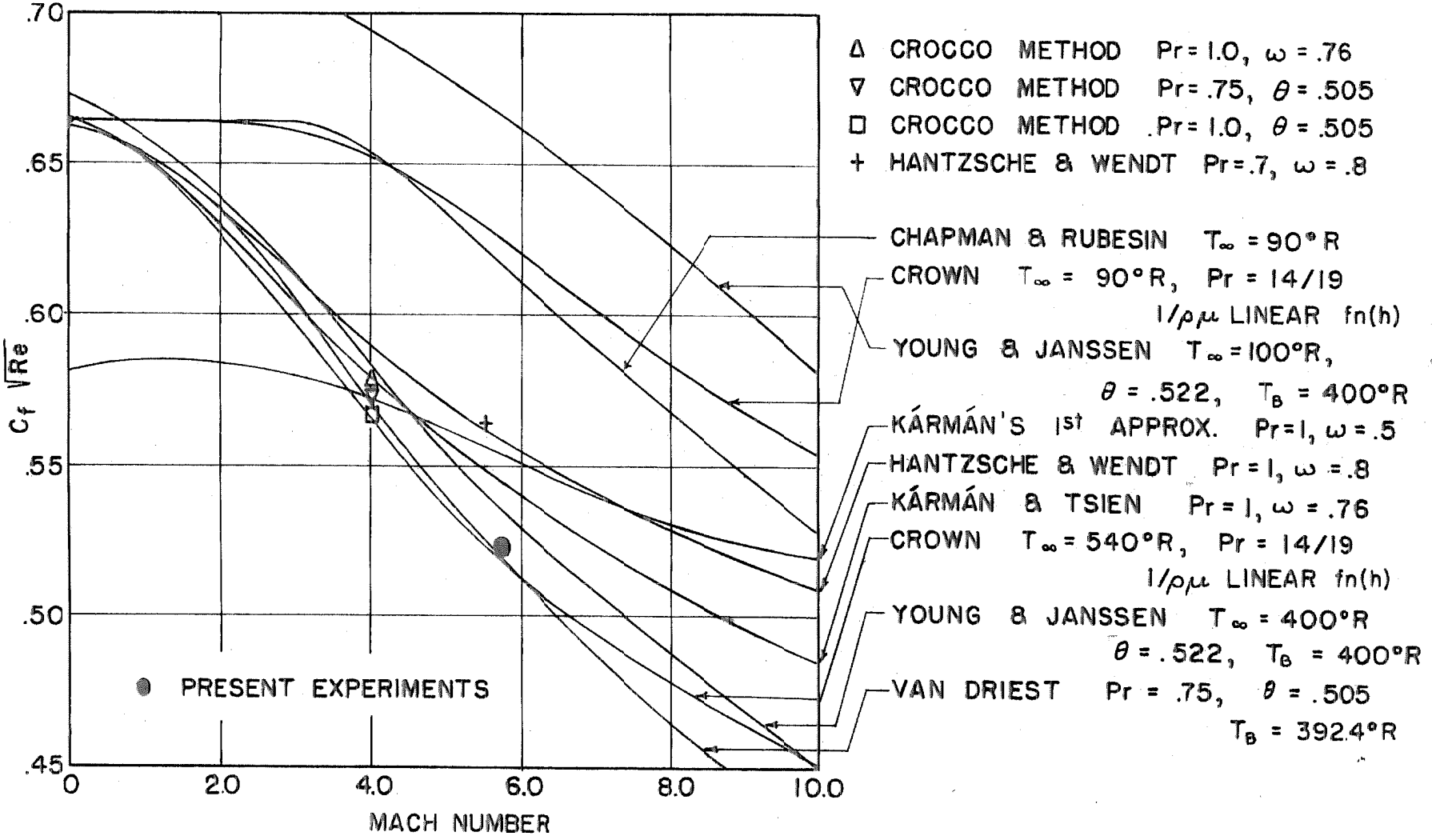

FIG. 23

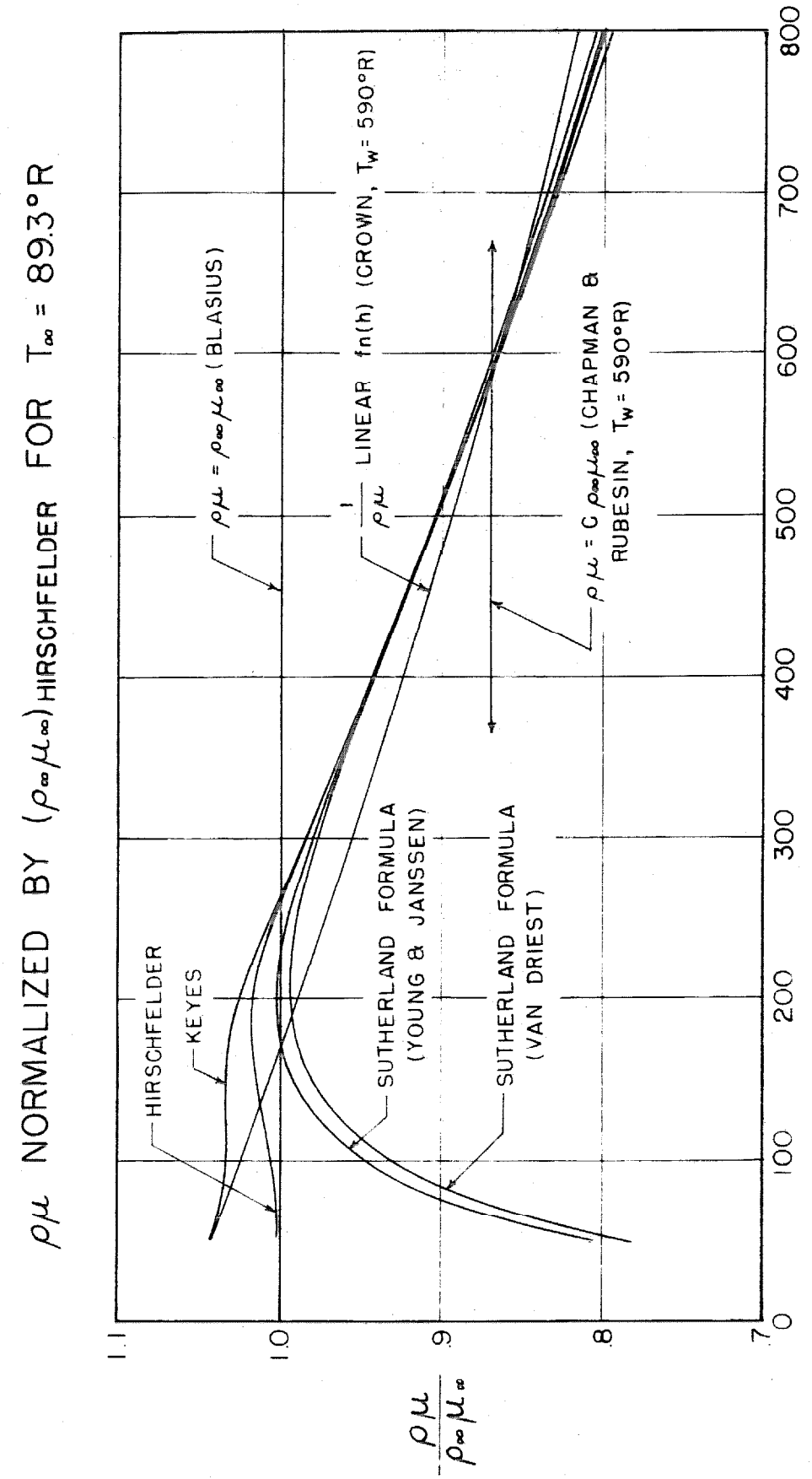
ρμ NORMALIZED BY (ρ∞μ∞) HIRSCHFELDER FOR T∞ = 89.3°R
ρμ = ρ∞μ∞ (BLASIUS)
1/ρμ LINEAR fn(h) (CROWN, Tw = 590°R)
ρμ = C ρ∞μ∞ (CHAPMAN & RUBESIN, Tw = 590°R)
HIRSCHFELDER
KEYES
SUTHERLAND FORMULA (YOUNG & JANSSEN)
SUTHERLAND FORMULA (VAN DRIEST)
ρμ / ρ∞μ∞
1.1
1.0
.9
.8
.7
0
100
200
300
400
500
600
700
800
T (°R)

FIG. 24

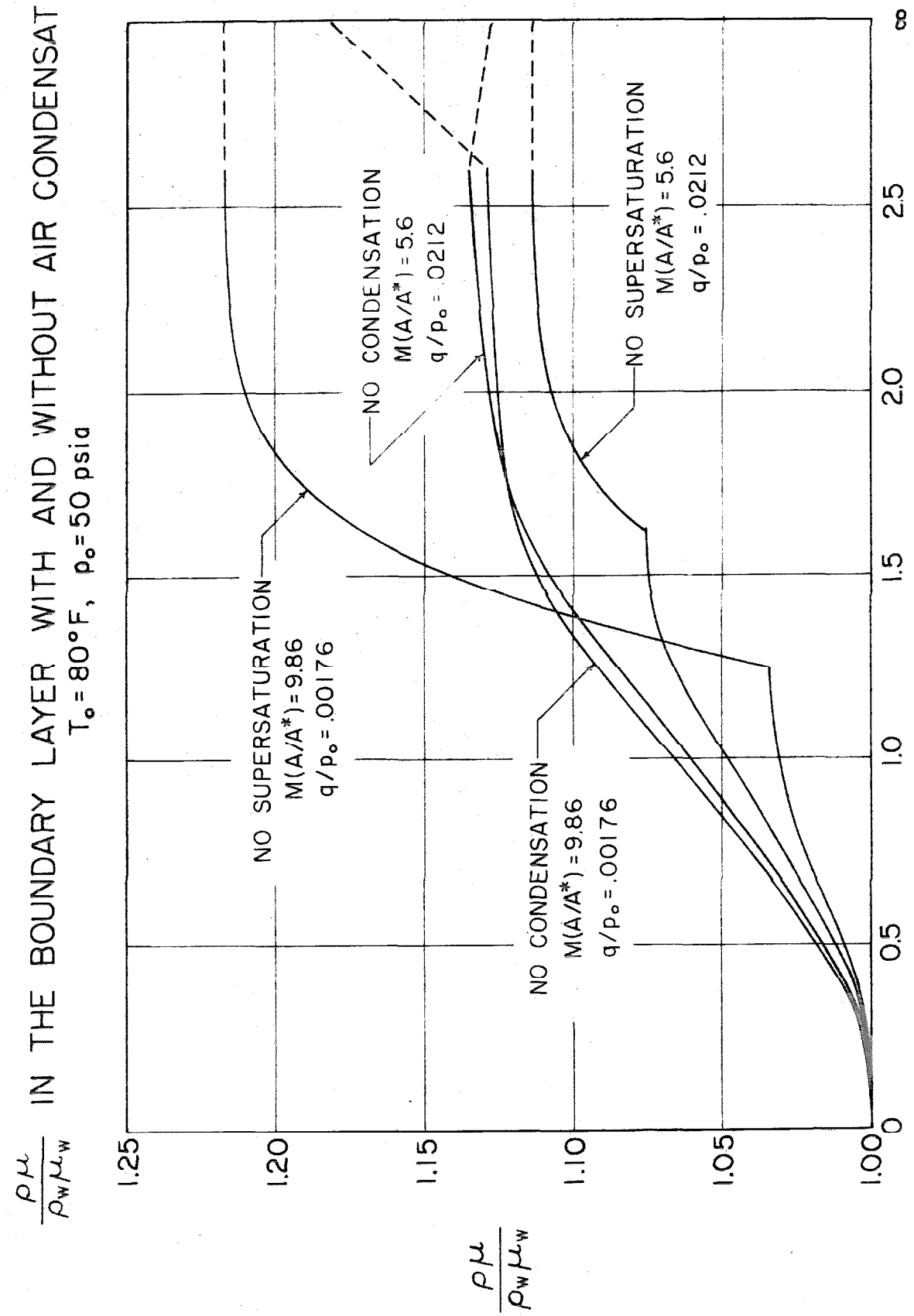
$\frac{\rho\mu}{\rho_w\mu_w}$ IN THE BOUNDARY LAYER WITH AND WITHOUT AIR CONDENSATION
$T_o = 80°F$, $p_o = 50$ psia
NO SUPERSATURATION
M(A/A*) = 9.86
q/p_o = .00176
NO CONDENSATION
M(A/A*) = 5.6
q/p_o = .0212
NO CONDENSATION
M(A/A*) = 9.86
q/p_o = .00176
NO SUPERSATURATION
M(A/A*) = 5.6
q/p_o = .0212
1.25
1.20
1.15
1.10
1.05
1.00
0
0.5
1.0
1.5
2.0
2.5
∞
η

FIG. 25

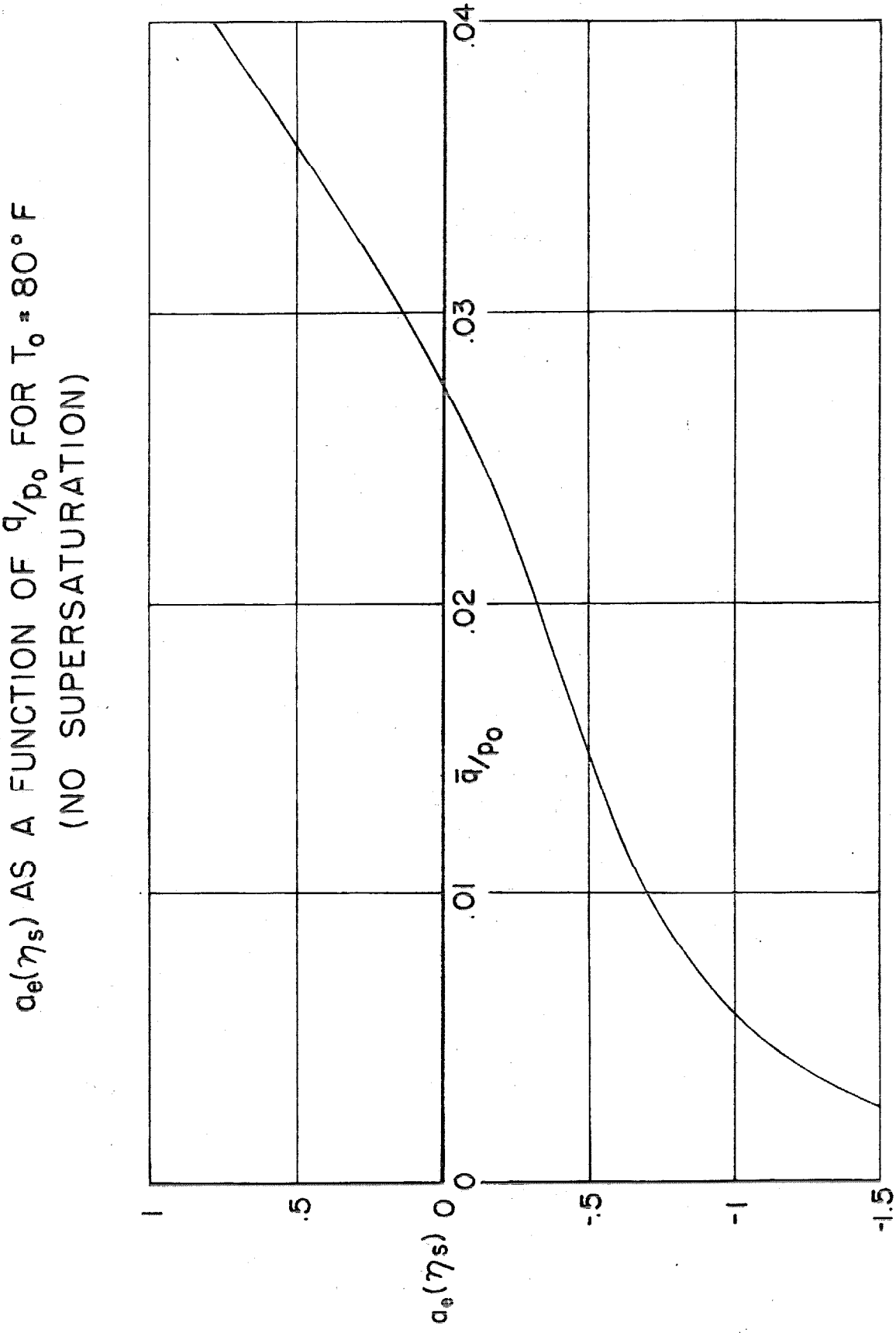
$a_e(\eta_s)$ AS A FUNCTION OF $\bar{q}/p_o$ FOR $T_o = 80°F$
(NO SUPERSATURATION)
$a_e(\eta_s)$
1
.5
0
-.5
-1
-1.5
$\bar{q}/p_o$
0
.01
.02
.03
.04

FIG.26